Synthesis and Characterization of Furan-Based Non-ionic Surfactants (FBNIOS)

by

Donghan Liu

A thesis

presented to the University of Waterloo

in fulfilment of the

thesis requirement for the degree of

Master of Science

in

Chemistry

Waterloo, Ontario, Canada, 2020

AUTHOR'S DECLARATION

I hereby declare that I am the sole author of this thesis. This is a true copy of the thesis, including any required final revisions, as accepted by my examiners.

I understand that my thesis may be made electronically available to the public.

Abstract

A series of furan-based non-ionic surfactants (*fbnios*) derived from 5-(chloromethyl)furfural (5-CMF), a feedstock prepared by Origin Materials through a carbon negative process, were prepared from commercially available 2,5-*bis*(hydroxymethyl) furan (2,5-*bis*HMF). The *fbnios* were synthesized by alkylating one hydroxyl of 2,5-*bis*HMF by Williamson ether synthesis and ethoxylating the other hydroxyl to generate an oligo(ethylene oxide) (OEO). Through systematic variations in the OEO length achieved by anionic polymerization, and the use of octyl and dodecyl groups, *fbnios* with different hydrophilic-lipophilic balances (HLBs) were synthesized. The number-average degree of polymerization (DP_n), and purity of the *fbnios* samples were determined by proton nuclear magnetic resonance (^{1}H NMR), gel permeation chromatography (GPC), and matrix-assisted laser desorption ionization-time of flight-mass spectroscopy (MALDI-ToF-MS). The amphiphilic properties of these *fbnios* were characterized by surface tension and fluorescence measurements. Surface tension was applied to determine the efficiency and effectiveness of the *fbnios*. The critical micelle concentration (CMC) of *fbnios* was determined by both characterization methods. The CMC of the *fbnios* prepared with an octyl chain was found to decrease about 3-fold upon increasing the DP_n of the OEO block from 3 to 14. The length of the OEO block had less influence on the CMC of the *fbnios* series prepared with a dodecyl chain. In contrast, the alkyl chain used to prepare the *fbnios* was found to affect their CMC, the CMC of the *fbnios* with an octyl chain being more than one order of magnitude larger than the CMC of the *fbnios* with a dodecyl chain. The range of CMC values found for the *fbnios* prepared in this thesis covered the range of CMCs found for well-known non-ionic surfactants (*nios*) such as the Triton X or Brij surfactant families. The *fbnios* with a dodecyl chain were found to have lower CMCs than the Brij surfactants prepared with the same alkyl chain. In summary, *fbnios* appear to behave as typical *nios* and show promising amphiphilic properties.

Acknowledgements

Words can hardly convey my deep gratitude toward my co-supervisors, Profs. Jean Duhamel and Mario Gauthier, for offering me the precious chance of working on this project. This thesis involved the complicated synthesis of novel chemicals and the usage of highly toxic and explosive ethylene oxide. It would have never been possible without their patient guidance and support.

Much appreciation also goes to my committee members Profs. Xiaosong Wang and Shawn Wettig. Their advice and help were critical for the success of my project.

I want to thank graduate student Remi Casier and Dr. Deepak Vishnu D. for teaching me how to carry out the anionic polymerization of ethylene oxide in a safe manner and providing advice during the course of my project. The precious help of graduate student Janine Thoma is also acknowledged for teaching me how to run and calibrate the GPC instrument.

Many thanks go to Dr. Richard Smith and Mrs. Valerie Goodfellow for teaching me how to operate the MALDI instrument, and to Mrs. Janet Venne for her training with the NMR instrument.

I want to thank all group members in the laboratories of Profs. Duhamel and Gauthier for their constant friendliness and help. Many difficulties encountered during the course of my project were resolved through discussions with them.

Finally, I would like to express my sincere gratitude to my dear parents for their unconditional love and support in my life.

Table of Contents

List of Figures

List of Schemes

List of Tables

Abbreviations

BHT	Butylated hydroxytoluene
Br-C_xH_{2x-1}	1-Bromoalkane with *x* carbons
CMC	Critical micelle concentration
C_x-F-OH	Monoalkylated furfuryl alcohol or 2,5-*bis*(hydroxymethyl)furan having one hydroxyl group etherified with an alkyl chain containing *x* carbons
C_x-F-EO_y	2,5-*bis*(Hydroxymethyl)furan having one hydroxyl group etherified with an alkyl chain containing *x* carbons and the other hydroxyl group ethoxylated with an oligo(ethylene oxide) chain containing *y* ethylene oxide monomers
DCM	Dichloromethane
DMSO	Dimethyl sulfoxide
DP_n	Number-average degree of polymerization
DRI	Differential refractive index
d_6-DMSO	Deuterated dimethyl sulfoxide
EO	Ethylene oxide
fbnios	Furan-based non-ionic surfactants
GPC	Gel permeation chromatography
HLB	Hydrophilic-lipophilic balance
I	Fluorescence intensity
I_E	Excimer fluorescence intensity
I_M	Monomer fluorescence intensity
I_1	Fluorescence intensity of the first peak in the fluorescence spectrum of pyrene

I_3	Fluorescence intensity of the third peak in the fluorescence spectrum of pyrene
LLE	Liquid-liquid extraction
MALDI-ToF MS	Matrix-assisted laser desorption ionization-time of flight mass spectroscopy
Me-F-EO_y	Ethoxylated 5-methylfuran-2-methanol containing *y* ethylene oxide units
Me-F-OH	5-Methylfurfuryl alcohol
2-MTHF	2-Methyltetrahydrofuran
M_n	Number-average molecular weight
M_w	Weight-average molecular weight
MWD	Molecular weight distribution
meq	Molar equivalents
nios	Non-ionic surfactant
NMR	Nuclear magnetic resonance
OrMat	Origin Materials®
OEO	Oligo(ethylene oxide)
pC_{20}	Efficiency of a surfactant
PDI	Polydispersity index
PEF	Pyrene excimer formation
PTB	Potassium *tert*-butoxide
PTP	Potassium *tert*-pentoxide
PMC	Phenylmagnesium chloride
RBF	Round-bottom flask
SDS	Sodium dodecyl sulfate

SSF	Steady-state fluorescence
T_b	Boiling point
V_e	Elution volume
2,5-*bis*HMF	2,5-*bis*(Hydroxymethyl)furan
5-CMF	5-Chloromethylfurfural

Chapter 1 - Introduction

1.1 Introduction

The ability of surfactants to reduce the interfacial tension between two phases has found numerous practical applications over the years. Surfactants are commonly used as detergents, which are the major ingredient in cleaning products, or as emulsifiers added to solubilize chemicals such as cosmetics, pesticides, or grease.[1] Surfactants are classified as ionic or non-ionic depending on their charge. Non-ionic surfactants (*nios*) have been the focus of tremendous research in recent years due to their cost-effectiveness,[2] stability against changes in ionic strength encountered in concentrated electrolyte solutions,[3-5] and their ability to form *niosomes* (vesicles prepared from *nios*).[6] Although the cost-effectiveness of *nios* is often reported in the scientific literature,[7-9] the origin of this claim is never clearly stated. It probably stems from their simple synthetic pathways and the biological origin of the hydro- and/or lipophilic moieties constituting many *nios* obtained from renewable biomass.[2,10] For instance, sorbitol produced from starch is used to prepare the ubiquitous Span surfactant family.[11,12] Span 60 is prepared by the esterification of sorbitol with stearic acid.[10] In 2004, mono- and diglycerides generated by the transesterification of soybean oil with excess glycerol were the most commonly used emulsifiers in the food industry. These *nios* were entirely generated from renewable biomass.[10] The chemical structure of Span 20 and the monoglyceride of soybean oil are shown in Figure 1.1A and B, respectively.[10]

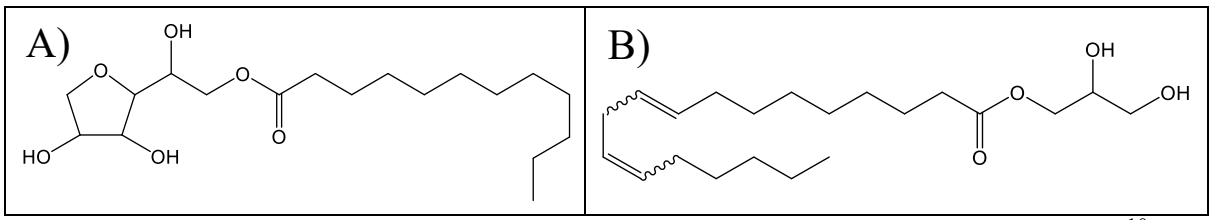

Figure 1.1. Chemical structure of A) Span 20 and B) the monoglyceride of soybean oil.[10]

Earlier studies have shown that the critical micelle concentration (CMC), which is the surfactant concentration above which micelles start to form, is lower by one-to-two orders of magnitude for *nios* as compared with traditional ionic surfactants prepared with the same hydrophobic component. For example, the ethoxylation of dodecanol to generate oligo(ethylene oxide)s (OEOs) with different degrees of polymerization yielded *nios* having a CMC in water ranging from 10^{-5} to 10^{-3} M.[13,14] These CMCs are lower than for sodium dodecyl sulfate (SDS), which equals 8×10^{-3} M.[15,16] In addition, the CMC of other common *nios* like the Triton X surfactants, and more particularly the Tween and Brij® surfactant families, are also orders of magnitude lower than 1 mM.[17] Such a reduction in CMC implies that much less *nios* is needed to achieve the same surface tension reduction than with a similar ionic surfactant. Consequently, this represents another justification for the cost-effectiveness of *nios* as compared to ionic surfactants.

In addition to their relatively low efficiency, the performance of ionic surfactants depends on the ionic strength of aqueous solutions, and is thus sensitive to changes in electrolyte concentration. For instance, an increase from 0 to 0.5 M NaCl results in a 95% decrease in the CMC of SDS from 8 to 0.5 mM.[3] In contrast, the CMC of *N*-octanoyl-*N*-methylglucamine only decreases by less than 30%, from 70 to 51 mM, when the NaCl concentration is increased from 0 to 0.5 M.[4,5] The reduction in CMC observed upon increasing the ionic strength of an aqueous solution of ionic surfactants is a consequence of their poorer solubility. A typical example is soap, which is a fatty acid salt. The deprotonated fatty acid precipitates in the presence of calcium or magnesium ions, typically found in hard water, through coordination of the divalent cation with two carboxylate anions, resulting in the formation of insoluble salts.[5] The detergency of an aqueous soap solution also decreases for increasing ionic strength and has been found to increase the roughness of fabrics.[5,18] In fact, the detrimental effects of salts on the properties of ionic surfactants like SDS or sodium oleate are well established.[5] In the case

of *nios* however, similar studies have shown that their performance is not affected by water hardness due to their non-ionic character.[6]

Nios can also be added to saline aqueous solutions of ionic surfactants, to increase the minimum salt concentration that induces the precipitation of an ionic surfactant.[19] Taking an anionic surfactant as example, its precipitation depends on its solubility product (K_{SP}) given by $[A^-]\times[C^+]$, where $[A^-]$ and $[C^+]$ are the concentrations of the free anionic surfactant and its counterion at saturation, respectively. The association of ionic surfactants with the *nios* micelles generated at low *nios* concentration reduces $[A^-]$, which brings the concentration product $[A^-]\times[C^+]$ below K_{SP}, thus increasing the solubility of the ionic surfactant. The enhanced solubility of ionic surfactants in the presence of *nios* is useful in applications where a high salinity can be detrimental to performance, such as in household detergents or enhanced oil recovery.[19]

The discovery that *nios* could form liposomes, or *niosomes*, has opened their application in drug delivery and has led to massive research on *nios*, which are increasingly preferred over ionic surfactants.[20,21] A schematic illustration of the structure of *niosomes* is presented in Fig. 1.2. The advantages for using *niosomes* in biological systems have been reviewed.[21] *Niososomes* are biocompatible, biodegradable, non-toxic, and more stable than the more traditional phospholipid liposomes due to their non-ionic character.[21] Another advantage of *nios* is that their shape and design can be easily adjusted through chemical modification of the functional groups in their hydrophilic moiety.[21]

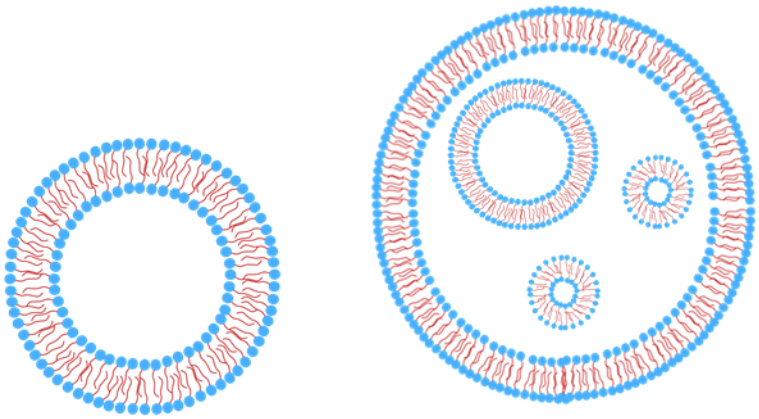

Figure 1.2. Illustration of the different structures taken by *niosomes*. *Niosomes* with diameter larger than 1 μm can form multi-lamellar vesicles where smaller *niosome(s)* are encapsulated in a larger *niosome*.[21]

These properties have led to many applications for *nios*. For example, Farmoudeh et al. have reported that methylene blue could be efficiently loaded into *niosomes*, which could then be applied to wounds to reduce reactive oxygen species generated during in vivo wound healing.[22] Abdelbary and El-Gendy demonstrated that *niosomes* prepared with a 1:1:0.1 Tween 60:cholesterol:dicetyl phosphate mixture could entrap up to 74% of the antibiotic gentamicin added to the mixture and deliver it in a controlled manner in simulated lacrimal fluid.[23] Puras et al. prepared *niosomes* from Tween 80, the cationic lipid 2,3-di(tetradecyloxy)propan-1-amine and squalene, and successfully applied it to gene transfection in rat retinas.[24] In addition, even *nios* that do not form *niosomes* still present advantageous properties such as promoting the transdermal permeation of biomacromolecules, altering the activity of enzymes, and synergizing the release of drugs, which all have great importance and potential in biological and pharmaceutical research.[25]

For all the reasons mentioned above, along with market pressure to produce more environmentally friendly surfactants, extensive studies have been conducted to explore

whether new types of *nios* could be produced in a more ecological manner, utilizing cheaper and renewable raw materials. In 2017, Dr. Masuno from Origin Materials (OrMat) introduced a novel catalytic process for the large-scale production of furan derivatives from renewable biomass like cardboard or wood chips,[26] as schematically depicted in Figure 1.3. This process yields furan derivatives from raw materials (e.g. used cardboard) that do not compete with food production.[27] Beside their obvious use as precursors in organic synthesis, furan derivatives such as 5-chloromethylfurfural (5-CMF), one of the major products of the catalytic process depicted in Figure 1.3, is a feedstock, that is produced through a carbon negative process by Origin Materials,[28] and that could also be employed to prepare *nios*. Such furan-based non-ionic surfactants (*fbnios*), produced from renewable and cost-effective non-food biomass, could have properties that might compete with those of more traditional *nios* like Triton X-100, prepared from petrochemicals, or Tween 80, produced from glucose. Thanks to their renewable origin, *fbnios* have the potential to ease the pressing demand on petroleum or food to produce feedstocks for the chemical industry, and to be less harmful to the environment. Moreover, *fbnios* might also have unique properties that would make them invaluable amphiphiles for applications in colloidal science. These promises make it worthwhile to investigate the feasibility of different synthetic protocols for the preparation of *fbnios*, and to characterize their amphiphilic properties. Furthermore, if *fbnios* could also form *niosomes*, they could also find valuable pharmaceutical applications.

These considerations were the motivations behind this thesis work, which was concerned with the synthesis and the characterization of two series of *fbnios*. The properties of the *fbnios* were characterized by surface tension and pyrene fluorescence measurements, whose principles are described in the following sections.

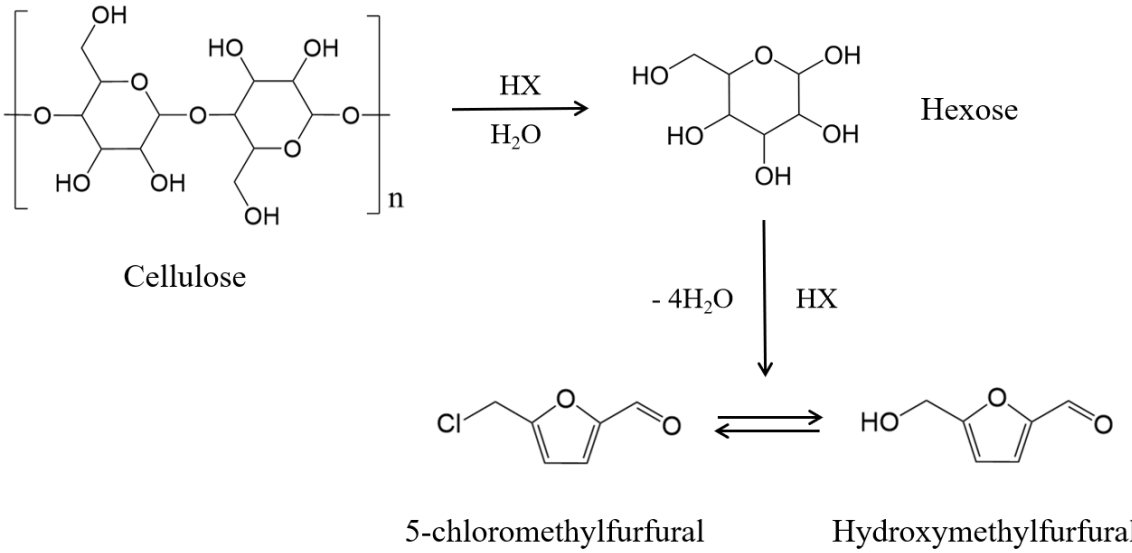

Figure 1.3. Reaction scheme for the synthesis of furan derivatives through a catalytic pathway, where HX represents a gaseous acid like hydrochloric acid.

1.2 Hydrophilic-Lipophilic Balance (HLB)

Previous work has shown that the HLB of *nios* has a determining effect on their efficiency and effectiveness in surface tension reduction, CMC, and thus on their performance and applications.[17,29,30] For instance, *nios* with HLB ranging from 3 to 6, 13 to 16, and 16 to 18 have been commonly used as water/oil emulsifier, detergent, and solubilizer, respectively.[31] The determination of the HLB of *nios* is based on the Griffin method, which states that HLB equals the weight fraction of the hydrophilic part in the surfactant molecule multiplied by 20.[31] The *fbnios* studied in this thesis are composed of a 2,5-*bis*(hydroxymethyl)furan (2,5-*bis*HMF) etherified on one side with a hydrophobic alkyl chain, and on the other side with a hydrophilic oligo(ethylene oxide) (OEO) segment as shown in Fig. 1.4. They are referred to as C_x-F-EO_y, where *x* and *y* represent the number of carbons in the alkyl substituent and the degree of polymerization of the OEO segment, respectively.

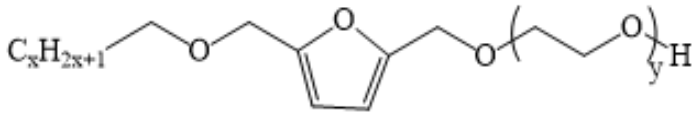

Figure 1.4. Chemical structure of the C_x-F-EO_y *fbnios* prepared with an OEO having a degree of polymerization *y* and an alkyl chain made of *x* carbons.

Thus, the HLB of these *fbnios* can be calculated with Equation 1.1, where M_{fbnios}, M_{OEO}, and M_{furan} represent the molar mass of the *fbnios* molecule, the OEO chain, and the alkylated furan ring in the *fbnios* molecule, respectively.

$$HLB = 20 \times \frac{M_{OEO} + M_{furan}}{M_{fbnios}} \tag{1.1}$$

1.3 Surface Tension of Aqueous Surfactant Solutions

The ability of a surfactant to reduce the surface tension of water is a critical parameter in assessing its performance. Numerous studies have shown that the surface tension of water decreases with increasing surfactant concentration until the concentration reaches the CMC, above which the surface tension remains constant.[2,13] Any surfactant addition past the CMC results in the formation of surfactant micelles, while the concentration of free surfactant remains constant and equal to the CMC. The performance of surfactants is assessed by determining their efficiency in surface tension reduction given by pC_{20}, their effectiveness, and their CMC. The parameter pC_{20} represents the negative logarithm (in base 10) of the surfactant concentration, such that the surface tension of water (72 mN/m) is reduced by 20 mN/m.[2] The effectiveness is quantified by the maximum surface tension reduction that can be achieved by a surfactant in water.[2,32] Many studies have also found that after the surface tension in water has decreased from 72 mN/m to about 52 mN/m, the surface tension decreases linearly with the surfactant concentration until the concentration reaches the CMC.[13] These observations are

summarized in Fig. 1.5, which represents the expected plot of surface tension against concentration for a surfactant in water.[2]

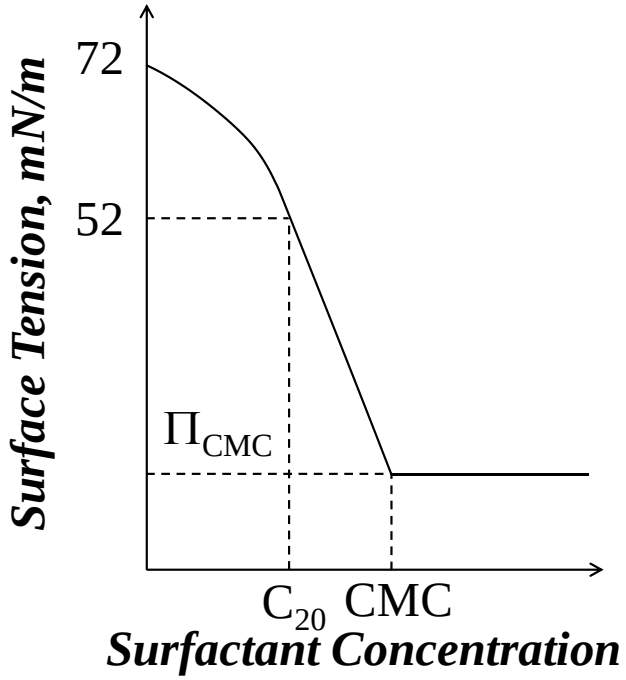

Figure 1.5. Typical semi-log plot of surface tension as a function of surfactant concentration in water.[2]

1.4 Pyrene Fluorescence to Determine the CMC of Surfactants

The CMC is an important parameter in the characterization of surfactants.[1,2] The CMC determines the amount of surfactant that must be added to the aqueous solution to produce micelles. The CMC value of surfactants can be measured by surface tension, as described in Section 1.3, and fluorescence as was done in this study.[33-35] The fluorescent dye used in these experiments was pyrene. With a solubility limit of 0.7 μM,[36] pyrene is highly hydrophobic and can be excited by UV light at 336 nm, which represents the $S_{0,0} \rightarrow S_{2,0}$ transition, and where its molar absorption coefficient (MAC) equals 32,600 $M^{-1}.cm^{-1}$.[37] The 0-0 transition of pyrene occurs at 375 nm. It is symmetry-forbidden and results in a very low MAC.[38] This explains why pyrene solutions are never excited at 375 nm.

Upon absorption of a photon, an excited pyrene can fluoresce as a monomer with its natural lifetime τ_M. The fluorescence spectrum of the pyrene monomer shows several sharp bands between 370 and 410 nm. However, an excited pyrene can also form an excimer upon encounter with a ground-state pyrene. The excimer decays with its natural lifetime τ_E and exhibits a broad structureless emission centered at 480 nm. Fig. 1.6 shows the fluorescence spectrum of a 1 mM C_8-F-EO_6 aqueous solution containing 5×10^{-7} M pyrene.

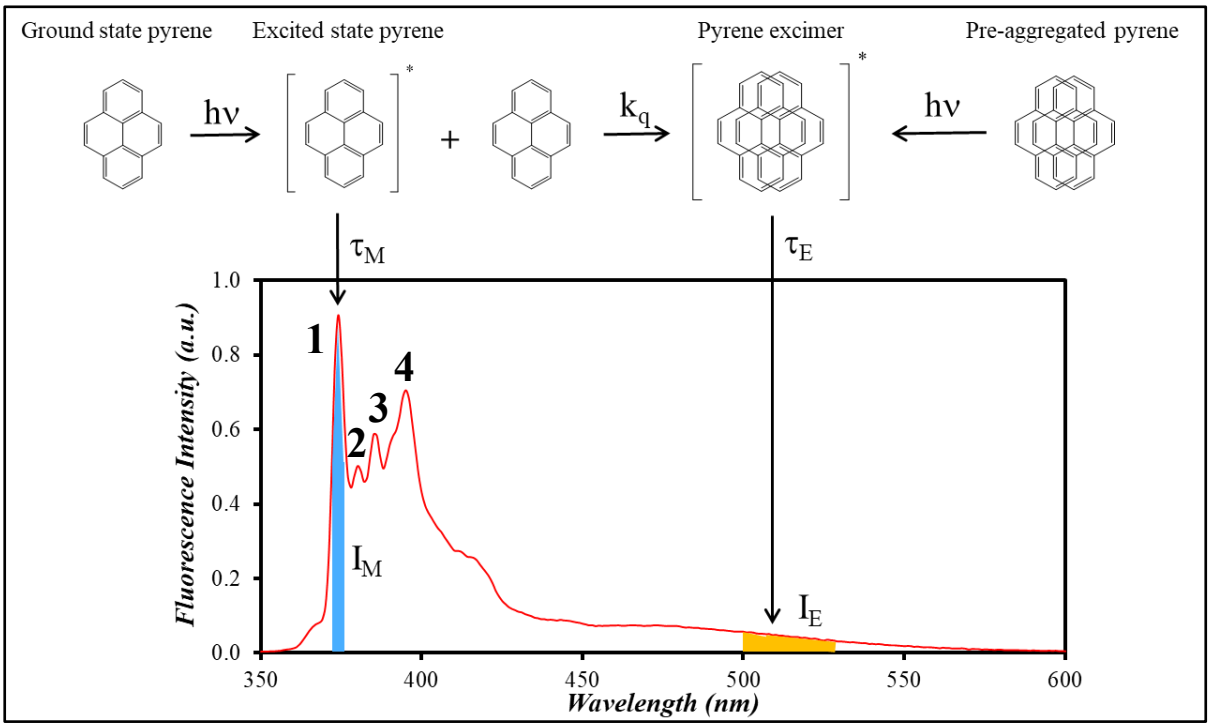

Figure 1.6. (Top) Kinetic scheme for pyrene excimer formation and (bottom) the corresponding steady-state fluorescence spectrum of 5×10^{-7} M molecular pyrene in a 1 mM C_8-F-EO_6 aqueous solution. I_M and I_E refer to the fluorescence intensity of the pyrene monomer and excimer, respectively. The position of the four first peaks in the fluorescence spectrum of the pyrene monomer have been assigned.

Because fluorescence is a relative measurement, the fluorescence intensity determined by steady-state fluorescence must be normalized. Pyrene is unique among all dyes because the

ratio of different bands in its fluorescence spectrum can be used to get a measure of the polarity of its local environment and of the local concentration ($[Py]_{loc}$) of ground-state pyrenes surrounding an excited pyrene. Taking the ratio of the intensity of the first peak (I_1) over that of the third peak (I_3) in the fluorescence spectrum of the pyrene monomer yields the I_1/I_3 ratio, whose value increases from 0.6 in apolar hexane to 1.8 in polar water.[39] The I_1/I_3 ratio takes an intermediate value of 1.05 when pyrene is located inside the hydrophobic interior of SDS micelles. Since the I_1/I_3 ratio decreases from 1.8 for pyrene in water to a substantially lower value when pyrene binds to a surfactant micelle, this ratio has been used effectively to determine the CMC of surfactants, and it will be used to determine the CMC of *fbnios*. Similarly, taking the ratio of the fluorescence intensity of the excimer (I_E) from 500 to 530 nm over that of the monomer (I_M) from $\lambda_1 - 3$ to $\lambda_1 + 3$ nm, where λ_1 corresponds to the 0-0 transition of pyrene and depends on the polarity of the local environment where pyrene is embedded yields the I_E/I_M ratio, which is proportional to the product $k_{diff} \times [Py]_{loc}$ where k_{diff} is the bimolecular rate constant for pyrene excimer formation by diffusion.

1.5 Thesis Outline

This thesis is divided into four chapters. Chapter 1 provided a general introduction about *fbnios* and the different techniques that will be applied to characterize them. The second chapter describes the synthesis of the *fbnios* considered in this thesis, namely *fbnios* constituted of a furan core flanked by a hydrophobic alkyl chain and a hydrophilic OEO block, which will be referred to as C_x-F-EO_y. In the third chapter, the fluorescence and surface tension techniques described in Chapter 1 are applied to characterize the *fbnios*. The final chapter of this thesis summarizes the results and suggests possible research directions for future work.

Chapter 2 - Synthesis and Characterization of Furan-based Non-ionic Surfactants

2.1 Synthetic Route Overview

As explained in Chapter 1, 5-chloromethylfurfural (5-CMF, compound **1** in Figure 2.1) can now be generated in large quantities from renewable biomass.[40] Chapter 2 focuses on the synthesis and characterization of environmentally friendly *fbnios* surfactants, that could be derived from 5-CMF according to the synthesis route described in Figure 2.1. In Figure 2.1, *fbnios* **7** and **8** are prepared by ethoxylation of the alkylated furfuryl alcohols (C_x-F-OH) **4** and **5**. Compound **5** and **8** was synthesized in this thesis from commercially available 2,5-*bis*HMF instead of 5-CMF. Compound **9** was prepared first from 5-methylfuran-2-methanol to examine the feasibility of the synthetic approach for the *fbnios*.

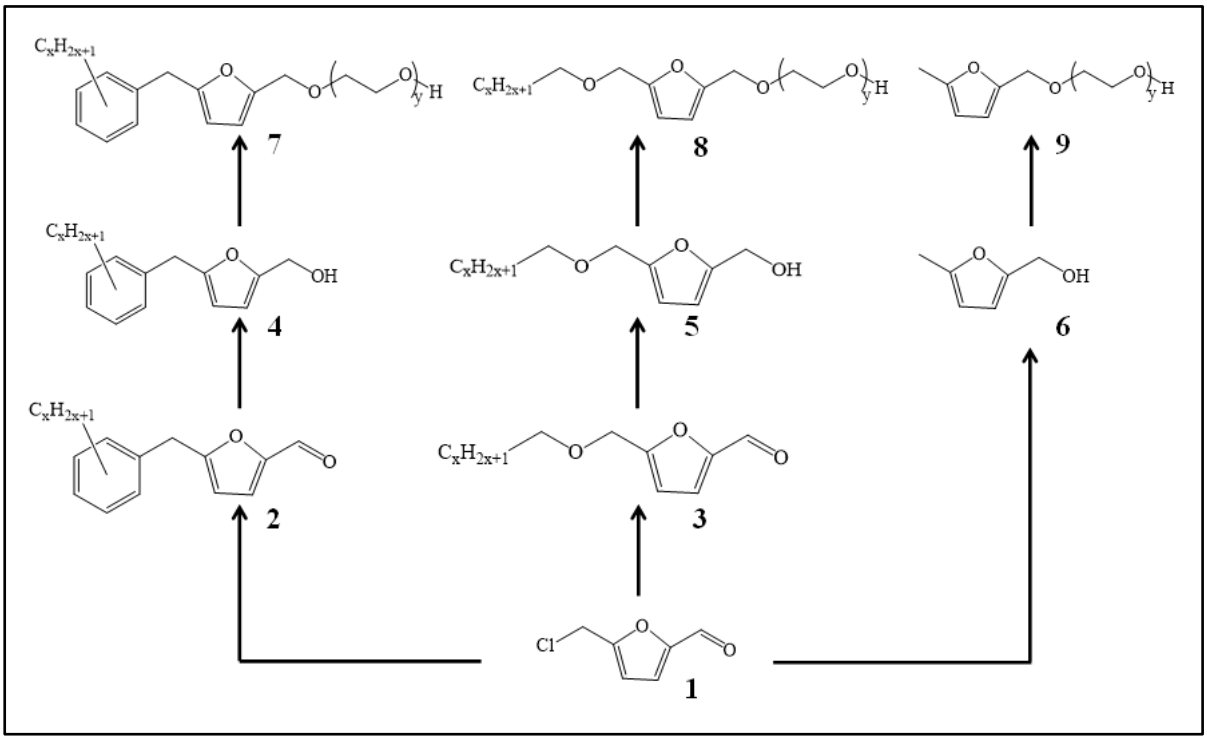

Figure 2.1. Scheme for the *fbnios* synthesis starting from 5-CMF (**1**).

A Williamson ether synthesis with an alkyl bromide was first applied to 2,5-*bis*HMF to generate the alkylated furfuryl alcohol (C_x-F-OH). It was followed by the anionic polymerization of ethylene oxide (EO) to convert C_x-F-OH into *fbnios* **8** in Figure 2.1. Due to the nature of the polymerization, EO oligomers (OEOs) produced from the addition of EO monomers were not uniform in length. The *fbnios* product was thus a polydisperse oligomer consisting of *fbnios* molecules bearing a well-defined alkyl chain made of *x* carbons, and OEOs made of *y* EO units on average. The numbers *x* and *y* could be controlled by the choice of the alkyl bromide used in the Williamson ether synthesis and by the EO-to-C_x-F-OH molar ratio used during the polymerization. The molecular weight distribution (MWD) of the C_x-F-EO_y samples was characterized by their number-average (M_n) and weight-average (M_w) molecular weights and their polydispersity index (PDI).[41,42] As for any polymeric surfactant, the properties of the C_x-F-EO_y samples depended strongly on their hydrophilic-lipophilic balance (HLB), and thus on the MWD of their OEO block. To assess the effect of the OEO block on the properties of the *fbnios*, anionic polymerization was selected for their preparation to produce *fbnios* with an OEO block of well-controlled chain length and with a narrow MWD.[43]

2.2 Chemicals

Dimethyl sulfoxide (DMSO, 99%), potassium *tert*-butoxide (PTB, 98%), potassium *tert*-pentoxide (PTP, 2 M in THF), acetic acid (99.7%), diethyl ether (with butylated hydroxytoluene (BHT) as inhibitor, 99%), hexanes (mixture of isomers, 98.5%), tetrahydrofuran (THF, 99%), phenylmagnesium chloride (PMC, 1 M in 2-methyl-tetrahydrofuran (MTHF)), dichloromethane (DCM, 99.8%), ethyl acetate (99.7%), acetone (99.9%), d_6-DMSO (99.9 atom% deuterium), chloroform-*d* (99.9 atom% deuterium), and dithranol (90%) were obtained from Sigma-Aldrich. 2,5-*Bis*(hydroxymethyl)furan (2,5-*bis*HMF, 97%) and tetrahydrofuran for

spectroscopy measurements (fluorescence grade, inhibitor-free) were purchased from Apollo Scientific and Fisher Scientific, respectively. Ultrapure water with resistivity 10 to 18 MΩ·cm was obtained with a Milli-Q® Direct water purification system. Ethylene oxide from Praxair was purified before its use in anionic polymerization as described in Section 2.5.

2.3 Instrumentation

^{1}H Nuclear Magnetic Resonance (^{1}H NMR): All samples were prepared in d_6-DMSO or chloroform-*d* for ^{1}H NMR analysis. The ^{1}H NMR spectra were acquired with 64 scans on a 300 MHz Bruker instrument and setting the relaxation times t_1 and t_2 at 8 and 1 sec, respectively. *Gel-Permeation Chromatography (GPC)*: All samples for GPC analysis were dissolved in THF at a concentration of 1 mg/mL. The solutions were filtered through a PTFE membrane with 0.22 μm pore size before being injected into a Viscotek VE 2001 GPC instrument equipped with three PolyAnalytik SupeRes mixed bed columns, a TDA 305 triple detector array (differential refractive index (DRI), pressure, and light scattering detectors), and a UV-Vis detector. THF was used for the mobile phase with a 1 mL·min^{-1} flow rate.

Matrix-Assisted Laser Desorption Ionization-Time of Flight Mass Spectroscopy (MALDI-ToF MS): A Bruker Autoflex Speed MALDI with a 2kHz Nd:YAG UV laser (355 nm) was applied to conduct all MALDI-ToF MS measurements in the reflection mode. The samples were dissolved in dithranol, which served as matrix solution before loading and drying on the sample plate for the MALDI measurements.

2.4 Williamson Ether Synthesis

The Williamson ether synthesis was used to prepare the alkylated furfuryl alcohols (C_x-F-OH) by reacting the corresponding 1-bromoalkane (Br-C_xH_{2x+1}) with 2,5-*bis*HMF. The synthesis of all C_x-F-OH compounds followed a similar procedure and the preparation of the octylfurfuryl

alcohol (C_8-F-OH) is described in more detail hereafter. 2,5-*bis*HMF (10 g, 0.078 molar equivalents (meq)) was placed in a 1 L round bottom flask (RBF) followed by the addition of PTB (9.2 g, 0.082 meq). DMSO (300 mL) was quickly transferred into the RBF and the flask was sealed. The solution was then stirred for 8 hours at 80 ºC. During this time, 2,5-*bis*HMF was deprotonated with PTB to generate a mixture of unreacted 2,5-*bis*HMF and potassium alkoxides. The mono potassium alkoxide is shown in Scheme 2.1.

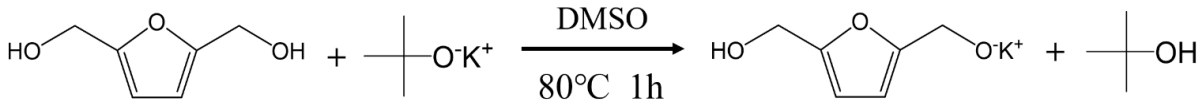

Scheme 2.1. Deprotonation of 2,5-*bis*HMF by PTB.

1-Bromooctane (13.47 mL, 0.078 meq) was then added dropwise to the solution with a syringe injector over a 30 min period to achieve a 1:1.05:1 molar ratio of 2,5-*bis*HMF:PTB:1-bromooctane. This ratio was expected to maximize the yield of C_8-F-OH. The mixture was maintained under stirring for another 8 h to ensure that 1-bromooctane would react with one or both sides of 2,5-*bis*HMF through nucleophilic attack. Scheme 2.2 shows the mechanism of the reaction.

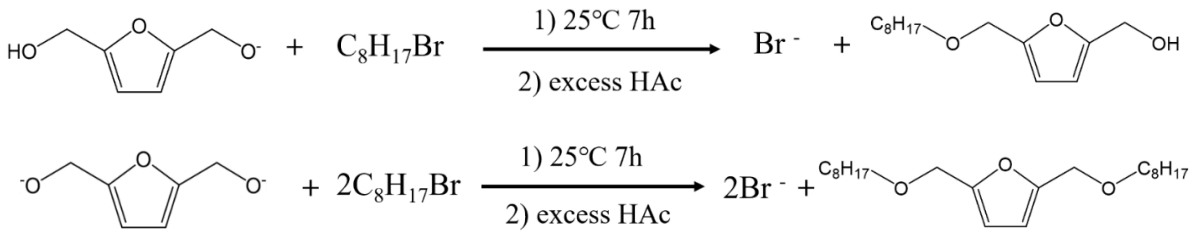

Scheme 2.2. Single and double alkylation of deprotonated 2,5-*bis*HMF by nucleophilic attack on 1-bromooctane.

After the reaction, a slight excess of acetic acid was added to the mixture to protonate the

potassium alkoxides and generate the final product. One side product generated during the Williamson ether synthesis was 1-octanol, due to the presence of residual water in the reaction as shown in Scheme 2.3.

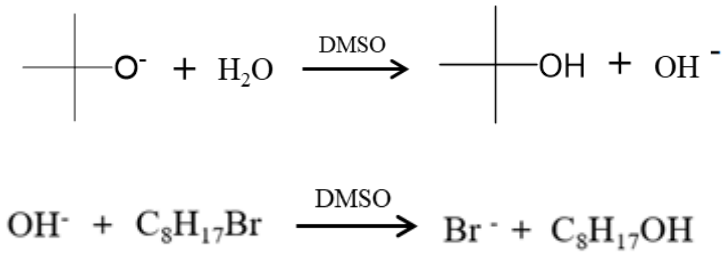

Scheme 2.3. The production of 1-octanol from 1-bromooctane.

Since the reaction mixture contained unreacted 2,5-*bis*HMF and residual 1-octanol, the C_8-F-OH product needed to be purified. To this end, the reaction mixture in DMSO was diluted with 1.2 L of deionized water. Liquid-liquid extraction (LLE) of the DMSO/water mixture with diethyl ether extracted C_8-F-OH into the ether phase, while potassium bromide and unreacted 2,5-*bis*HMF remained in the DMSO/water mixture. The ether fraction was a yellow liquid containing a mixture of 1-octanol as well as singly and doubly alkylated 2,5-*bis*HMF. The ether was removed on a rotary evaporator. The doubly alkylated C_8-F-C_8 compound was separated from the C_8-F-OH product by column chromatography using hexane as the elution solvent. C_8-F-OH and residual 1-octanol, which are relatively polar, were then collected by changing the elution solvent to diethyl ether. The purity of C_8-F-OH could be quantified from the ^{1}H NMR spectrum as shown in Figure 2.2. All the ^{1}H NMR signals expected for the protons of C_8-F-OH were assigned. In particular, the signal at 3.6 ppm was characteristic of the *d*-protons α to the octanol hydroxyl oxygen, while the signal at 3.5 ppm was due to the *e*-protons on the octyl chain α to the ether oxygen. Integration of the respective proton signals led to the conclusion that the C_8-F-OH sample retained about 5% octanol.

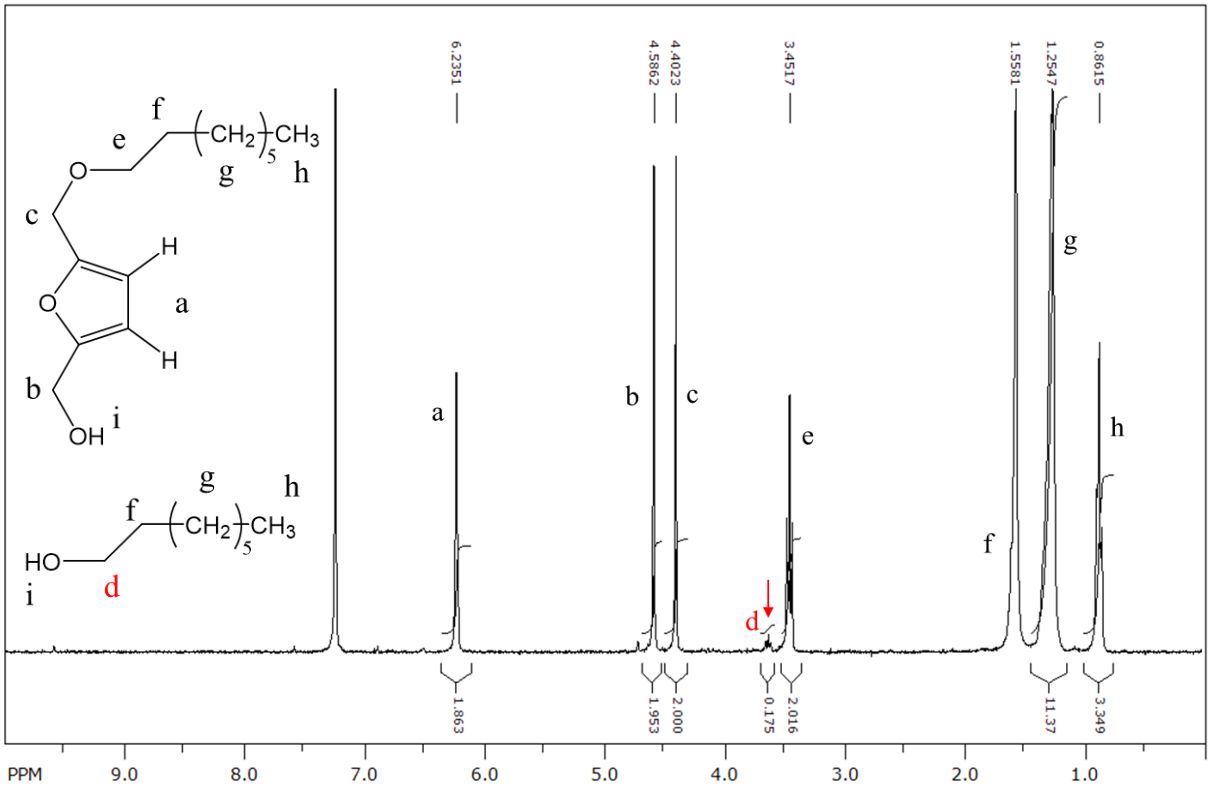

Figure 2.2. Chemical structure of octanol and C_8-F-OH with letter labeling of the different protons, and 300 MHz ^{1}H NMR spectrum of the C_8-F-OH product in chloroform-*d*: δ 6.2 (d, 2H), 4.6 (s, 2H), 4.4 (s, 2H), 3.6 (t, 2H), 3.5 (t, 2H), 1.3 (m, 10H), 0.9 (t, 3H). Residual solvent peaks are found at 7.3 ppm for chloroform and 1.6 ppm for water. The signals generated by the *f* hydrogens are merged with the water signal at 1.6 ppm.

To separate 1-octanol from the C_8-F-OH product, the mixture was distilled under reduced pressure (~3 mm Hg) at 50 ºC to remove the octanol. A viscous liquid with a palm yellow color was obtained as the residue after the distillation. The ^{1}H NMR spectrum shown in Figure 2.3 indicates the disappearance of the residual peak at 3.6 ppm, thus demonstrating the removal of 1-octanol from the C_8-F-OH sample. Consequently, the C_8-F-OH sample could be used in the anionic polymerization of ethylene oxide to produce *fbnios*. The same procedure was applied to prepare C_{12}-F-OH and the ^{1}H NMR spectra of Me-F-OH provided by OrMat and C_{12}-F-OH are presented in Appendix A as Figures A2.1 and A2.2, respectively.

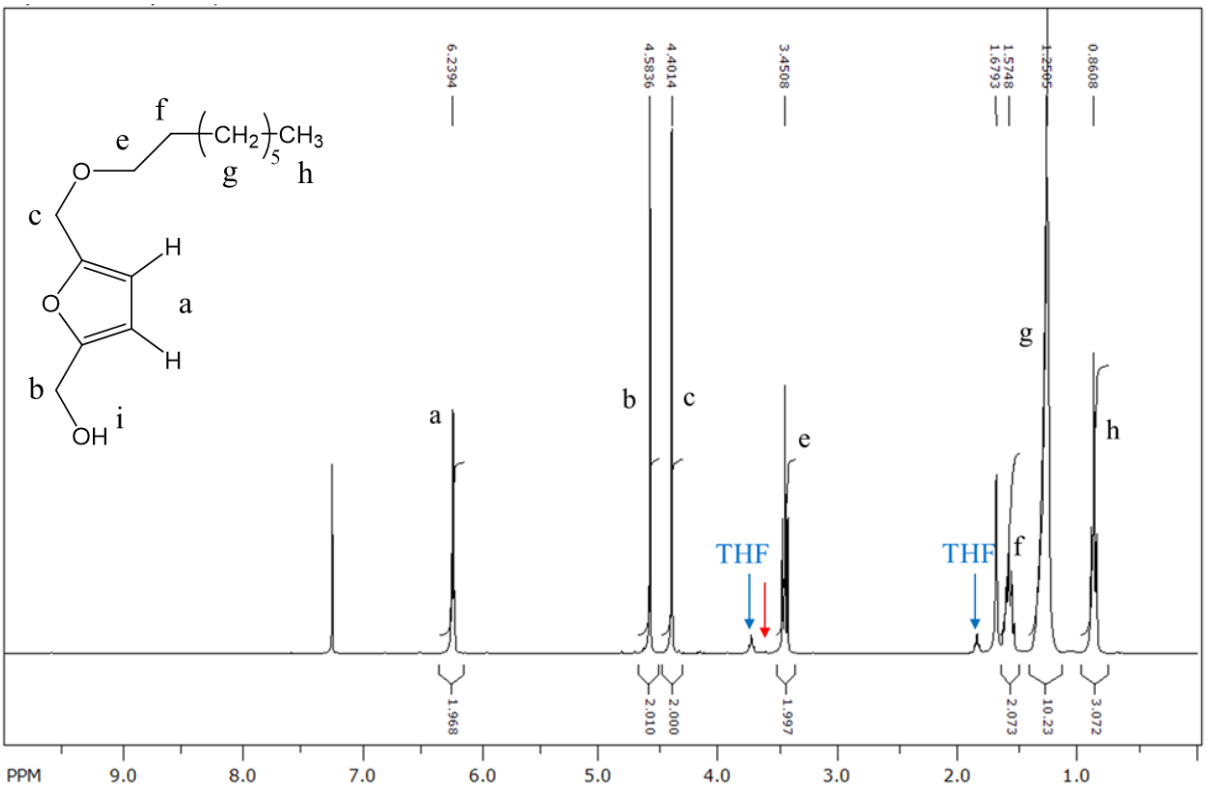

Figure 2.3. 300 MHz ^{1}H NMR spectrum of C_8-F-OH in chloroform-*d* after distillation: δ 6.2 (d, 2H), 4.6 (s, 2H), 4.4 (s, 2H), 3.5 (t, 2H), 1.6 (p, 2H), 1.3 (m, 10H), 0.9 (t, 3H). Residual solvent peaks are seen at 7.3 ppm for chloroform, 3.8 and 1.9 for THF, and 1.7 ppm for water.

2.5 Anionic Polymerization

Anionic polymerization of methylfurfuryl alcohol (Me-F-OH) and the alkyl furfuryl alcohols (C_x-F-OH) prepared by Williamson ether synthesis was conducted in a similar manner. The anionic polymerization of Me-F-OH was performed first to demonstrate that the ethoxylation of the furfuryl alcohol would yield Me-F-EO_y samples with narrow molecular weight distributions (MWD). The procedure was then applied to the C_x-F-OH samples, whose MWD was also characterized. Since the Me-F-EO_y samples were too water-soluble to exhibit any dispersing properties, the anionic polymerization of C_8-F-OH is described in more details, as this compound is more representative of an *fbnios*.

2.5.1 Apparatus Used for The Anionic Polymerization of Ethylene Oxide

Anionic polymerization requires that all chemicals and glassware be devoid of moisture. All chemicals were purified, and the glassware cleaned to remove impurities that could interfere with the polymerization. To this end, the distilled C_8-F-OH sample was desiccated in a vacuum oven for 12 h. The cleaned glass manifold and the ethoxylation and storage ampules shown in Figure 2.4 were dried in an oven at 80 ^oC for 24 h before being assembled as part of the high vacuum system used to conduct the polymerization.

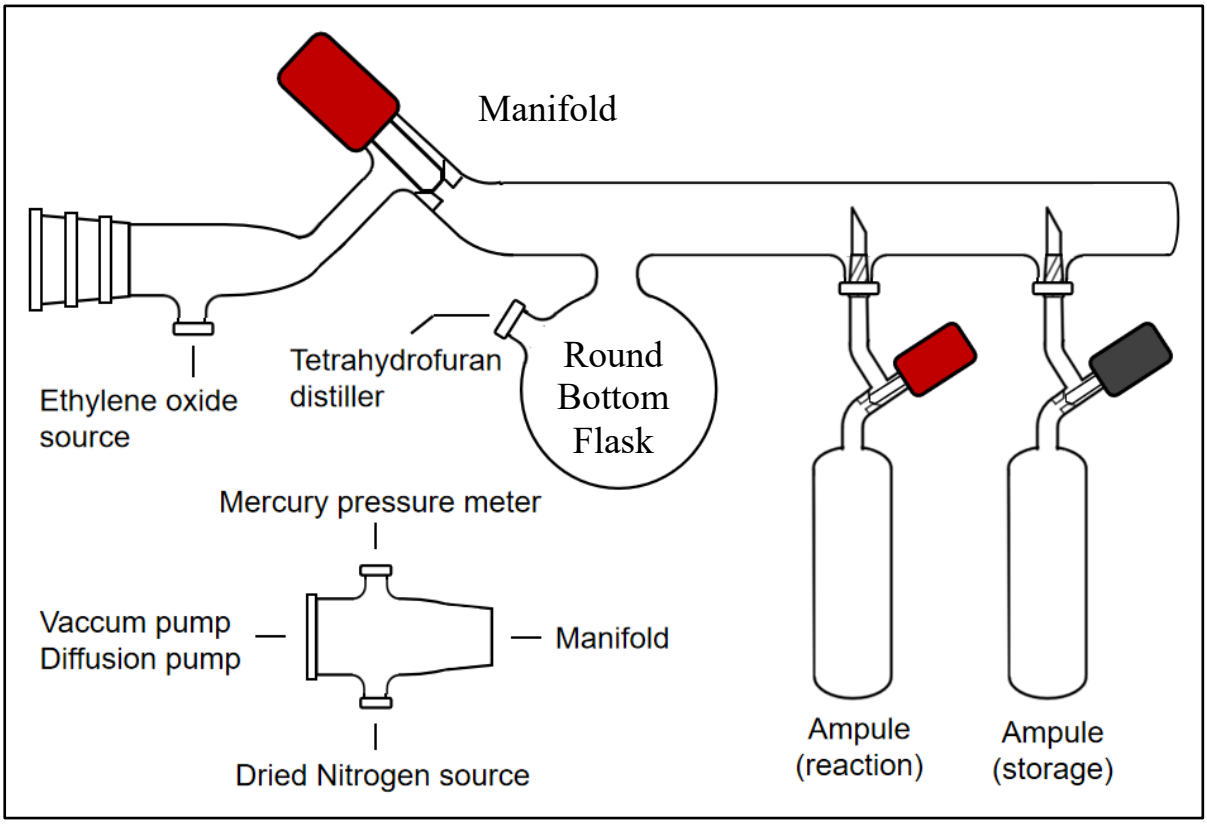

Figure 2.4. Schematic illustration of the apparatus used for the anionic polymerization of ethylene oxide.

The polymerization setup, succinctly described in Figure 2.4, included diffusion and rotary pumps in series, that were protected by a cold trap. A mercury manometer was used to monitor the pressure inside the system. An ethylene oxide tank and a THF still were connected

to the polymerization setup to supply monomer and distilled solvent, respectively. The entire system could be maintained under dry nitrogen or vacuum with the manifold. Two reaction ampules and two storage ampules were used to enable the production of two batches of *fbnios* with distinct degrees of polymerization in one operation.

After the apparatus was assembled, low vacuum was applied first with the rotary pump to the manifold and the two reaction ampules, before applying high vacuum with the diffusion pump. As the apparatus and the ampules were kept under high vacuum, they were flamed to remove residual moisture. The dried ampules were then sealed, and dry nitrogen was introduced into the manifold to restore the pressure before the reaction ampules could be removed from the manifold. Then two storage ampules were connected to the manifold and flame-dried under high vacuum through the same process.

2.5.2 Purification of Ethylene Oxide

After the storage ampules were dried, sealed, and removed from the manifold, the manifold was maintained under nitrogen atmosphere and an appropriate volume of degassed 1 M phenylmagnesium chloride (PMC) solution in MTHF (~ 1 mL for one gram of ethylene oxide to be dried) was introduced in the RBF of the manifold. In the meantime, the storage ampules were weighted before being connected back to the manifold. The vacuum was applied again to the manifold to remove the MTHF. PMC served as a strong drying agent scavenging water from ethylene oxide. After the MTHF had evaporated, the manifold was subjected to high vacuum and then sealed. Ethylene oxide from Praxair was introduced to condense in the RBF of the manifold in Figure 2.5, which was immersed in liquid nitrogen. The ethylene oxide in the RBF was subjected to a series of freeze-pump-thaw cycles, whereby the Dewar filled with liquid nitrogen was replaced by an ice-water bath to melt the ethylene oxide and allow it to mix with PMC with stirring. An ice-water bath was used to prevent the ethylene oxide from boiling off. After 5 min stirring, the mixture was frozen again with liquid nitrogen and maintained

under high vacuum for 5 min. Three freeze-pump-thaw cycles were applied. Then with the manifold sealed, the RBF was placed in an ice-water bath and the ethylene oxide was allowed to melt. The liquid ethylene oxide was stirred for 40 min before being transferred to the storage ampules, which had been kept under high vacuum. The bottom part of one of the storage ampules was immersed in liquid nitrogen and upon opening the ampule, ethylene oxide condensed in it. The first ampule was sealed, and the same operation was applied to the second storage ampule. While maintaining the manifold under a gentle flow of dry nitrogen, both storage ampules were replaced by the reaction ampules. The storage ampules were weighted again to determine the mass of ethylene oxide (m_{EO}) in each of them, as the weight of the empty ampules had been measured beforehand. The mass of C_8-F-OH ($m_{C8\text{-}F\text{-}OH}$) required to be added in the reaction ampules for a given degree of polymerization (y) was calculated by Eq. 2.1, where $M_{C8\text{-}F\text{-}OH}$ and M_{EO} are the molar mass of C_8-F-OH and ethylene oxide equal to 240 and 44 g/mol, respectively.

$$m_{C8-F-OH} = \frac{m_{EO}}{M_{EO}} \times \frac{1}{y} \times M_{C8-F-OH} \quad (2.1)$$

The density of C_8-F-OH was measured and found to be approximately 1 g/mL. The required volume of C_8-F-OH needed for the ethoxylation was measured with a syringe and it was transferred into the reaction ampules through a long needle, while keeping the reaction ampules under a gentle flow of dry nitrogen. An approximate 0.8:1 molar ratio of C_8-F-OH to potassium *tert*-pentoxide (PTP) was employed to minimize the addition of ethylene oxide onto PTP, while not interfering with the polymerization. The required volume of the PTP solution was introduced in the reaction ampules in the same manner as for the addition of C_8-F-OH. PTP is anticipated to be a stronger base than PTB, and therefore applied to minimize the side reaction identified in section 2.5.4.2.

2.5.3 Reaction Procedure

The anionic polymerization of ethylene oxide involved three stages: Initiation (deprotonation of the C_8-F-OH hydroxyl), propagation (successive attachment of ethylene oxide monomers), and termination (protonation of the living oligo(ethylene oxide) (OEO) chain).

2.5.3.1 Initiation

As indicated in Section 2.5.1, the amounts of C_8-F-OH and PTP added to the reaction ampules, where ethylene oxide would ultimately be transferred, depended on the exact mass of ethylene oxide transferred to the storage ampules. The reaction ampules were filled with the desired amounts of reactants (C_8-F-OH and PTP). Vacuum was applied and the manifold was isolated, before opening the valve connecting the manifold to the THF still via Teflon tubing. Distilled THF was pumped into the RBF by the pressure difference between the manifold and the THF still. The valve was closed after enough THF had been collected in the RBF of the manifold (ca. 25 mL per gram of C_8-F-OH). THF was then transferred into one of the cold reaction ampules, that had been immersed in liquid nitrogen. The ampule was sealed afterwards and THF was allowed to melt and dissolve C_8-F-OH and PTP. The same procedure was applied to the other reaction ampule and the solutions were stirred for 1 h to allow the initiation reaction shown in Scheme 2.3 to take place. This reaction generated a methoxide anion enabling the nucleophilic attack on either carbon of ethylene oxide.

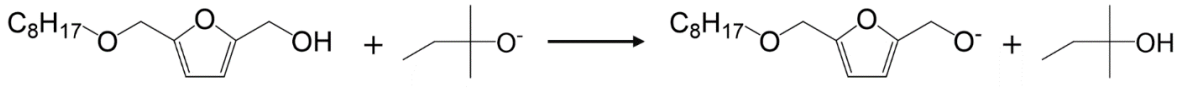

Scheme 2.4. Deprotonation of C_8-F-OH by potassium *tert*-pentoxide.

2.5.3.2 Propagation

After stirring for 1 h, most C_8-F-OH molecules were assumed to be deprotonated by PTP. One

of the two reaction ampules still attached to the manifold was sealed and replaced by a storage ampule containing the amount of ethylene oxide needed to conduct the polymerization in the remaining reaction ampule. The bottom of the reaction ampule was immersed in liquid nitrogen to freeze the solution in THF and high vacuum was applied, before the manifold was sealed again. The stopcocks of the reaction and storage ampules were opened to enable the transfer of ethylene oxide through the manifold from the storage ampule to the reaction ampule, that contained the deprotonated C_8-F-OH. Five minutes after the transfer of ethylene oxide was completed, the reaction ampule was sealed and the solid mixture was melted by replacing the Dewar filled with liquid nitrogen, in which the bottom of the reaction ampule was immersed, with a warm water bath. The reaction ampule was then placed in a silicone oil bath on a stir plate (300 rpm, 50 ºC) to start the propagation reaction as shown in Scheme 2.4. A reaction temperature of 50 ºC was selected to maximize the polymerization rate, while remaining well below the boiling point of THF (T_b = 66 ºC). The reaction was allowed to proceed for approximately 48 h. The same treatment was applied to the other pair of storage and reaction ampules, allowing 2 batches of product to be synthesized in a same experiment.

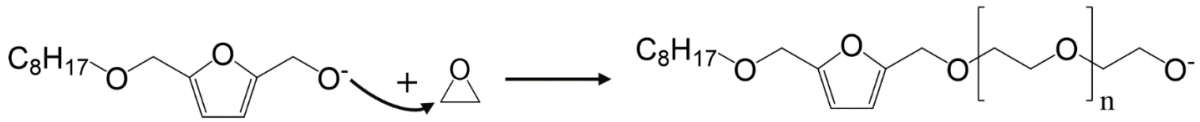

Scheme 2.5. Reaction scheme for living polymerization of ethylene oxide.

2.5.3.3 Termination

After 48 h, the polymerization at 50 ºC had consumed all the ethylene oxide. The reaction ampules were opened and Milli Q® water (3 mL for each gram of C_8-F-OH used) was added to the THF solution to terminate the polymerization as shown in Scheme 2.5. The mixture was left stirring for 15 min and acetic acid was introduced to complete the termination.

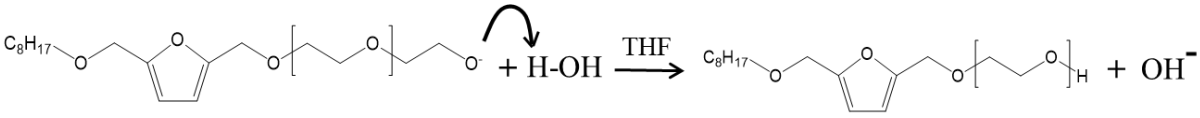

Scheme 2.6. Termination of the anionic polymerization of ethylene oxide by addition of Milli Q® water.

2.5.4 Purification and Separation of The Product

At this point, the polymerization product was obtained in a mixture of THF and water that also contained potassium ions, acetic acid, *tert*-pentanol, and residual C_x-F-OH. The same procedure described in detail for the purification of C_8-F-EO_y was applied to isolate the products.

2.5.4.1 Liquid-Liquid Extraction

Upon termination, the mixture in the reaction ampule was transferred to a 500 mL RBF. Most of the THF, acetic acid, and some of the water were removed on a rotary evaporator. A precipitate formed, which dissolved upon addition of dichloromethane (DCM). Since DCM is not miscible with water, the mixture was transferred to a separatory funnel to conduct a LLE between the aqueous solution and DCM. The extraction was repeated three times. For the first two extractions, equal amounts of aqueous solution saturated with sodium chloride (first extraction) or sodium carbonate (second extraction), 50 mL for each gram of precursor used, were mixed with the organic solution in DCM to remove potassium ions and acetic acid. A third extraction was done with a saturated sodium chloride aqueous solution and DCM, to scavenge residual ions while minimizing the amount of organic surfactant that would dissolve in the aqueous phase. Two batches of crude C_8-F-EO_y products with number-average degrees of polymerization ($DP_n = y$) of 4.5 and 11.5 were obtained as orange viscous liquids. Each of these crude products were further separated into two samples with distinct DP_n through column chromatography, to make their molecular weight distribution narrower.

2.5.4.2 Column Chromatography

After loading the crude product on a silica gel column, an ether wash followed by an ethyl acetate wash were applied first, to flush out hydrophobic impurities from the product. The elution solvent was then changed to a 50:50 (v/v) ethyl acetate:acetone mixture for the elution of *fbnios*. The chain length distribution of the C_8-F-EO_y samples prepared by anionic polymerization follows a Poisson distribution,[44,45] thus the more hydrophobic *fbnios* molecules with a shorter OEO chain eluted from the silica gel column before those with a longer OEO chain. Consequently, silica gel column chromatography enabled the fractionation of the C_8-F-$EO_{4.5}$ and C_8-F-$EO_{11.5}$ samples into four *fbnios* having a DP_n of 3, 6, 10, and 14. ^{1}H NMR spectra of C_8-F-EO_{14} and C_{12}-F-EO_{23} are shown in Figures 2.5 and 2.6. ^{1}H NMR spectra for Me-F-EO_y and other C_x-F-EO_y samples prepared in this thesis are presented in Figures A2.3 – S2.20 in Appendix A.

According to the NMR spectra, the only impurity present in the *fbnios* samples was identified by its peak at 1.0 ppm, and corresponded to OEO chains initiated by *tert*-pentoxide used to deprotonate the alkylfurfuryl alcohol according to the mechanism shown in Scheme 2.7.

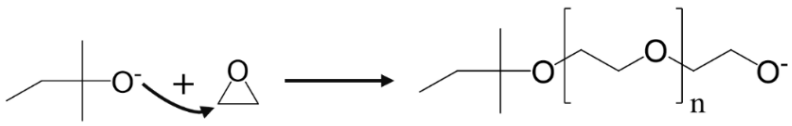

Scheme 2.7. Side reaction encountered during the anionic polymerization yielding *tert*-pentoxide modified OEO.

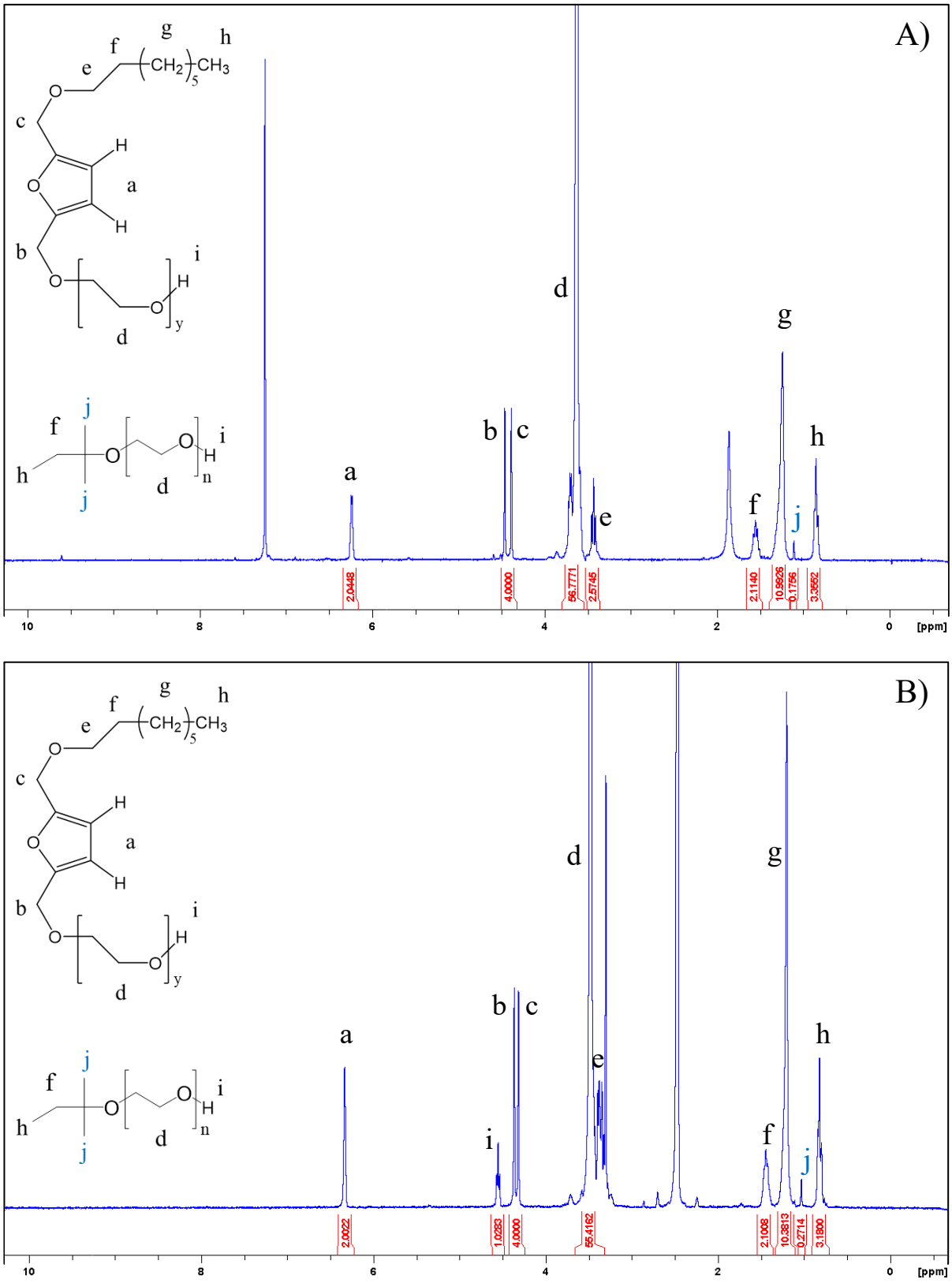

Figure 2.5. 300 MHz ^{1}H NMR spectra of A) C_8-F-EO_{14} in chloroform-*d*: δ 6.2 (d, 2H), 4.5 (s, 2H), 4.4 (s, 2H), 3.6 (m, 56H), 3.4 (t, 2H), 1.6 (p, 2H), 1.3 (m, 10H), 1.1 (s, 6H), 0.9 (t, 3H). Residual solvent peaks are found at 7.3 ppm for chloroform and 1.9 ppm for water; B) C_8-F-

EO_{14} in d_6-DMSO: δ 6.3 (d, 2H), 4.6 (t, 1H), 4.4 (s, 2H), 4.3 (s,2H), 3.5 (m, 56H), 3.3 (t, 2H), 1.4 (p, 2H), 1.2 (m, 10H), 1.0 (s, 6H), 0.8 (t, 3H). Residual solvent peaks are found at 2.5 ppm for chloroform and 3.3 ppm for water.

Since the rate-limiting step in anionic polymerization is the propagation step, the average OEO chains initiated by *tert*-pentoxide were expected to have the same DP_n as the *fbnios*. The DP_n for the OEO segments was determined from Equation 2.2 by integration of the signal from the *b* and *c* protons of the two furan-methylene groups, the *j* protons of the pentoxide group, and the *d* protons of the EO chain in the ^{1}H NMR spectra of the *fbnios* samples in chloroform shown in Figure 2.5. Because each ethylene oxide unit contains 4 hydrogen atoms, and the two methylene groups on either side of the furan ring contribute 4 hydrogen atoms, the number of EO units was calculated through Equation 2.2 from the ratio of the number of EO units and the total number of chain ends.

$$DP_n = \frac{\frac{d}{4}}{\frac{b+c}{4}+\frac{j}{8}} \tag{2.2}$$

The DP_n of the *fbnios* samples, calculated according to Equation 2.2, could be used to determine their HLB with Equation 1.1. The DP_n and HLB values of the *fbnios* samples are summarized in Section 2.7. ^{1}H NMR analysis indicates that all samples display similar signals at the expected chemical shifts based on the chemical structure of the C_8-F-EO_y samples. Integration of the NMR signals demonstrated that the C_8-F-EO_y samples contained less than 8% of OEO chains initiated by *tert*-pentoxide.

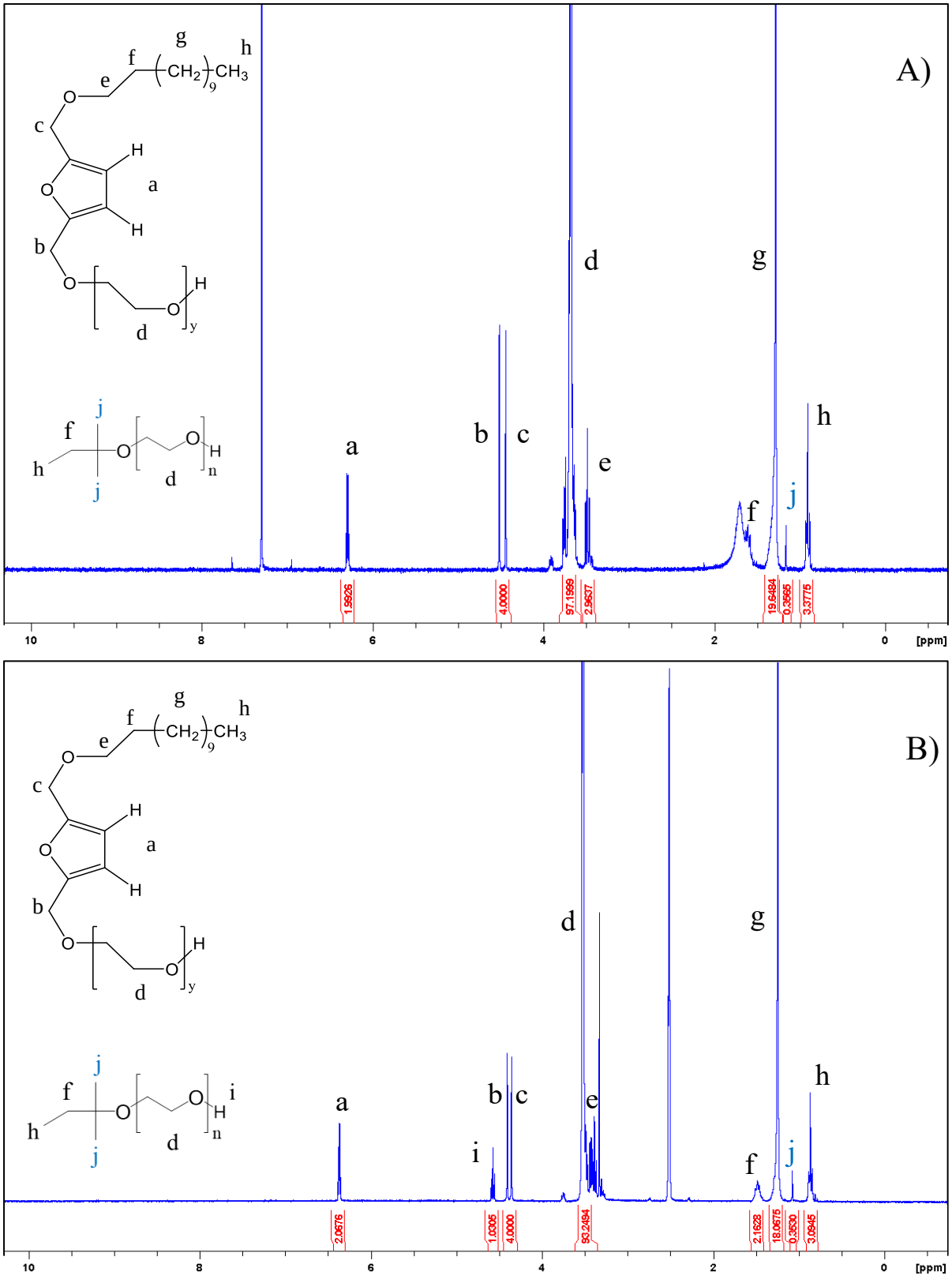

Figure 2.6. 300 MHz ^{1}H NMR spectra of A) C_{12}-F-EO_{23} in chloroform-*d*: δ 6.2 (d, 2H), 4.5 (s, 2H), 4.4 (s, 2H), 3.6 (m, 92H), 3.4 (t, 2H), 1.6 (p, 2H), 1.3 (m, 18H), 1.1 (s, 6H), 0.9 (t, 3H). Residual solvent peaks are found at 7.3 ppm for chloroform and 1.6 ppm for water; B) C_{12}-F-

EO_{23} in d_6-DMSO: δ 6.3 (d, 2H), 4.6 (t, 1H), 4.4 (s, 2H), 4.3 (s,2H), 3.5 (m, 92H), 3.3 (t, 2H), 1.4 (p, 2H), 1.2 (m, 18H), 1.0 (s, 6H), 0.8 (t, 3H). Residual solvent peaks are found at 2.5 ppm for chloroform and 3.3 ppm for water.

2.6 Characterization of *fbnios*

The DP_n values and molecular weight distribution (MWD) of the Me-F-EO_y, C_8-F-EO_y, and C_{12}-F-EO_y samples obtained by ^{1}H NMR were further confirmed by gel permeation chromatography (GPC) and matrix-assisted laser desorption ionization-time of flight mass spectroscopy (MALDI-ToF MS).

2.6.1 Gel Permeation Chromatography

The GPC traces obtained with the DRI detector for the C_8-F-EO_{14} and C_{12}-F-EO_{23} samples are given as a function of elution volume (V_e) in Figure 2.7. The GPC traces of the THF used to dissolve the samples, the Me-F-EO_y samples, and the other *fbnios* samples are provided in Appendix A as Figures A2.21 – 2.31.

The main signal in the plots represents the C_8-F-EO_{14} and C_{12}-F-EO_{23} samples, while the solvent peaks appear at 19.1 mL and higher elution volumes. A calibration curve was generated with PEO standards of narrow MWD, with molecular weights ranging from 150 to 34,800 Da. It was applied to analyze the GPC traces obtained with the Me-F-EO_y, C_8-F-EO_y, and C_{12}-F-EO_y samples. GPC analysis yielded the M_n, M_w, and PDI of each sample. In turn, DP_n was determined by subtracting the molar mass of the Me-F or C_x-F part from M_n and dividing the result of this subtraction by the molar mass of EO (= 44 g/mol). The parameters describing the MWD of Me-F-EO_y and the *fbnios* obtained by GPC analysis are presented in Section 2.7.

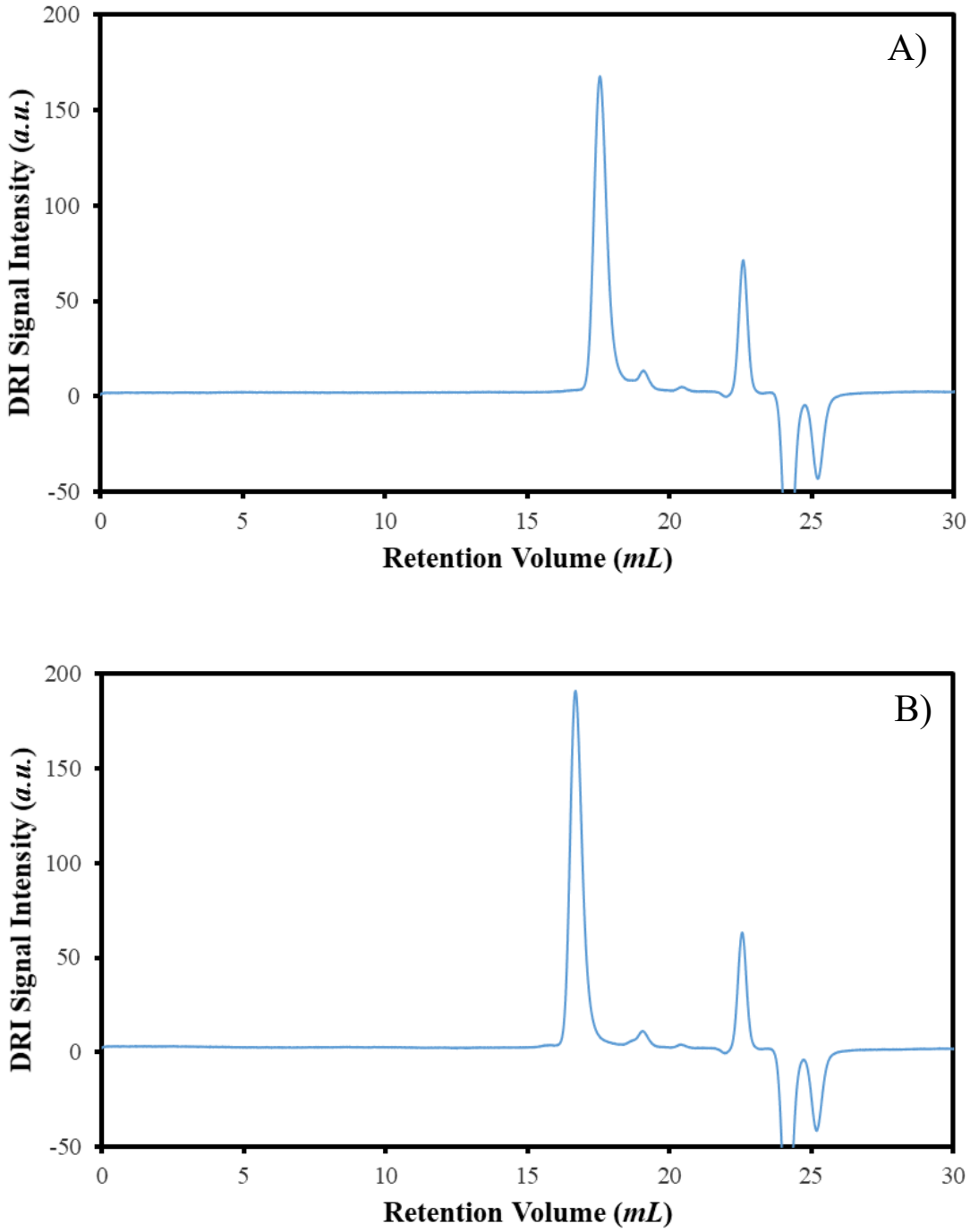

Figure 2.7. GPC traces obtained with the DRI detector for A) C_8-F-EO_{14} and B) C_{12}-F-EO_{23}.

2.6.2 Matrix-Assisted Laser Desorption Ionization-Time of Flight Mass Spectroscopy

The MWD of the Me-F-EO_y and *fbnios* samples was also characterized by MALDI-ToF MS. The samples were dissolved in water to generate a 4 mg/mL solution. A volume (10 μL) of the

sample solution was mixed with 5 µL of a 10 mg/mL LiCl water solution and 15 µL of a 10 mg/mL dithranol solution in THF. The mixture was loaded onto a metal sample plate.[46] A blank was also prepared for comparison by mixing 10 µL of MilliQ water with 5 µL of a 10 mg/mL LiCl water solution and 15 µL of a 10 mg/mL dithranol solution in THF. The resulting mass spectra of C_8-F-EO_{14} and C_{12}-F-EO_{23} are shown in Figure 2.8. The mass spectra obtained with the blank comparison and other samples are included in Appendix A as Figures A2.32 – 2.40.

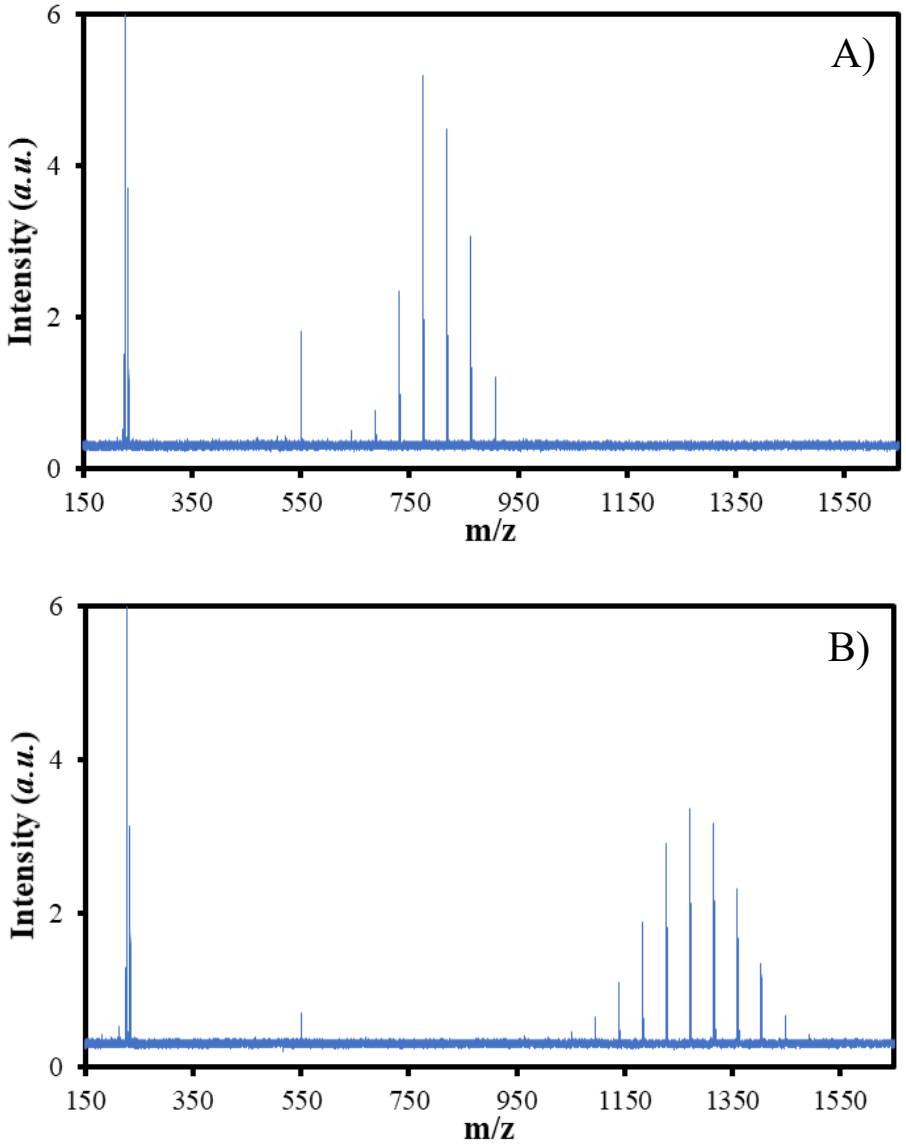

Figure 2.8. MALDI-ToF MS spectra for A) C_8-F-EO_{14} and B) C_{12}-F-EO_{23}. The *m/z* ratio refers to the mass to charge ratio. The signal peak at *m/z* = 550, also observed in a blank sample, was generated by an unknown chemical.

The intensities of the peaks refer to the relative abundance of the corresponding species with different OEO chain lengths in the C_8-F-EO_{14} and C_{12}-F-EO_{23} samples. All detected species are found to contain only 1 positive charge. Therefore, their *m/z* ratio is equal to the sum of their molar mass and the molar mass of $^7Li^+$. The MWD of the Me-F-EO_y and *fbnios* samples could thus be directly obtained.[47] The MALDI-ToF-MS results were analyzed to obtain the DP_n and PDI of all Me-F-EO_y and *fbnios* samples and they have been summarized in Tables 2.1 and 2.2, which are discussed in the following section.

2.7 Summary and Discussion

A synthetic route has been proposed to prepare *fbnios* from the 2,5-*bis*HMF precursor. The successful synthesis of the C_8-F-OH and C_{12}-F-OH intermediates was confirmed through ^1H NMR analysis of the synthesized compounds. The validity of the anionic polymerization procedure to obtain *fbnios* with a narrow molecular weight distribution was verified first by ethoxylating Me-F-OH. The Me-F-EO_y samples, that were generated in this thesis, were characterized by NMR, GPC, and MALDI-ToF MS. The results of these analyses demonstrated the successful synthesis of a series of Me-F-EO_y samples, where their preparation allowed control over the DP_n of the OEO chain and resulted in low PDI and low impurity content (in terms of OEO chains initiated by *tert*-butoxide groups), as shown in Table 2.1. The Me-F-EO_3 and Me-F-EO_{10} samples were only purified by LLE and therefore have a relatively large PDI.

Having established a effective synthetic procedure to obtain the Me-F-EO_y samples, C_8-F-OH and C_{12}-F-OH were synthesized and deprotonated to initiate the anionic polymerization with ethylene oxide. A series of C_8-F-EO_y and C_{12}-F-EO_y samples with a low PDI were successfully synthesized. The appearance of the samples ranged from palm yellow viscous liquids to white solids, depending on the average length of their OEO moiety. The only impurity in the C_8-F-EO_y and C_{12}-F-EO_y samples determined by ^1H NMR analysis was *tert*-

pentoxide-initiated OEO chains, whose content was less than 8%, as shown in Table 2.2 for each sample except for C_{12}-F-EO_8 and C_{12}-F-EO_{13}, which contained larger amounts of impurity for currently unknown reasons. The results obtained from the ^{1}H NMR, GPC, and MALDI-ToF MS analysis for all the Me-F-EO_y, C_8-F-EO_y and C_{12}-F-EO_y samples are presented in Tables 2.1 and 2.2. The HLB of all samples were also calculated and included in the tables.

In MALDI-ToF MS measurements, *tert*-pentoxide-modified OEO chains were only observed in the C_{12}-F-EO_8 and C_{12}-F-EO_{13} samples and resulted in a very weak signal. This suggests that the affinity of *tert*-butoxide and *tert*-pentoxide-modified OEOs to Li^+ ion is significantly less than for the Me-F-EO_y and *fbnios* samples, likely due to the absence of a furan ring. Consequently, the *tert*-pentoxide-modified OEOs, with a molecular weight different from Me-F-EO_y or *fbnios* in the same sample, did not contribute to the MWD of the sample probed by the MALDI-ToF MS. The MALDI-ToF MS analysis thus yielded smaller PDI values as compared to GPC, and this difference is more pronounced for the C_{12}-F-EO_8 and C_{12}-F-EO_{13} samples, which have a larger impurity content. NMR and GPC analysis demonstrated the presence of Me-F-EO_1 and Me-F-EO_2 species in the Me-F-EO_3 sample (see Figure A2.20), which is expected according to the Poisson distribution theory. However, both species bear extremely short OEO chains and thus lack the ability to form a complex with lithium ions. As a result, Me-F-EO_1 and Me-F-EO_2 molecules were not detected by the MALDI-ToF MS and the DP_n for Me-F-EO_3 appears to be significantly larger in the MALDI-ToF MS analysis.

Table 2.2 shows that all *fbnios* samples had a narrow MWD. Good agreement was found between the DP_n values obtained by NMR and MALDI-ToF MS. The amphiphilic properties of these *fbnios* were further characterized in Chapter 3 by fluorescence and surface tension measurements to determine their CMC, efficiency, and effectiveness.

Table 2.1. Summary of the impurity content (in terms of OEO chains initiated by TPO), HLB, DP_n and PDI values obtained by different techniques for the Me-F-EO_y samples.

	Impurity content (molar%)	DP_n (NMR)	DP_n (GPC)	DP_n (MALDI)	PDI (GPC)	PDI (MALDI)	HLB
Me-F-EO_3	1.2	2.6	1.6	5.4	1.22	1.02	19.9
Me-F-EO_6	4.2	6.2	5.6	6.5	1.03	1.01	19.9
Me-F-EO_8	3.1	8.4	7.7	8.9	1.02	1.01	19.9
Me-F-EO_{10}	5.9	10.3	9.6	13.0	1.08	1.06	20.0

Table 2.2. Summary of the impurity content (in terms of OEO chains initiated by TPO), HLB, DP_n and PDI values obtained by different techniques for the C_8-F-EO_y and C_{12}-F-EO_y samples.

	Impurity content (molar%)	DP_n (NMR)	DP_n (GPC)	DP_n (MALDI)	PDI (GPC)	PDI (MALDI)	HLB
C_8-F-EO_3	5.9	2.8	3.2	3.1	1.04	1.004	13.9
C_8-F-EO_6	6.1	5.7	5.1	5.8	1.02	1.015	15.5
C_8-F-EO_{10}	5.1	10.4	7.0	9.0	1.02	1.006	16.7
C_8-F-EO_{14}	2.8	13.8	9.5	12.6	1.01	1.005	17.4
C_{12}-F-EO_8	20.4	7.7	5.0	8.5	1.08	1.027	14.8
C_{12}-F-EO_{13}	20.4	12.7	7.1	12.0	1.07	1.012	16.1
C_{12}-F-EO_{18}	5.7	18.1	12.2	19.6	1.01	1.006	16.9
C_{12}-F-EO_{23}	5.6	23.0	14.0	23.3	1.01	1.004	17.3

Chapter 3 - Surface Tension and CMC Measurements on *Fbnios*

3.1 Introduction

Surfactants are usually described in terms of three parameters: Their critical micelle concentration (CMC), the negative logarithm in base 10 of the surfactant concentration that reduces the surface tension of water by 20 $mN.m^{-1}$ (also referred to as their efficiency or pC_{20} value), and their effectiveness, which is the maximum decrease in surface tension that can be achieved by the surfactant. These parameters were determined for the *fbnios* synthesized in Chapter 2 through a combination of surface tension and steady-state fluorescence measurements. The results of these experiments are now described.

3.2 Experimental

Surface Tension: All surface tension measurements were conducted at room temperature (~25 ^{o}C) with a DuNuoy ring tensiometer from Central Scientific Co., equipped with a platinum-iridium ring having a ring to wire radius ratio of 51.179. The surface tension measured by the tensiometer was corrected according to the procedure recommended by the manufacturer. More information about the surface tension measurements can be found in an earlier publication.[48]

Steady-state fluorescence: The steady-state fluorescence (SSF) spectra of pyrene dissolved in aqueous solutions of *fbnios* were acquired with a Horiba QM-400 spectrofluorometer equipped with a xenon arc lamp. The solutions were irradiated with an excitation wavelength of 336 nm, using an excitation slit width of 5 nm. The SSF spectra were acquired from 350 to 600 nm with a 1 nm emission monochromator slit width. The I_1/I_3 ratio, used to assess the polarity of the environment probed by pyrene,[39] was obtained by taking the fluorescence intensity ratio of the

first peak (I_1) over the third peak (I_3) in the SSF spectrum of pyrene. Similarly, the fluorescence intensity ratio (I_E/I_M) of the excimer over the monomer was obtained by integrating the area under the SSF spectrum centered at the wavelength of the first peak in the spectrum of the pyrene monomer from $\lambda_1 - 3$ to $\lambda_1 + 3$ nm, where λ_1 corresponds to the 0-0 transition of pyrene, and from 500 to 530 nm for the excimer to yield I_M and I_E, respectively.

Correction of fluorescence spectra: For some *fbnios*, distortions in the fluorescence spectra of pyrene were observed at high surfactant concentration (see Figure 3.1A for C_{12}-F-EO_{13}). These distortions were induced by the intrinsic fluorescence of some surfactants (see trace *a* in Figure 3.1A). As the surfactant concentration was decreased from 61.6 mM to 6.1 and 0.0067 mM, the expected spectral feature of the fluorescence spectrum of pyrene were recovered as shown in Figures 3.1D – F. Since the intrinsic fluorescence of some surfactants covered the entire wavelength range of the pyrene fluorescence, it would affect the determination of the I_1/I_3 and I_E/I_M ratios of pyrene. Consequently, the fluorescence spectra of the aqueous *fbnios* solutions containing 5×10^{-7} M pyrene were corrected by subtracting trace *a* for the fluorescence of C_{12}-F-EO_{13} in Figure 3.1A, after normalization of trace *a* to the value of the fluorescence intensity of pyrene averaged from 585 to 600 nm. The corrected fluorescence spectra obtained through this procedure are shown in Figures 3.1D – F and show the spectral features expected from a pyrene solution.

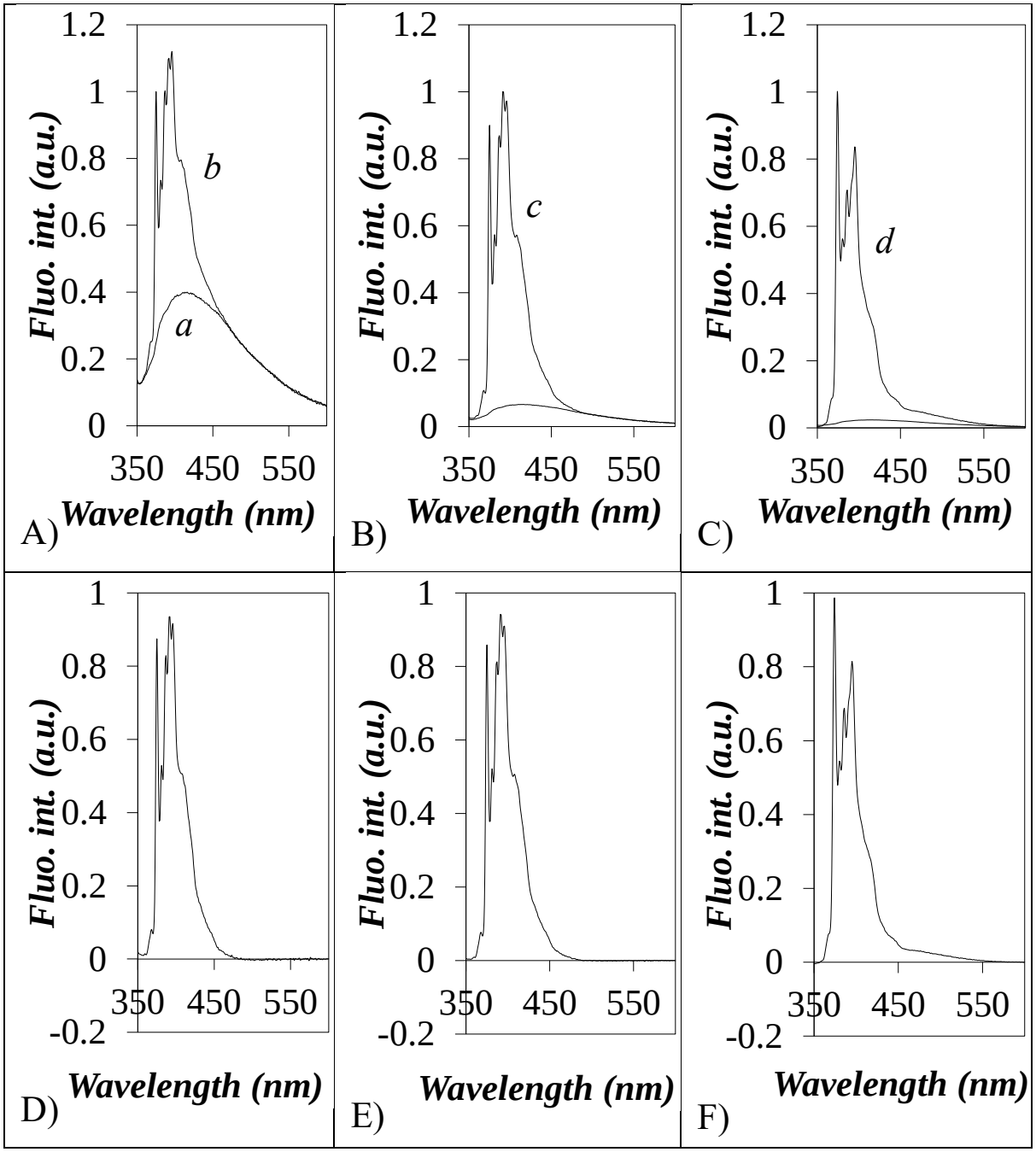

Figure 3.1. Fluorescence spectra of A) 61.6 mM C_{12}-F-EO_{13} aqueous solution with no pyrene (trace *a*) and with 5×10^{-7} M pyrene (trace *b*); B) 6.1 mM C_{12}-F-EO_{13} aqueous solution with 5×10^{-7} M pyrene (trace *c*) with trace *a* normalized at 600 nm; C) 0.067 mM C_{12}-F-EO_{13} aqueous solution with 5×10^{-7} M pyrene (trace *d*) with trace *a* normalized at 600 nm. Corrected fluorescence spectra of D) 61.6 mM, E) 6.13 mM, and F) 0.067 mM C_{12}-F-EO_{13} aqueous solutions with 5×10^{-7} M pyrene after subtraction of the normalized trace *a*.

When a correction appeared to be necessary, particularly at high surfactant concentrations,

the same trace *a* was used to apply this correction to all *fbnios* solution that required a correction, since all *fbnios* molecules consist of an alkyl chain, a furan ring, and an OEO chain, and the fluorescence generated by all *fbnios* molecules was expected to be similar. In particular, this correction was applied to all spectra obtained with aqueous solutions of C_8-F-EO_{10}, C_{12}-F-EO_8, and C_{12}-F-EO_{13}. The corrected spectra were used to determine the I_1/I_3 and I_E/I_M ratios, that served to assess whether pyrene was located in either water or the hydrophobic interior of the *fnios* micelles.

3.3 Results

3.3.1 Surface Tension Measurements

A dilute (5×10^{-7} M) stock solution of pyrene was prepared in water. The *fbnios* samples synthesized in Chapter 2 were weighed and mixed with the pyrene stock solution to generate 6 mL of a 0.1 M *fbnios* aqueous solution, so that the same *fbnios* solutions could be used in both the surface tension and fluorescence measurements. The surface tension of this solution was measured in triplicate while it was kept in the dark, to minimize exposure of pyrene to light and its potential degradation. The solution was then split in two parts, keeping 2 mL of the solution in the dark to conduct fluorescence measurements and using the other 4 mL to prepare a more dilute *fbnios* solution by mixing it with the 5×10^{-7} M pyrene stock solution. Each diluted *fbnios* aqueous solution was stored in the dark and its surface tension was measured in triplicate. This procedure ensured that the same *fbnios* solutions were used for the surface tension and fluorescence measurements, which enabled easier comparison of the results obtained from both characterization methods. Moreover, since the pyrene concentration is almost negligible, the presence of pyrene could not affect the surface tension of the *fbnios* solutions. The surface tension of the *fbnios* samples prepared in Chapter 2 were plotted in Figure 3.2 as a function of *fbnios* concentration.

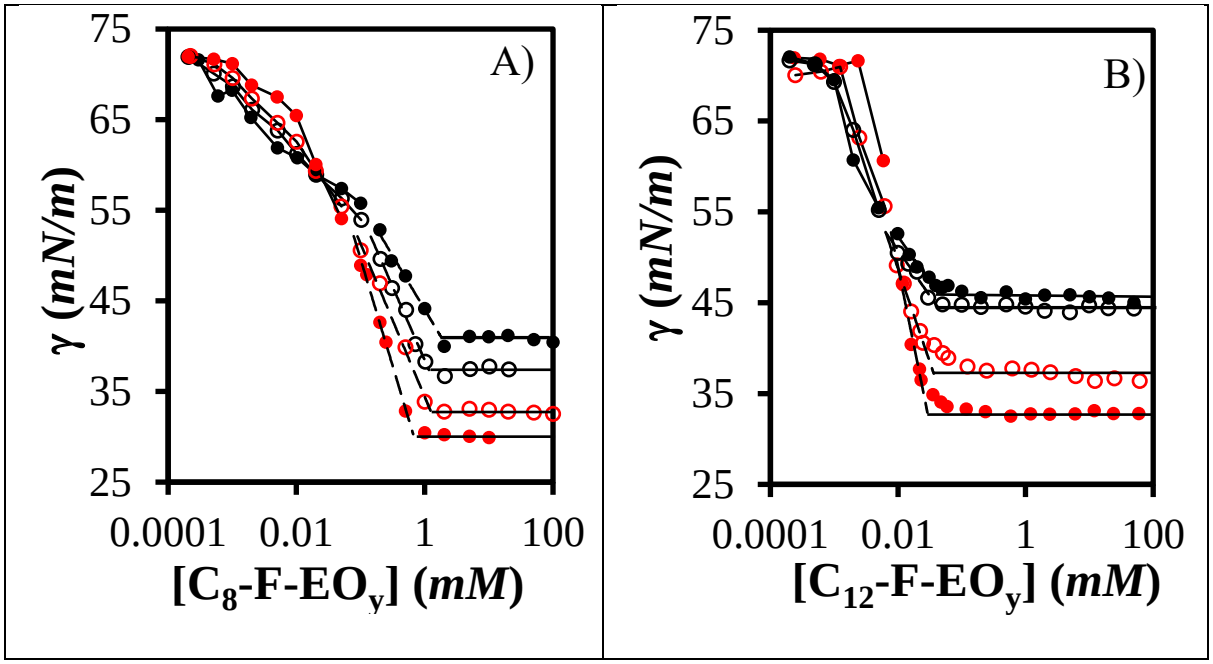

Figure 3.2. Plot of surface tension (γ) as a function of *fbnios* concentration for aqueous solutions of A) (●) C_8-F-EO_3, (○) C_8-F-EO_6, (○) C_8-F-EO_{10}, and (●) C_8-F-EO_{14} and B) (●) C_{12}-F-EO_8, (○) C_{12}-F-EO_{13}, (○) C_{12}-F-EO_{18}, and (●) C_{12}-F-EO_{23}.

The profiles shown in Figure 3.2 matched perfectly those expected for a typical surfactant shown in Figure 1.5. Starting with the surface tension of water (γ_{water} = 72 mN/m at 25 °C), an increase in the *fbnios* concentration led to a precipitous decrease in surface tension (γ) of the *fbnios* aqueous solutions until a clear break point was reached, that corresponded to the CMC of the *fbnios*. The surface tension of the *fbnios* aqueous solutions remained constant for *fbnios* concentrations greater than the CMC, at which point any increase in surfactant concentration resulted in the formation of more micelles. In Figure 3.2B, C_{12}-F-EO_8 and C_{12}-F-EO_{13} were found to show a transition that was not as pronounced at the CMC instead of the clear break point obtained for all other samples. This might be a consequence of the relatively large content of *tert*-pentoxide-modified OEO present in both samples, which must have a different CMC and thus affect the surface tension profiles.

The CMC, efficiency, and effectiveness of each *fbnios* sample were obtained from

Figure 3.2 and they are listed in Table 3.1, along with the HLB of the *fbnios* calculated with Equation 1.1. For the same *fbnios* series, the results shown in Table 3.1 demonstrate the strong relationship that exists between the HLB and the behavior of that *fbnios* series. However, for the same HLB, the CMC of the C_8-F-EO_y surfactants was found to be 20-to-30 times larger than the CMC of the C_{12}-F-EO_y surfactants, the efficiency of the C_8-F-EO_y surfactants was about 2-to-3 times smaller than that of the C_{12}-F-EO_y surfactants, and the effectiveness of the C_8-F-EO_y surfactants was slightly larger than that of the C_{12}-F-EO_y surfactants.

As shown in Table 3.1, the CMC increased with increasing HLB for a same series of *fbnios* samples. Trends similar to those shown in Figure 3.2 have also been observed for the Brij and Triton X family surfactants, whose chemical structures are shown in Figure 3.3. It can be seen that these surfactants are made of a hydrophobic group modified with an OEO chain. Their structure is thus similar to that of the *fbnios*. The CMCs of the Brij and Triton X family surfactants and *fbnios* were plotted against their HLB in Figure 3.4A, where the increase of CMC with HLB is illustrated.[49,50]

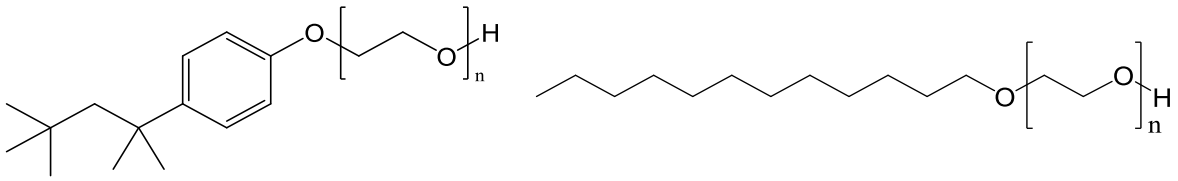

Figure 3.3. Chemical structure of the A) Triton X and B) Brij family surfactants.

Table 3.1. CMC, efficiency, and effectiveness of the *fbnios* samples.

Sample	HLB	CMC (mM)	Efficiency	Effectiveness (mN/m)
C_8-F-EO_3	13.9	0.67 ± 0.02	1.10 ± 0.06	41.83 ± 0.20
C_8-F-EO_6	15.5	1.24 ± 0.06	1.04 ± 0.07	39.18 ± 0.19
C_8-F-EO_{10}	16.7	1.17 ± 0.04	0.84 ± 0.06	34.66 ± 0.39
C_8-F-EO_{14}	17.4	1.89 ± 0.13	0.67 ± 0.08	31.24 ± 0.43
C_{12}-F-EO_8	14.8	0.029 ± 0.009	2.09 ± 0.87	39.13 ± 0.22
C_{12}-F-EO_{13}	16.1	0.036 ± 0.004	2.16 ± 0.48	34.81 ± 0.57
C_{12}-F-EO_{18}	16.9	0.042 ± 0.016	2.12 ± 0.41	27.49 ± 0.29
C_{12}-F-EO_{23}	17.3	0.044 ± 0.013	1.97 ± 0.29	26.00 ± 0.58

Figure 3.4A illustrates that the range of CMCs obtained with the *fbnios* covers handily the range of CMCs obtained for the Brij and Triton X surfactants, also given in the figure. It suggests that the modular chemical structure of the *fbnios* can be adjusted to cover a wide range of CMCs, that should include the range of CMCs obtained for the majority of other families of surfactants in use today.

The efficiency, the effectiveness, and the surface excess (Γ_i, obtained from the slope of the linear region of the *γ-vs*-[*fbnios*] plots just before the CMC in Figure 3.2) increased for decreasing EO_y lengths. The efficiency and effectiveness of *fbnios* were plotted with their error bars against their HLB in Figure 3.4B. The C_8-F-EO_y surfactants were found to have a lower efficiency and a higher effectiveness than the C_{12}-F-EO_y surfactants. G_i was obtained by applying Equation 3.1, where R is the ideal gas constant equal to 8.3145 $J \cdot K^{-1} \cdot mol^{-1}$, T is the absolute temperature in Kelvin, and [*fbnios*] is expressed in mol/L.

$$\Gamma_i = -\frac{1}{4.605RT} \times \frac{d\gamma}{d\, log_{10}[fbnios]} \qquad (3.1)$$

The area-per-molecule (A^{Γ}) expressed in m^2 could be derived from Equation 3.2, where

N_A is Avogadro's constant. The radius (R_{fbnios}) of the cross section of the head group of the *fbnios* was then determined and it is plotted in Figure 3.5 as a function of the DP of the OEO block.

$$A^{\Gamma} = \frac{1}{\Gamma_i \times N_A} \tag{3.2}$$

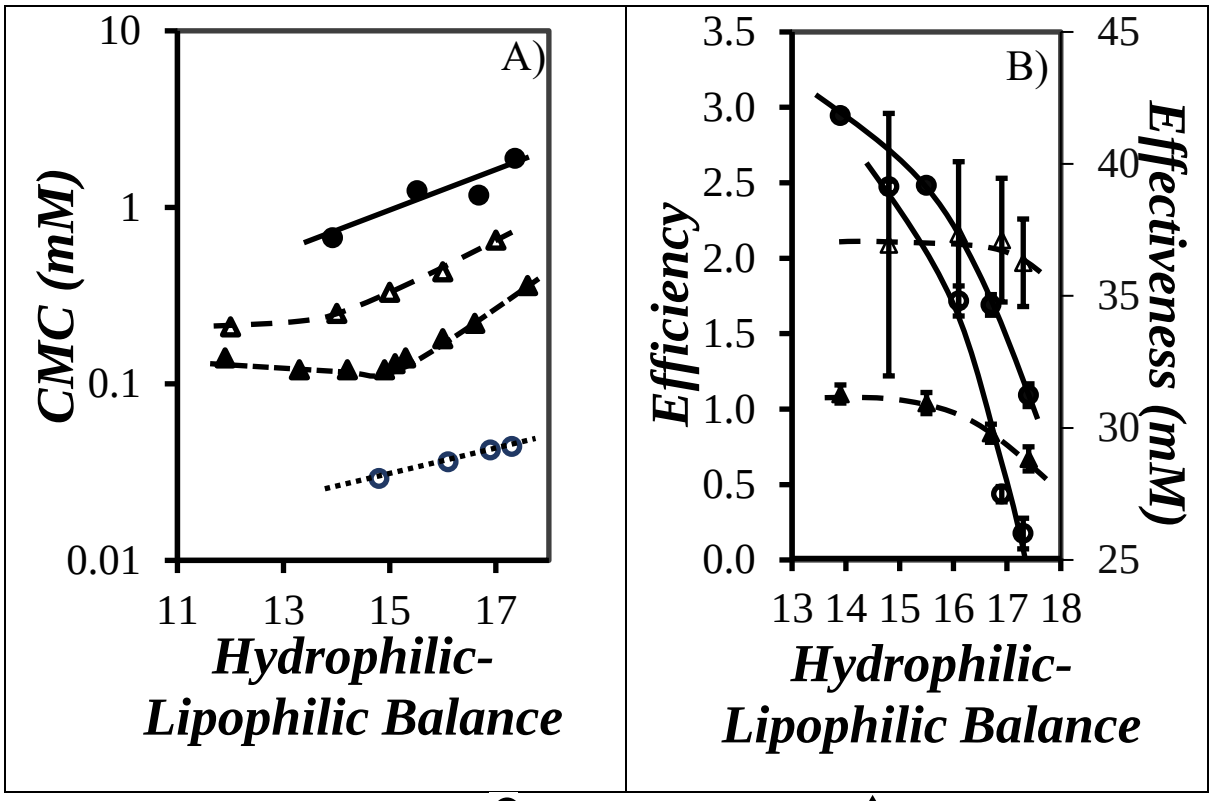

Figure 3.4. Plots of A) the CMC of (○) the C_{12}-F-EO_y series, (△) the Triton X surfactant family, (▲) the Brij surfactant family, and (●) the C_8-F-EO_y series, and B) (△,▲) the efficiency and (○,●) effectiveness of the (hollow) C_{12}-F-EO_y and (filled) C_8-F-EO_y series as a function of their HLB.

Figure 3.5 indicates that as the DP of the OEO block of the *fbnios* increases, so does R_{fbnios}, as expected. Except for the C_{12}-F-EO_8 and C_{12}-F-EO_{13} samples, which had a higher content of impurities, all other *fbnios* yielded R_{fbnios} values that clustered around a straight line regardless of whether they were prepared with a C8 or C12 alkyl group. This result suggested that the area

generated at the air-water interface by the OEO block of the *fbnios* is independent of the alkyl group used to prepare the *fbnios*.

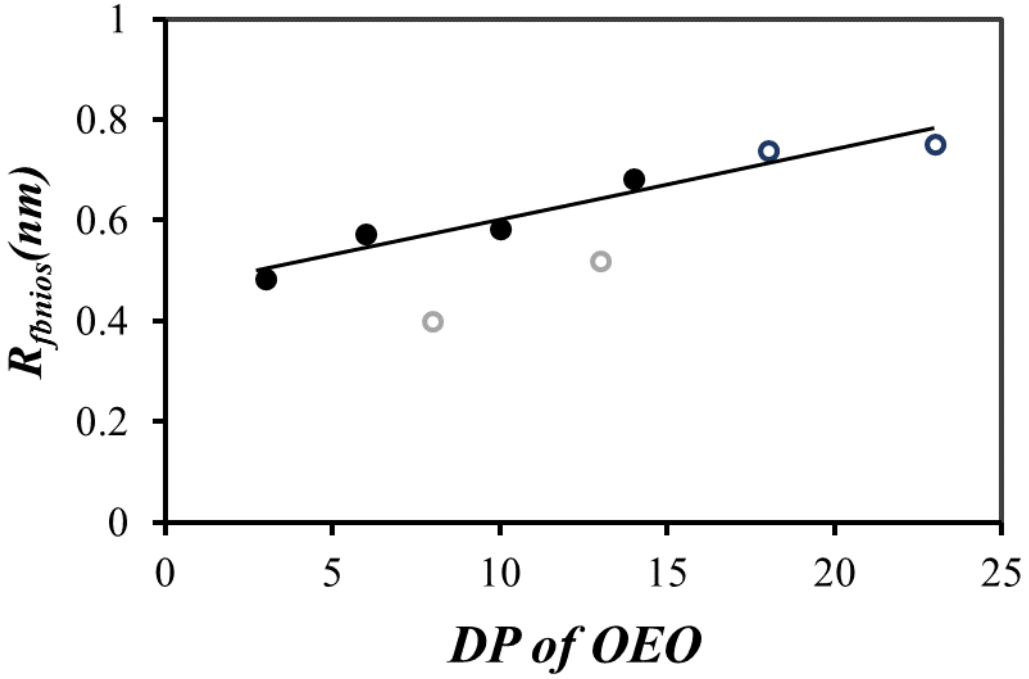

Figure 3.5. Plot of R_{fbnios} as a function of the degree of polymerization of the OEO block for (●) the C_8-F-EO_y series and (O) the C_{12}-F-EO_y series (grey for C_{12}-F-EO_8 and C_{12}-F-EO_{13} and black for C_{12}-F-EO_{18} and C_{12}-F-EO_{23}).

3.3.2 Steady State Fluorescence Measurements

The SSF spectra of the aqueous solutions of the *fbnios* samples with 5×10^{-7} M pyrene, that had been used in the surface tension experiments, were acquired. The SSF spectra of C_8-F-EO_{14} aqueous solutions are shown in Figure 3.5. Similar results were obtained for the other *fbnios* samples, and the corresponding spectra are included in Appendix A.

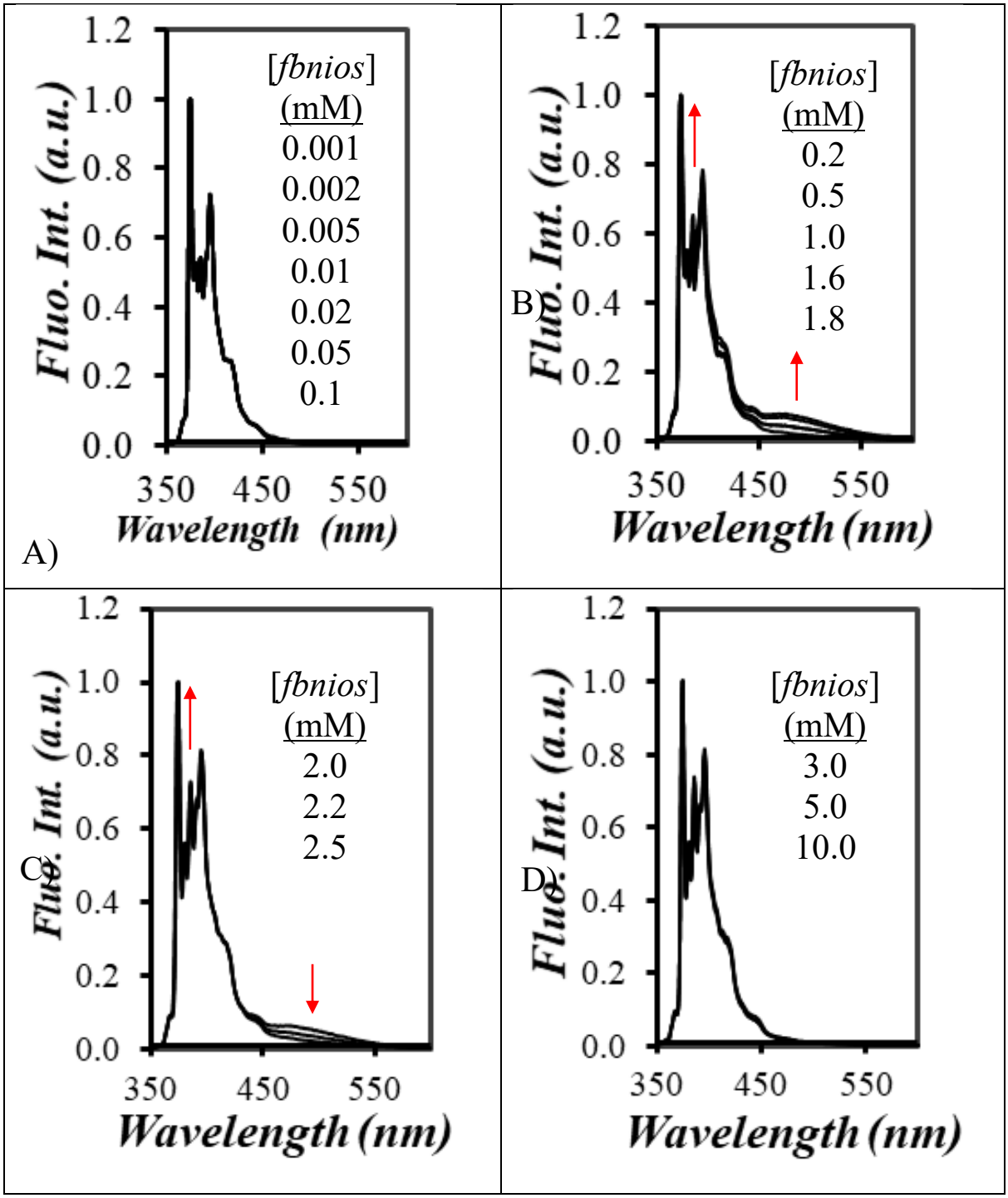

Figure 3.6. SSF spectra of 5×10^{-7} M pyrene in aqueous solutions of C_8-F-EO_{14} with concentration ranging from A) 0.001 to 0.1 mM, B) 0.2 to 1.8 mM, C) 2.0 to 2.5 mM, and D) 3 to 10 mM. λ_{ex} = 336 nm.

Changes in the SSF spectra shown in Figure 3.5 for C_8-F-EO_{14} were described based on the fluorescence intensity ratio (I_1/I_3) of the first (I_1) over the third (I_3) bands of the pyrene

monomer, and second, the excimer-to-monomer fluorescence intensity ratio (I_E/I_M). For C_8-F-EO_{14} concentrations below 0.1 mM, no change in the fluorescence spectra were observed in Figure 3.5A and no pyrene excimer fluorescence was observed. Both features suggested that pyrene did not interact with the surfactant in this concentration range. For C_8-F-EO_{14} concentrations between 0.2 and 1.8 mM in Figure 3.5B, the fluorescence intensity of the third peak was clearly enhanced with respect to that of the first peak. Furthermore, a clear excimer fluorescence centered at 480 nm was observed, taking a maximum value for a C_8-F-EO_{14} concentration of 1.8 mM. When the C_8-F-EO_{14} concentration was further increased from 1.8 to 2.5 mM in Figure 3.5C, the relative fluorescence intensity of the third peak continued to increase, while the fluorescence intensity of the excimer decreased. Hardly any excimer fluorescence was detected for C_8-F-EO_{14} concentration above 2.5 mM, as shown in Figure 3.5D.

These spectral changes were better represented by plotting the I_1/I_3 and I_E/I_M ratios of the C_8-F-EO_{14} aqueous solutions as a function of the C_8-F-EO_{14} concentration in Figure 3.6. At low *fbnios* concentrations the pyrene is located in water and its I_1/I_3 ratio equals 1.9, which is typical of pyrene dissolved in water.[51,52] The I_1/I_3 ratio shows a significant decrease when the C_8-F-EO_{14} concentration is increased from 0.5 to 2.2 mM, before plateauing at a lower value of 1.4. The lower I_1/I_3 value observed at high C_8-F-EO_{14} concentration indicates that pyrene probes an environment that is more hydrophobic than water, and corresponds to the interior of the C_8-F-EO_{14} micelles. Micelle formation also affected the I_E/I_M ratio in Figure 3.6. At low C_8-F-EO_{14} concentration, pyrene is homogeneously distributed in water and the extremely low pyrene concentration of 5×10^{-7} M prevents excimer formation. Thus, the I_E/I_M ratio takes a very small value. Close to the CMC of C_8-F-EO_{14}, where micelles begin to form, the few pyrene molecules in the solution are concentrated inside a few micelles where the high local pyrene concentration ($[Py]_{loc}$) promotes pyrene excimer formation (PEF), which is reflected by a sharp increase in the I_E/I_M ratio in Figure 3.6. As the C_8-F-EO_{14} concentration is further increased,

more micelles are created among which the pyrene molecules distribute themselves, thus decreasing $[Py]_{loc}$ and the I_E/I_M which returns to a low value as all pyrene molecules are sequestered in different micelles. These effects are clearly observed in Figure 3.6, thus demonstrating, along with the trend obtained with the I_1/I_3 ratio, that C_8-F-EO_{14} forms micelles in water. Taking the position of the I_E/I_M maximum in Figure 3.6 suggests that the CMC of C_8-F-EO_{14} equals 1.8 (±0.2) mM, in good agreement with the value of 1.89 ± 0.13 mM found by surface tension measurements. The plots of I_E/I_M and I_1/I_3 obtained as a function of concentration for the other *fbnios* samples are included in Appendix A.

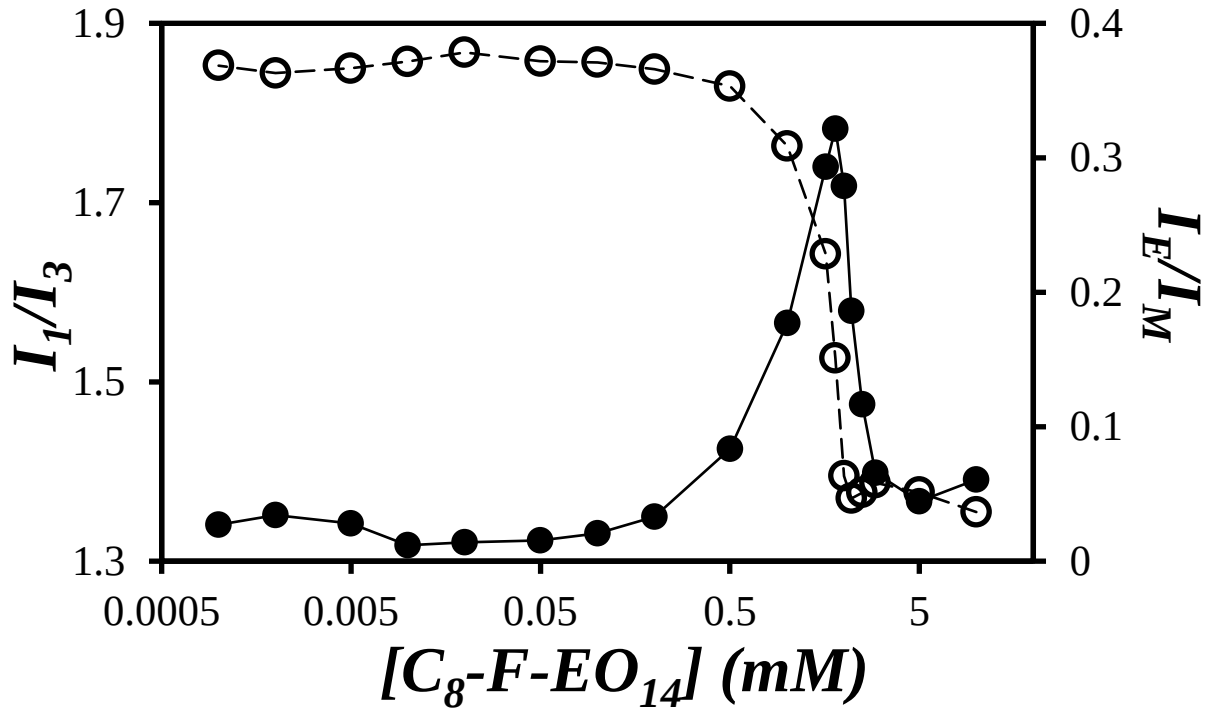

Figure 3.7. Plot of the (●, solid line) I_E/I_M and (○, dashed line) I_1/I_3 ratios as a function of C_8-F-EO_{14} concentration. $[Py] = 5\times10^{-7}$ M.

Similar trends of I_E/I_M and I_1/I_3 against *fbnios* concentration were obtained for all *fbnios* samples and their CMC was determined in a similar manner. The CMCs are listed in Table 3.1, which also includes the CMC determined by surface tension for comparison. Although the

CMCs obtained by both methods showed some differences, they were in fairly good agreement with each other. For instance, the CMC values obtained for the C_8-F-EO_y series by fluorescence were also found to be about one order of magnitude larger than those of the C_{12}-F-EO_y series, as had been found by surface tension measurements. The CMCs obtained for the C_{12}-F-EO_y series appear to be less sensitive to changes in the OEO segment length.

Table 3.2. Comparison of the CMC of *fbnios* samples determined by SSF and surface tension measurements.

Sample	HLB	CMC (mM) by fluorescence	CMC (mM) by surface tension
C_8-F-EO_3	13.9	0.7 ± 0.3	0.67 ± 0.02
C_8-F-EO_6	15.5	0.9 ± 0.1	1.24 ± 0.06
C_8-F-EO_{10}	16.7	1.3 ± 0.2	1.17 ± 0.04
C_8-F-EO_{14}	17.4	1.8 ± 0.2	1.89 ± 0.13
C_{12}-F-EO_8	14.8	0.068 ± 0.009	0.029 ± 0.009
C_{12}-F-EO_{13}	16.1	0.074 ± 0.012	0.036 ± 0.004
C_{12}-F-EO_{18}	16.9	0.075 ± 0.025	0.042 ± 0.016
C_{12}-F-EO_{23}	17.3	0.068 ± 0.007	0.044 ± 0.013

3.4 Conclusions

In this chapter, the amphiphilic properties of *fbnios* were characterized by surface tension and fluorescence measurements. These measurements demonstrated that the *fbnios* prepared in this thesis behaved similarly to typical surfactants. The CMCs of the eight synthesized *fbnios* samples were successfully determined by surface tension and pyrene fluorescence measurements. The HLB had a similar effect on the behavior of *fbnios* as that reported for other non-ionic surfactants such as the Triton X and Brij family surfactants.[3,4] In particular, it was found that the C_{12}-F-EO_y samples, bearing the same hydrophobic chain as Brij family surfactants, had much smaller CMCs.

All trends obtained by plotting the surface tension against *fbnios* concentration showed

consistent results and high similarity to the plots obtained for typical surfactants. These results were used as evidence that *fbnios* can be viewed as surfactants. The CMCs were also determined by SSF measurements. For all synthesized *fbnios* samples, the I_1/I_3 ratio of pyrene dissolved in aqueous solutions of the *fbnios* decreased drastically in the concentration range where the I_E/I_M ratio passed through a maximum. Both ratios remained constant within experimental error for *fbnios* concentrations higher or lower than the range of concentrations around the CMC. The results from both surface tension and SSF measurements were in agreement with each other, which suggests that the CMCs obtained by the two different experimental methods are reliable.

Chapter 4 – Conclusions

A synthetic pathway to convert 2,5-*bis*(hydroxymethyl)furan (2,5-*bis*HMF) into furan-based non-ionic surfactants (*fbnios*) was introduced in this thesis. After alkylating one of the hydroxyl groups of 2,5-*bis*HMF by Williamson ether synthesis, the second hydroxyl group was ethoxylated by anionic polymerization of ethylene oxide. The extension of the oligo(ethylene oxide) (referred to as either OEO or EO_y, where *y* represents the number of EO units) from the second alcohol of 2,5-*bis*HMF by anionic polymerization was first demonstrated by the successful ethoxylation of 5-(methyl-2-furyl)methanol for several Me-F-EO_y samples. The Me-F-EO_y samples were characterized further by ^{1}H NMR, gel permeation chromatography (GPC), and MALDI-ToF MS, to demonstrate control over the EO chain length and the molecular weight for all Me-F-EO_y samples. The only impurity observed in the ^{1}H NMR spectra of Me-F-EO_y was *tert*-butoxide-modified OEO, which was produced from the addition of EO onto the *tert*-butoxide anion. Due to the similarity in polarity between the *tert*-butoxide group and Me-F-EO_y, attempts made to remove the impurity were unsuccessful. Nevertheless, the content of *tert*-butoxide-modified OEO was less than 8% in the Me-F-EO_y samples. Considering the low impurity content and the structural similarity between the impurity and the Me-F-EO_y samples, the presence of *tert*-butoxide-modified OEO was expected to have a minor effect on the properties of Me-F-EO_y samples. Because their structural similarity, this expectation could be extended to *tert*-pentoxide-modified OEO in the corresponding *fbnios*. The synthesis of *fbnios* with an octyl (C_8) or dodecyl (C_{12}) alkyl chain was carried out.

The C_8-F-OH and C_{12}-F-OH samples were synthesized by Williamson ether synthesis, and no impurity was observed in their ^{1}H NMR spectra. Anionic polymerization was then conducted by deprotonation of C_8-F-OH with potassium *tert*-pentoxide, yielding two crude products that were further separated by column chromatography into four final products,

namely C_8-F-EO_3, C_8-F-EO_6, C_8-F-EO_{10}, and C_8-F-EO_{14}. An identical procedure was applied to prepare C_{12}-F-OH, which after ethoxylation yielded C_{12}-F-EO_8, C_{12}-F-EO_{13}, C_{12}-F-EO_{18}, and C_{12}-F-EO_{23}. All 8 *fbnios* samples were characterized by ^{1}H NMR, GPC, and MALDI-ToF MS. The *tert*-pentoxide-modified OEO content of the C_{12}-F-EO_8 and C_{12}-F-EO_{13} samples was 25 mol%, while it accounted for less than 8 mol% in all other *fbnios* samples.

The number-average degree of polymerization (DP_n) of the *fbnios* samples calculated from the NMR spectra matched the DP_n obtained from the MALDI-ToF MS analysis. The DP_n values obtained by GPC were lower, probably due to structural differences between the *fbnios* and the PEO standards used to calibrate the GPC column. Both the GPC and MS techniques indicated that the purified (fractionated) *fbnios* samples had extremely narrow molecular weight distributions (MWDs), with polydispersity indices (PDI) approaching unity. These characterization techniques demonstrated the successful synthesis of the C_x-F-EO_y samples.

The amphiphilic properties of the *fbnios* were determined by conducting surface tension and fluorescence measurements. The surface tension measurements resulted in plots of surface tension as a function of *fbnios* concentration, which exhibited similar features for all samples. Starting from the surface tension of water at low f*bnios* concentrations, the surface tension decreased precipitously before plateauing after reaching the critical micelle concentration (CMC). Since this behavior is typical of surfactants, it confirmed that *fbnios* behaved like surfactants. The CMC of the *fbnios* samples showed a more than ten-fold decrease when the octyl group was replaced by a dodecyl chain, thus reflecting the effect of the hydrophobic tail as observed with typical surfactants.

The fluorescence measurements allowed monitoring of changes in the fluorescence spectrum of pyrene dissolved at very low concentration upon changing the *fbnios* concentration. These changes in the fluorescence spectra were quantified by considering the I_1/I_3 and I_E/I_M ratios. Corrections needed to be applied to the fluorescence spectra obtained with the C_8-F-

EO_{10}, C_{12}-F-EO_8, and C_{12}-F-EO_{13} samples due to their inherent fluorescence. After these corrections were applied, the I_1/I_3 and I_E/I_M ratios were calculated for all *fbnios* samples as described in Chapter 3. For all *fbnios* samples, a significant decrease in the I_1/I_3 ratio was observed in the *fbnios* concentration range where I_E/I_M reached its maximum value, and both ratios remained constant within experimental error when the *fbnios* concentration was higher or lower than the CMC. The changes in the I_1/I_3 and I_E/I_M ratios were attributed to the formation of *fbnios* micelles, and the concentration where the I_E/I_M ratio passed through a maximum was assigned to the CMC.

For all *fbnios* samples, the CMC determined from surface tension measurements agreed with the CMC obtained from fluorescence measurements within experimental error. This is strong evidence that the CMC values are reliable, and reflect the amphiphilic properties of the *fbnios*. The effect of different molecular parameters, such as the length of the alkyl or OEO chains, on the properties of the *fbnios* were illustrated by plotting the CMC obtained by surface tension measurements as a function of their HLB. These plots showed similar trends, whereby the CMC decreased for decreasing HLB for each *fbnios* series, but increased by more than one order of magnitude upon replacing the dodecyl chain by an octyl chain. The effect of the HLB on the CMC observed for the *fbnios* samples was similar to that found for other well-known *nios* such as the Triton X and Brij surfactant families. Moreover, the C_{12}-F-EO_y samples bearing identical hydrophobic moiety as the Brij family were found to have much lower CMC values.

In conclusion, utilizing 2,5-*bis*HMF as starting material, 8 *fbnios* were successfully synthesized with control over their EO chain length and maintaining a narrow MWD, through Williamson ether synthesis and anionic polymerization. The only impurity observed in the *fbnios* samples was *tert*-pentoxide-modified OEO, which accounted for 25 mol% in the C_{12}-F-EO_8 and C_{12}-F-EO_{13} samples, but less than 8 mol% in the other *fbnios* samples. The effect of the *tert*-pentoxide-modified OEO on the latter *fbnios* samples is likely to be insignificant due

their low content and similarity with the *fbnios*. Surface tension measurement demonstrated that the *fbnios* synthesized in this thesis could be considered as a novel family of surfactants. They displayed a behavior similar to other widely applied *nios*, the CMC of C_{12}-F-EO_y being significantly lower than that of the Brij family prepared with an identical hydrophobic moiety. This study suggests that *fbnios* can be viewed as novel environmentally friendly surfactants.

Future Work

One aspect that could be considered in future work would be to improve the GPC analysis of the *fbnios* by using the monodisperse Me-F-EO_y samples as standards to calibrate the GPC column, as their M_n was already determined by ^{1}H NMR and MALDI-ToF MS. Such a calibration would be expected to yield more accurate DP_n for the *fbnios*. In an effort to prepare *fbnios* with a lower amount of *tert*-pentoxide-modified OEO impurity, the C_{12}-F-EO_8 and C_{12}-F-EO_{13} samples should be synthesized again with a stronger base for the anionic polymerization, or else with a longer equilibration time, to hopefully minimize the content of *tert*-pentoxide-modified OEO. The aggregation number of the *fbnios* micelles should be determined by time-resolved fluorescence. More experiments need to be conducted to explore the properties of these *fbnios* samples in more details. For instance, gelation was observed for some of the *fbnios* at high surfactant concentrations. More detailed information will need to be gathered on these interesting molecules, to determine potential applications for *fbnios* in the future.

References

1. Myers, D. *Surfactant science and technology*, 4th ed.; John Wiley & Sons, Inc.: Hoboken, 2020; pp 6-8.
2. Rosen, M. J. *Surfactants and Interfacial Phenomena,* 4th ed.; John Wiley & Sons, Inc: Hoboken, New Jersey, 2004, pp. 32, 123-124, 235-239.
3. Raimbault, J.; Casier, R.; Little, H.; Duhamel, J. Hydrophobic and Elastic Forces Experienced by a Series of Pyrene End-Labeled Poly(Ethylene Oxide)s Interacting with Sodium Dodecyl Sulfate Micelles. *Macromolecules* **2018**, *51*, 5933-5943.
4. Miyagishi, S.; Okada, K.; Asakawa, T. Salt Effect on Critical Micelle Concentrations of Nonionic Surfactants, N-AcylN-methylglucamides (MEGAn). *J. Colloid Interface Sci.* **2001**, *238*, 91-95.
5. Gotoh, K.; Horibe, K.; Mei, Y.; Tsujisaka, T. Effect of Water Hardness on Textile Detergency Performance in Aqueous Cleaning Systems. *J. Oleo Sci.* **2016**, *65*, 123-133.
6. Uchegbu, I. F.; Vyas, S. P. Non-Ionic Surfactant-Based Vesicles (Niosomes) in Drug Delivery. *Int. J. Pharm*. **1998**, *172*, 33-70.
7. Wan, Y.; Shi, Y.; Zhao, D. Designed Synthesis of Mesoporous Solids via Nonionic-Surfactant-Templating Approach. *Chem. Commun.* **2007**, *9*, 897-926.
8. Vyas, S.; Singh, R.; Jain, S.; Mishra, V.; Mahor, S.; Singh, P.; Gupta, P.; Rawat, A.; Dubey, P. Non-Ionic Surfactant Based Vesicles (Niosomes) for Non-Invasive Topical Genetic Immunization Against Hepatitis B. *Int. J. Pharm.* **2005**, *296*, 80-86.
9. Pal, N.; Babu, K.; Mandal, A. Surface Tension, Dynamic Light Scattering, and Rheological Studies of a New Polymeric Surfactant for Application in Enhanced Oil Recovery. *J. Petrol. Sci. Eng.* **2016**, *146*, 591-600.
10. Foley, P.; Kermanshahi Pour, A.; Beach, E.; Zimmerman, J. Derivation and Synthesis of Renewable Surfactants. *Chem. Soc. Rev.* **2012**, *41*, 1499-1518.

11. Xuefan Gu; Gao, L.; Li, Y.; Chen, S.; Zhang, J.; Du, W.; Qu, C.; Chen, G. Performance and Mechanism of Span Surfactants as Clean Flow Improvers for Crude Oil. *Pet. Chem.* **2020**, *60*, 140-145.
12. Naoe, K.; Ura, O.; Hattori, M.; Kawagoe, M.; Imai, M. Protein Extraction Using Non-Ionic Reverse Micelles of Span 60. *Biochem. Eng. J.* **1998**, *2*, 113-119.
13. Rosen, M. J.; Cohen, A. W.; Dahanayake, M.; Hua, X. Relationship of Structure to Properties in Surfactants. 10. Surface and Thermodynamic Properties of 2-Dodecyloxypoly(ethenoxyethanol)s, C12H25(OC2H4)xOH, in Aqueous Solution. *J. Phys. Chem.* **1982**, *86*, 541-545.
14. Corkill, J. M.; Goodman, J. F.; Harrold, S. P. Thermodynamics of Micellization of Non-Ionic Detergents. *Trans. Faraday Soc.* **1964**, *60*, 202-207.
15. Khan, A. M.; Shah, S. S. Determination of Critical Micelle Concentration (CMC) of Sodium Dodecyl Sulfate (SDS) and the Effect of Low Concentration of Pyrene on its CMC Using ORIGIN Software. *J. Chem. Soc. Pak.* **2008**, *30*, 186-191.
16. Ray, G. B.; Chakraborty, I.; Moulik, S. P. Pyrene Absorption Can Be a Convenient Method for Probing Critical Micellar Concentration (cmc) and Indexing Micellar Polarity. *J. Colloid Interface Sci.* **2006**, *294*, 248-254.
17. Hait, S.; Moulik, S. Determination of Critical Micelle Concentration (CMC) of Nonionic Surfactants by Donor-Acceptor Interaction with Lodine and Correlation of CMC with Hydrophile-Lipophile Balance and Other Parameters of the Surfactants. *J. Surfactants Deterg.* **2001**, *4*, 303-309.
18. Stellner, K.; Scamehorn, J. Hardness Tolerance of Anionic Surfactant Solutions. 1. Anionic Surfactant with Added Monovalent Electrolyte. *Langmuir* **1989**, *5*, 70-77.
19. Stellner, K.; Scamehorn, J. Surfactant Precipitation in Aqueous Solutions Containing Mixtures of Anionic and Nonionic Surfactants. *J. Am. Oil Chem. Soc.* **1986**, *63*, 566-574.

20. Mehta, S. K.; Jindal, N.; Kaur, G. Quantitative Investigation, Stability and in Vitro Release Studies of Anti-TB Drugs in Triton Niosomes. *Colloids Surf. B.* **2011**, *87*, 173-179.
21. Moghassemi, S.; Hadjizadeh, A. Nano-Niosomes as Nanoscale Drug Delivery Systems: An Illustrated Review. *J. Control. Release* **2014**, *185*, 22-36.
22. Farmoudeh, A.; Akbari, J.; Saeedi, M.; Ghasemi, M.; Asemi, N.; Nokhodchi, A. Methylene Blue-Loaded Niosome: Preparation, Physicochemical Characterization, and in Vivo Wound Healing Assessment. *Drug Deliv. Trans. Re.* **2020**.
23. Abdelbary, G.; El-gendy, N. Niosome-Encapsulated Gentamicin for Ophthalmic Controlled Delivery. *AAPS PharmSciTech.* **2008**, *9*, 740-747.
24. Puras, G.; Mashal, M.; Zárate, J.; Agirre, M.; Ojeda, E.; Grijalvo, S.; Eritja, R.; Diaz-Tahoces, A.; Martínez Navarrete, G.; Avilés-Trigueros, M.; Fernández, E.; Pedraz, J. A Novel Cationic Niosome Formulation for Gene Delivery to the Retina. *J. Control. Release* **2014**, *174*, 27-36.
25. Cserhati, T. Alkyl Ethoxylated And Alkylphenol Ethoxylated Nonionic Surfactants: Interaction with Bioactive Compounds and Biological Effects. *Environ. Health Perspectives* **1995**, *103*, 358.
26. Masuno, M. N.; Bissell, II N.; L. Smith, R.; Higgins, B.; Wood, A. Utilizing a Multiphase Reactor for the Conversion of Biomass to Produce Substituted Furans. U.S. Patent 9,637,463 B2, May 2, **2017**.
27. Barros-Rios, J.; Romani, A.; Garrote, G.; Ordas, B. Biomass, Sugar, and Bioethanol Potential of Sweet Corn. *GCB Bioenergy* **2015**, *7*, 153-160.
28. Bioplastics Magazine, Nov 03, **2020.**
29. Partearroyo, M.; Alonso, A.; Goñi, F.; Tribout, M.; Paredes, S. Solubilization of Phospholipid Bilayers by Surfactants Belonging to the Triton X Series: Effect of Polar Group Size. *J. Colloid Interface Sci.* **1996**, *178*, 156-159.

30. Barakat, Y.; Gendy, T.; Basily, I.; Mohamad, A. Polymeric Surfactants for Enhanced Oil Recovery. Part II—The Hlb-Cmc Relationship of Ethoxylated Alkylphenol-Formaldehyde Polymeric Surfactants. *Br. Polym. J.* **1989**, *21*, 451-457.

31. Griffin W.C. Classification of Surface-active Agents by " HLB ", *J. Soc. Cosmet. Chem.* **1949**, *1*, 311-326.

32. Tanford, C. Micelle Shape and Size. *J. Phys. Chem.* **1972**, 76, 3020-3024.

33. Lee, S.; Lee, J.; Yu, H.; Lim, J. Synthesis of Environment Friendly Nonionic Surfactants from Sugar Base and Characterization of Interfacial Properties for Detergent Application. *J. Ind. Eng. Chem.* **2016**, *38*, 157-166.

34. Wolszczak, M.; Miller, J. Characterization of Non-Ionic Surfactant Aggregates by Fluorometric Techniques. *J. Photochem. Photobiol. A.* **2002**, *147*, 45-54.

35. Garrido, P.; Brocos, P.; Amigo, A.; García-Río, L.; Gracia-Fadrique, J.; Piñeiro, Á. STAND: Surface Tension for Aggregation Number Determination. *Langmuir* **2016**, *32*, 3917-3925.

36 Yekta, A.; Duhamel, J.; Adiwidjaja, H.; Brochard, P.; Winnik, M. A. A Fluorescence Probe Study of Micelle Like Cluster Formation in Aqueous Solutions of Hydrophobically Modified Poly(ethylene oxide). *Macromolecules* **1993**, *26*, 1829-36.

37. Kim, D.; Amos, R.; Gauthier, M.; Duhamel, J. Assemblies of Hydrophobically Modified Starch Nanoparticles Probed by Surface Tension and Pyrene Fluorescence. *ACS Symposium Series-Molecular Assemblies: Characterization and Applications.* Ed. Nagarajan, R. **2020**, Chapter 5, pp 61-75.

38. Duhamel, J. New Insights in the Study of Pyrene Excimer Fluorescence to Characterize Macromolecules and their Supramolecular Assemblies in Solution. *Langmuir* **2012**, *28*, 6527-6538

39. Kalyanasundaram, K.; Thomas, J. K. Environmental Effects on Vibronic Band Intensities in Pyrene Monomer Fluorescence and Their Application in Studies of Micellar Systems. *J. Am. Chem. Soc.* **1977**, *99*, 2039-2044.

40. Masuno, M. N.; Bissell, J.; Smith, R. L.; Higgins, B.; Wood, B. A.; Foster, M. Utilizing a Multiphase Reactor for the Conversion of Biomass to Produce Substituted Furans. U.S. Patent 9,637,463 B2, May 2, **2017**.

41. Rogošić, M.; Mencer, H.; Gomzi, Z. Polydispersity Index and Molecular Weight Distributions of Polymers. *Eur. Polym. J.* **1996**, *32*, 1337-1344.

42. Dispersity in Polymer Science (IUPAC Recommendations 2009). *Chemistry International -- Newsmagazine for IUPAC* **2009**, *31*, 351-353.

43. Hadjichristidis, N.; Hirao, A. *Anionic polymerization*; Springer Japan, Tokyo, **2015**, pp. 68, 79, 81, 90, 93-97, 111, 116.

44. Lee, W.; Lee, H.; Cha, J.; Chang, T.; Hanley, K.; Lodge, T. Molecular Weight Distribution of Polystyrene Made by Anionic Polymerization. *Macromolecules* **2000**, *33*, 5111-5115.

45. Ryu, J.; Im, K.; Yu, W.; Park, J.; Chang, T.; Lee, K.; Choi, N. Molecular Weight Distribution of Branched Polystyrene: Propagation of Poisson Distribution. *Macromolecules* **2004**, *37*, 8805-8807.

46. Mass, V.; Rode, K.; Rittig, F.; Ostrowski, T.; Pasch, H. Analysis of Fatty Alcohol Ethoxylates Regarding Chain Length and Endgroups by MALDI-TOF MS Using Collision-Induced Dissociation. *Macromol. Chem. Phys.* **2012**, *213*, 747–756.

47. Chen, H.; He, M. Quantitation of Synthetic Polymers Using an Internal Standard by Matrix-Assisted Laser Desorption/Ionization Time-of-Flight Mass Spectrometry. *J. Am. Soc. Mass Spectrom.* **2005**, *16*, 100–106.

48. Siu, H.; Prazeres, T. J. V.; Duhamel, J.; Olesen, K.; Shay, G. Characterization of the Aggregates Made by Short Poly(ethylene oxide) Chains Labelled at one End with the Dye Pyrene. *Macromolecules* **2005**, *38*, 2865-2875.

49. Diallo, M. S.; Abriola, L. M.; Weber, W. J. Solubilization of Nonaqueous Phase Liquid Hydrocarbons in Micellar Solutions of Dodecyl Alcohol Ethoxylates. *Environmental Science & Technology* **1994**, *28*, 1829–1837.

50. Partearroyo, M.; Alonso, A.; Goñi, F.; Tribout, M.; Paredes, S. Solubilization of Phospholipid Bilayers by Surfactants Belonging to the Triton X Series: Effect of Polar Group Size. *J. Colloid Interface Sci.* **1996**, *178*, 156-159.

51. Dong, D. C.; Winnik, M. A. The Py Scale of Solvent Polarities. Solvent Effects on the Vibronic Structure of the Pyrene Fluorescence and Empirical Correlations with *E*T and *Y* Values. *Photochem. Photobiol.* **1982**, *35*, 17-21.

52. Dong, D. C.; Winnik, M. A. The Py Scale of Solvent Polarities. *Can. J. Chem.* **1984**, *62*, 2560-2565.

Appendix A

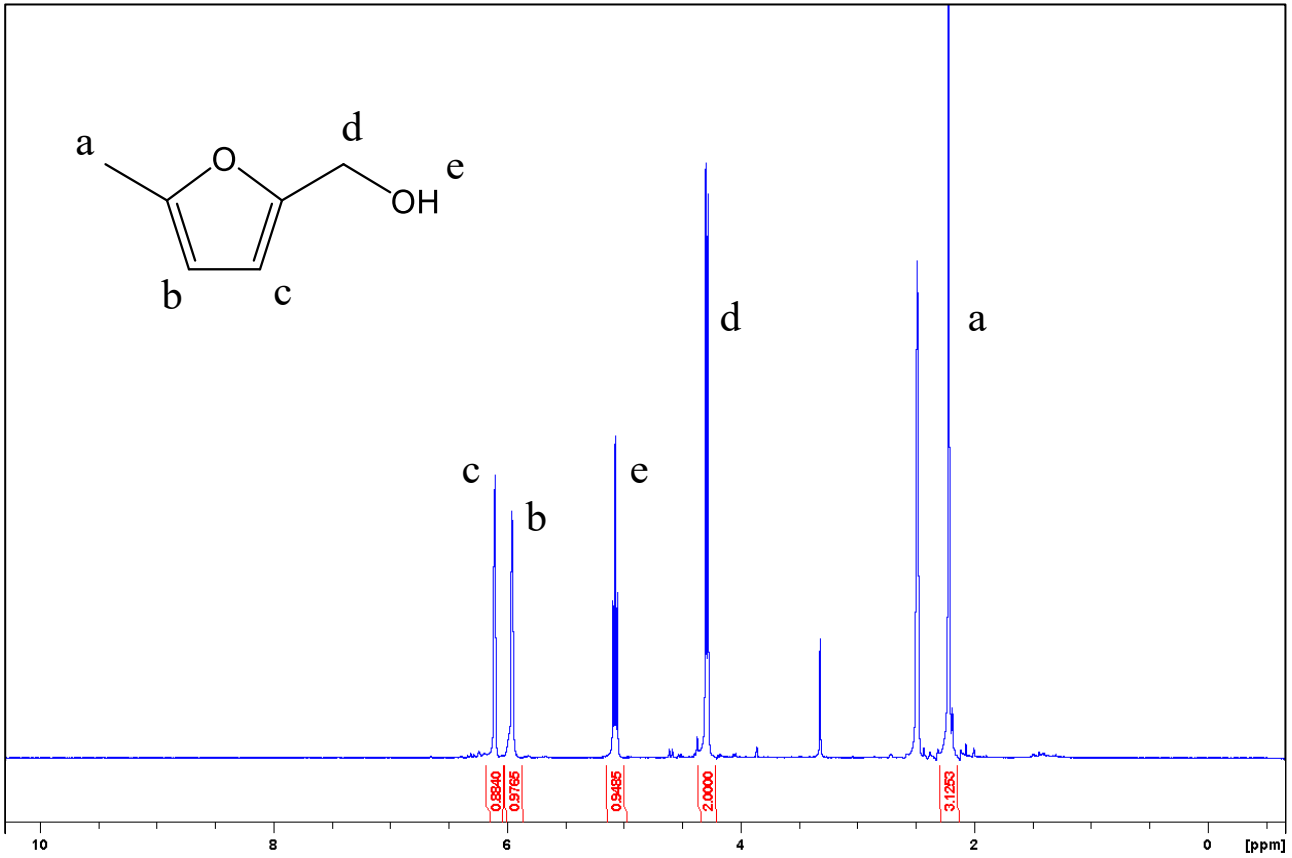

Figure A2.1. 300 MHz ^{1}H NMR spectrum of Me-F-OH in *d*$_6$-DMSO: δ 6.1(s, 1H), 5.9 (s, 1H), 5.1 (t, 1H), 4.3 (d, 2H), 2.2 (s, 3H). Residual solvent peaks are seen at 2.5 ppm for DMSO and 3.3 ppm for water.

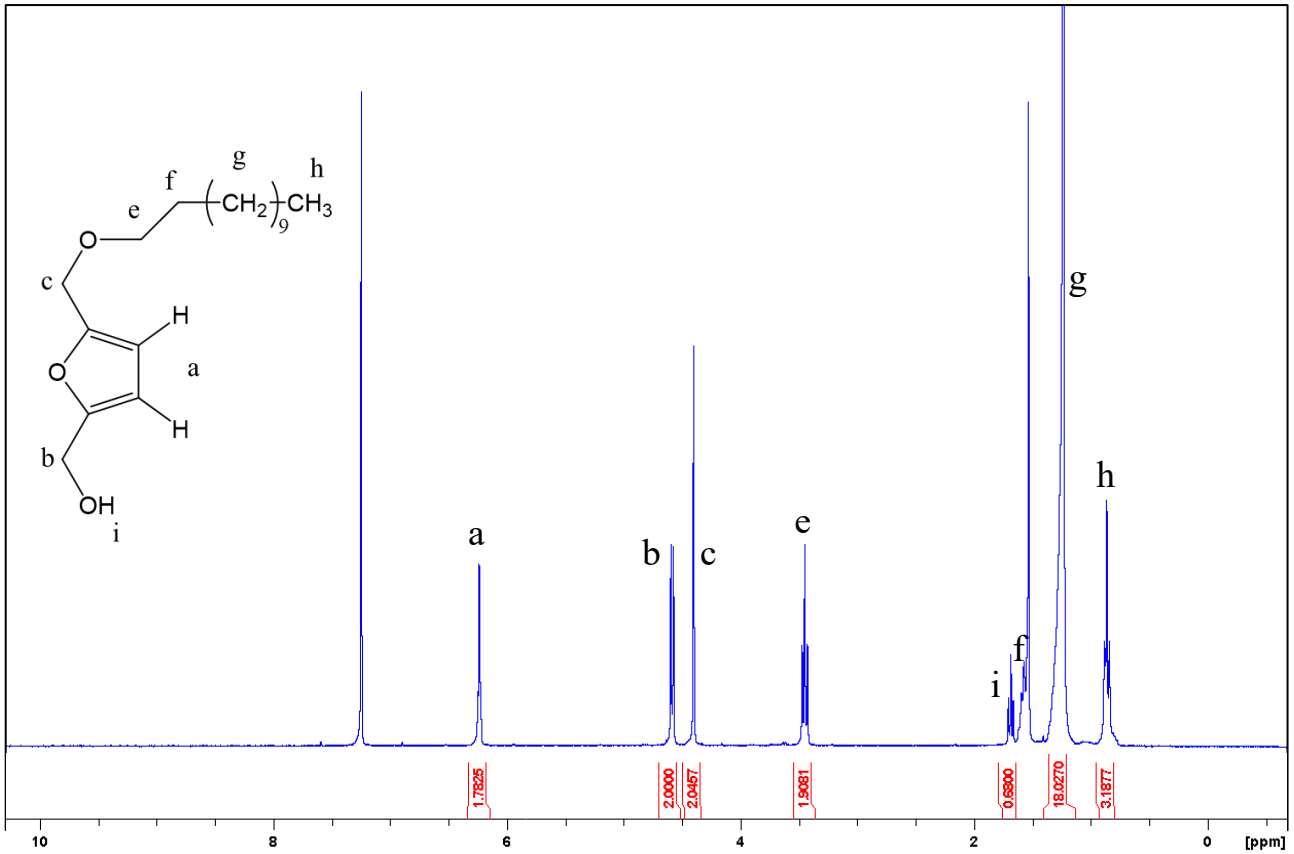

Figure A2.2. 300 MHz ^{1}H NMR spectrum of C_{12}-F-OH in chloroform-*d*: δ 6.2 (d, 2H), 4.6 (d, 2H), 4.4 (s, 2H), 3.5 (t, 2H), 1.7 (t, 1H), 1.6 (p, 2H), 1.2 (m, 18H), 0.9 (t, 3H). Residual solvent peaks are seen at 7.3 ppm for chloroform and 1.5 ppm for water.

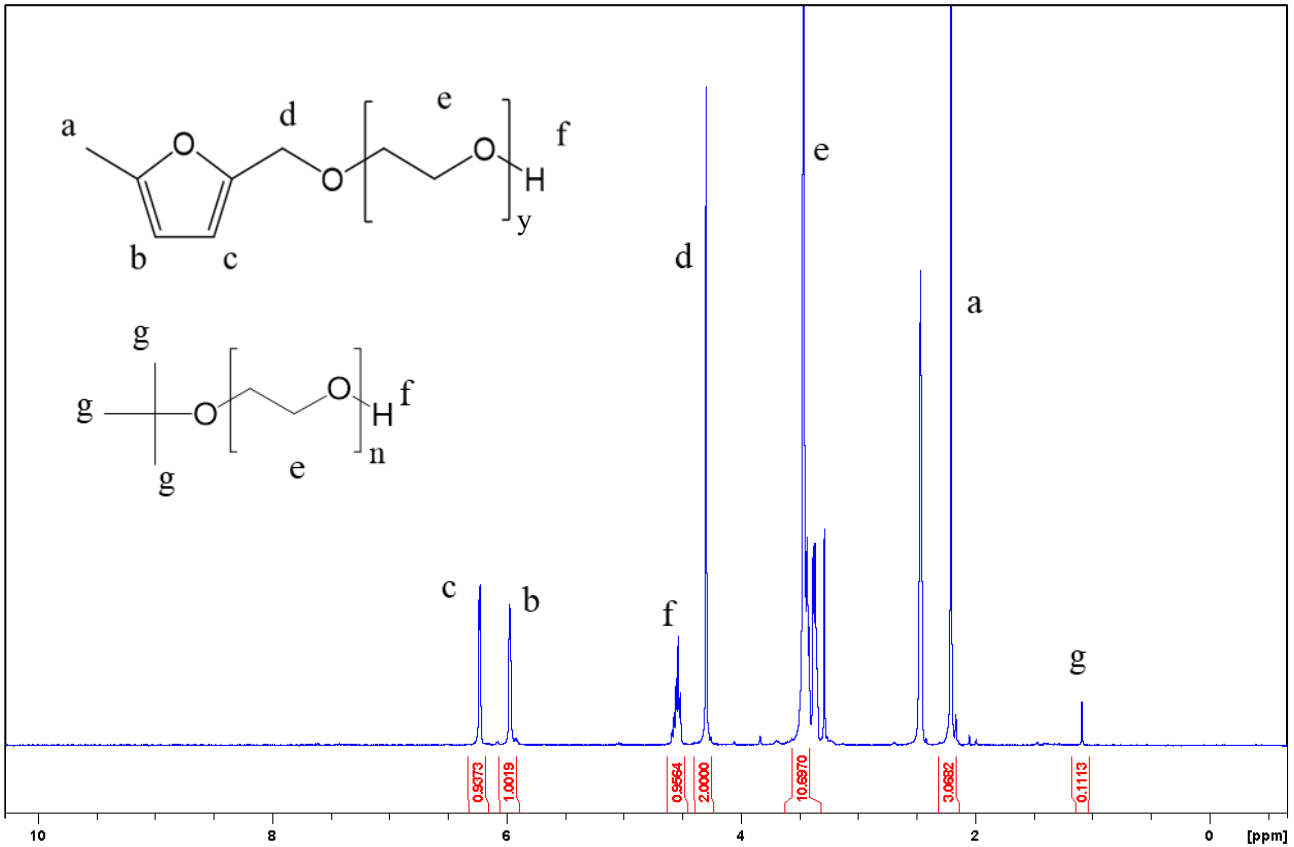

Figure A2.3. 300 MHz ^{1}H NMR spectrum of Me-F-EO$_3$ in d_6-DMSO: δ 6.2 (d, 1H), 6.0 (d, 1H), 4.5 (t, 1H), 4.3 (d, 2H), 3.5 (m, 12H), 2.2 (s, 3H), 1.1 (s, 9H). Residual solvent peaks are seen at 2.5 ppm for DMSO and 3.3 ppm for water.

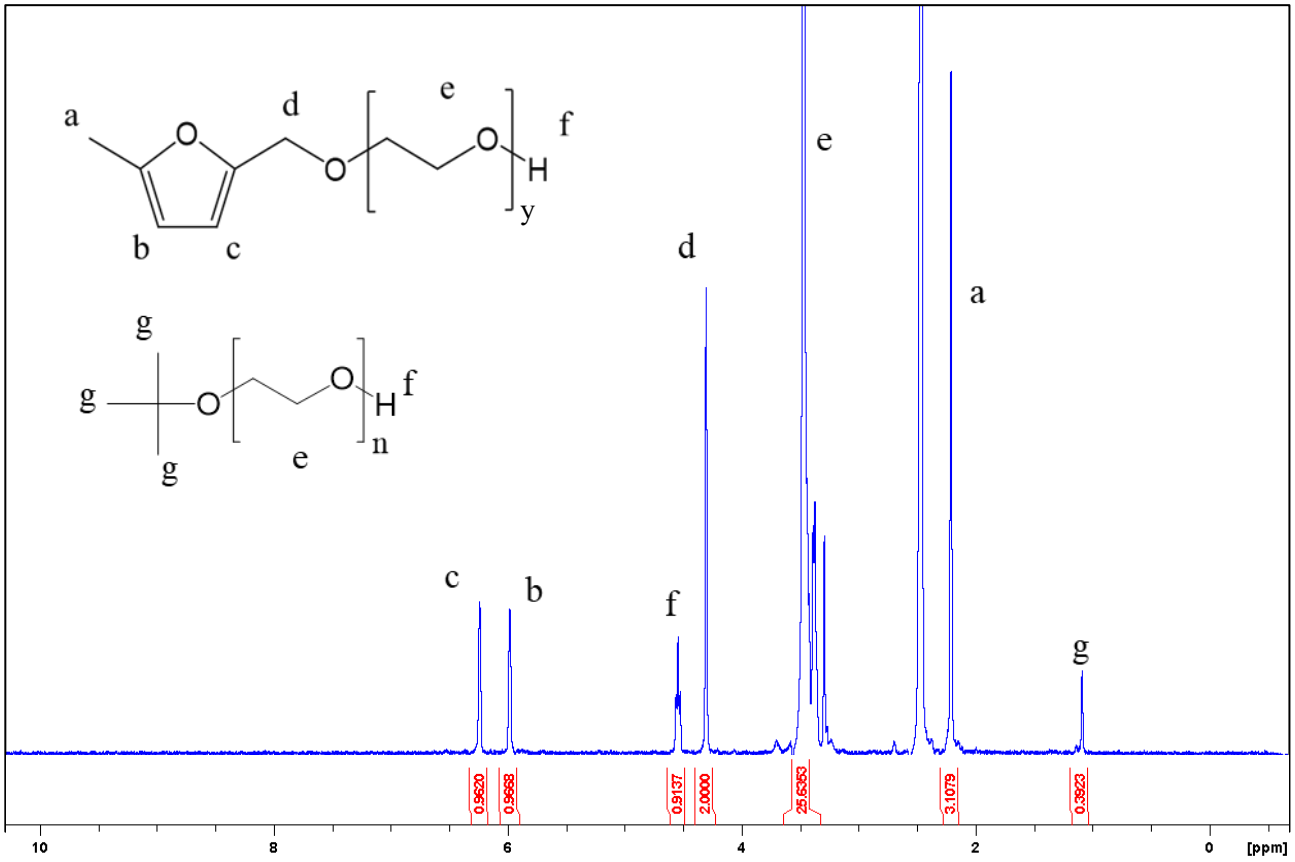

Figure A2.4. 300 MHz ^{1}H NMR spectrum of Me-F-EO$_6$ in d_6-DMSO: δ 6.2 (d, 1H), 6.0 (d, 1H), 4.5 (t, 1H), 4.3 (d, 2H), 3.5 (m, 24H), 2.2 (s, 3H), 1.1 (s, 9H). Residual solvent peaks are seen at 2.5 ppm for DMSO and 3.3 ppm for water.

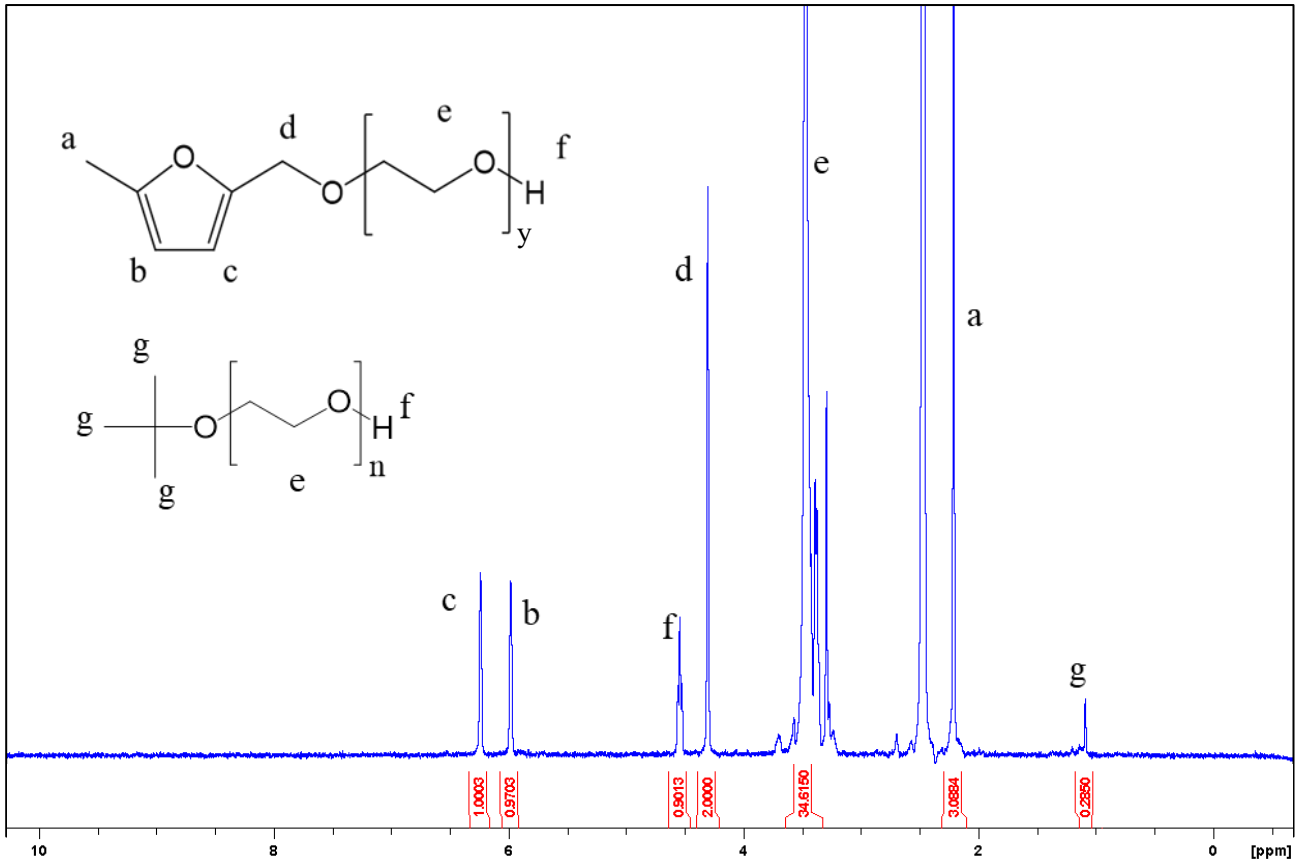

Figure A2.5. 300 MHz ^{1}H NMR spectrum of Me-F-EO$_8$ in *d*$_6$-DMSO: δ 6.2 (d, 1H), 6.0 (d, 1H), 4.5 (t, 1H), 4.3 (d, 2H), 3.5 (m, 32H), 2.2 (s, 3H), 1.1 (s, 9H). Residual solvent peaks are seen at 2.5 ppm for DMSO and 3.3 ppm for water.

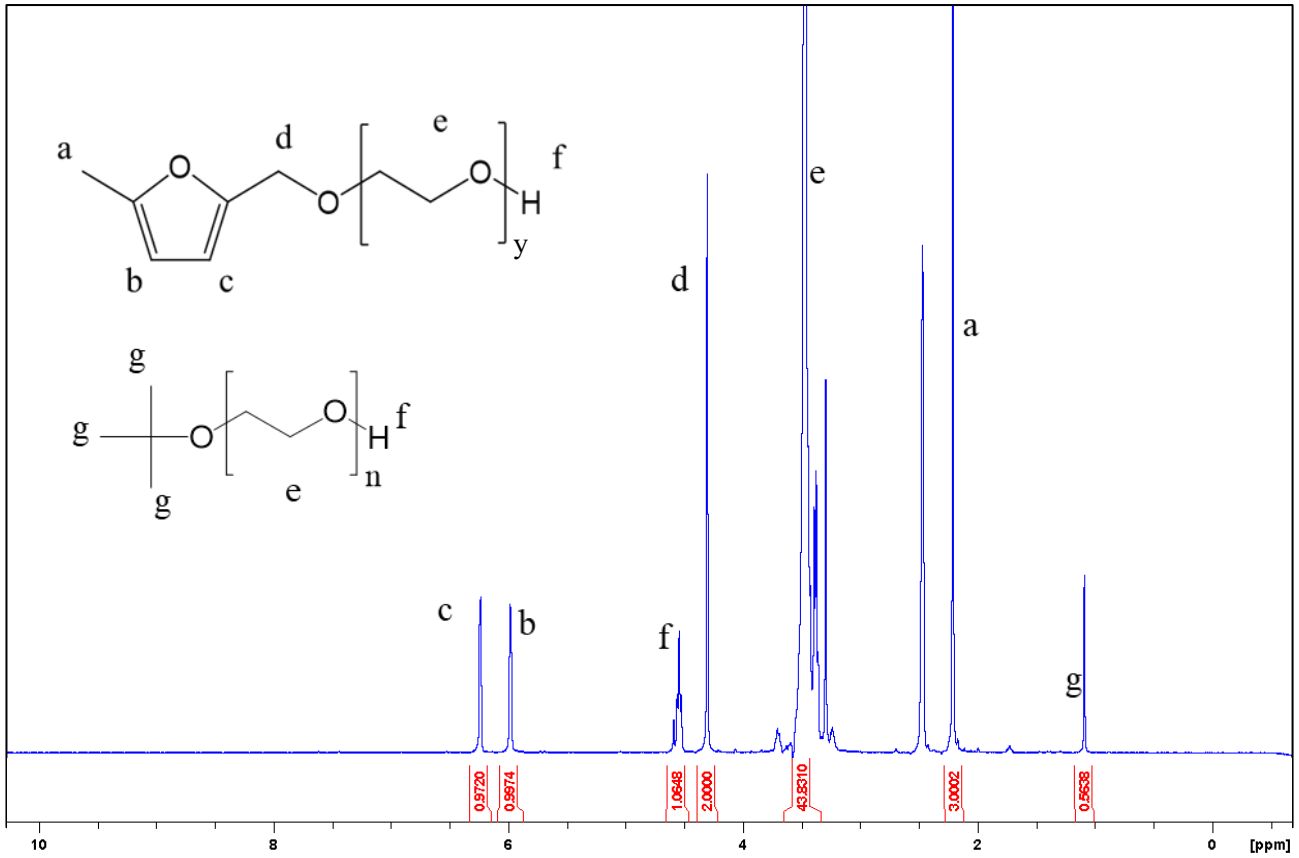

Figure A2.6. 300 MHz ^{1}H NMR spectrum of Me-F-EO$_{10}$ in d_6-DMSO: δ 6.2 (d, 1H), 6.0 (d, 1H), 4.5 (t, 1H), 4.3 (d, 2H), 3.5 (m, 40H), 2.2 (s, 3H), 1.1 (s, 9H). Residual solvent peaks are seen at 2.5 ppm for DMSO and 3.3 ppm for water.

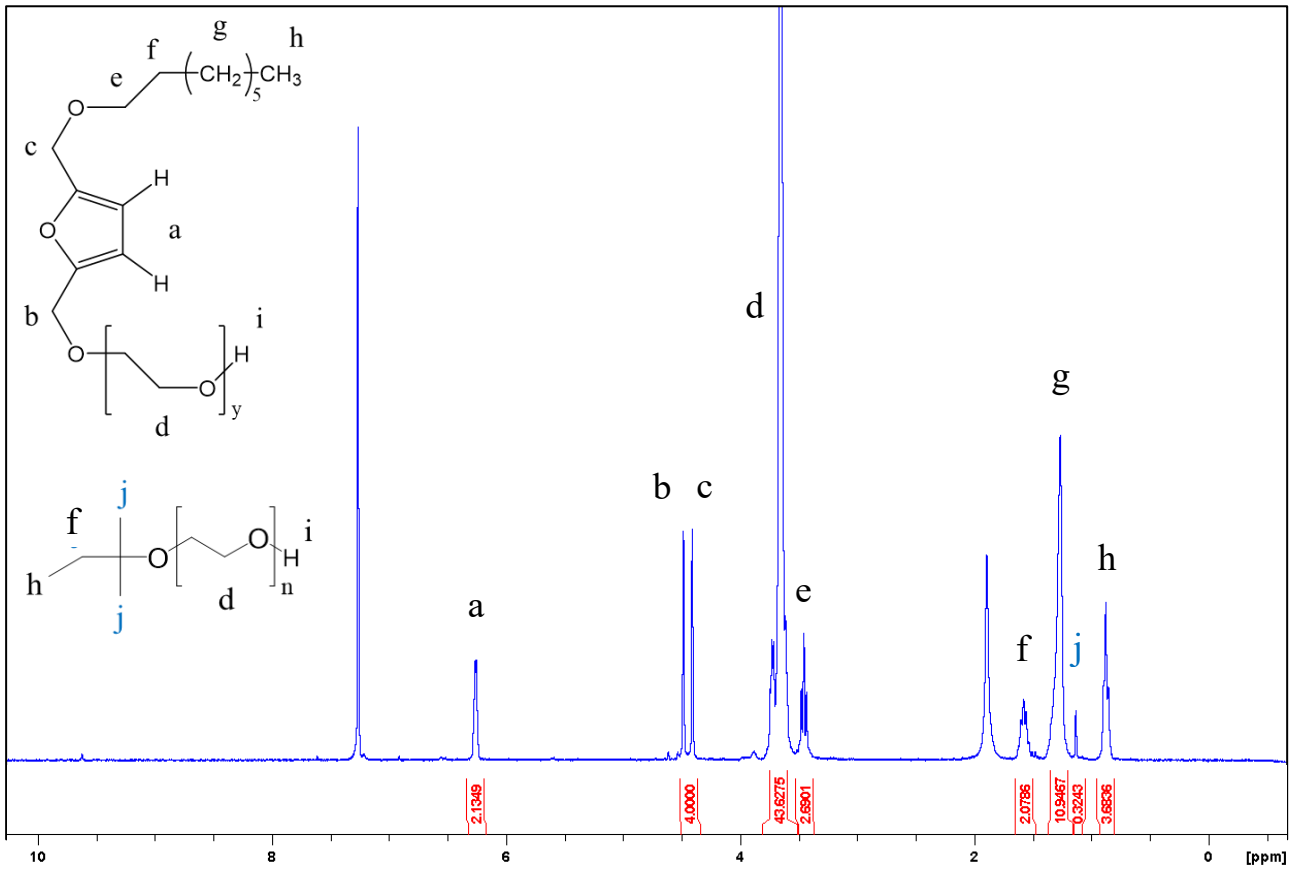

Figure A2.7. 300 MHz ^{1}H NMR spectrum of C_8-F-EO_{10} in chloroform-*d*: δ 6.2 (d, 2H), 4.5 (s, 2H), 4.4 (s, 2H), 3.6 (m, 40H), 3.4 (t, 2H), 1.6 (p, 2H), 1.3 (m, 10H), 1.1 (s, 6H), 0.9 (t, 3H). Residual solvent peaks are found at 7.3 ppm for chloroform and 1.9 ppm for water.

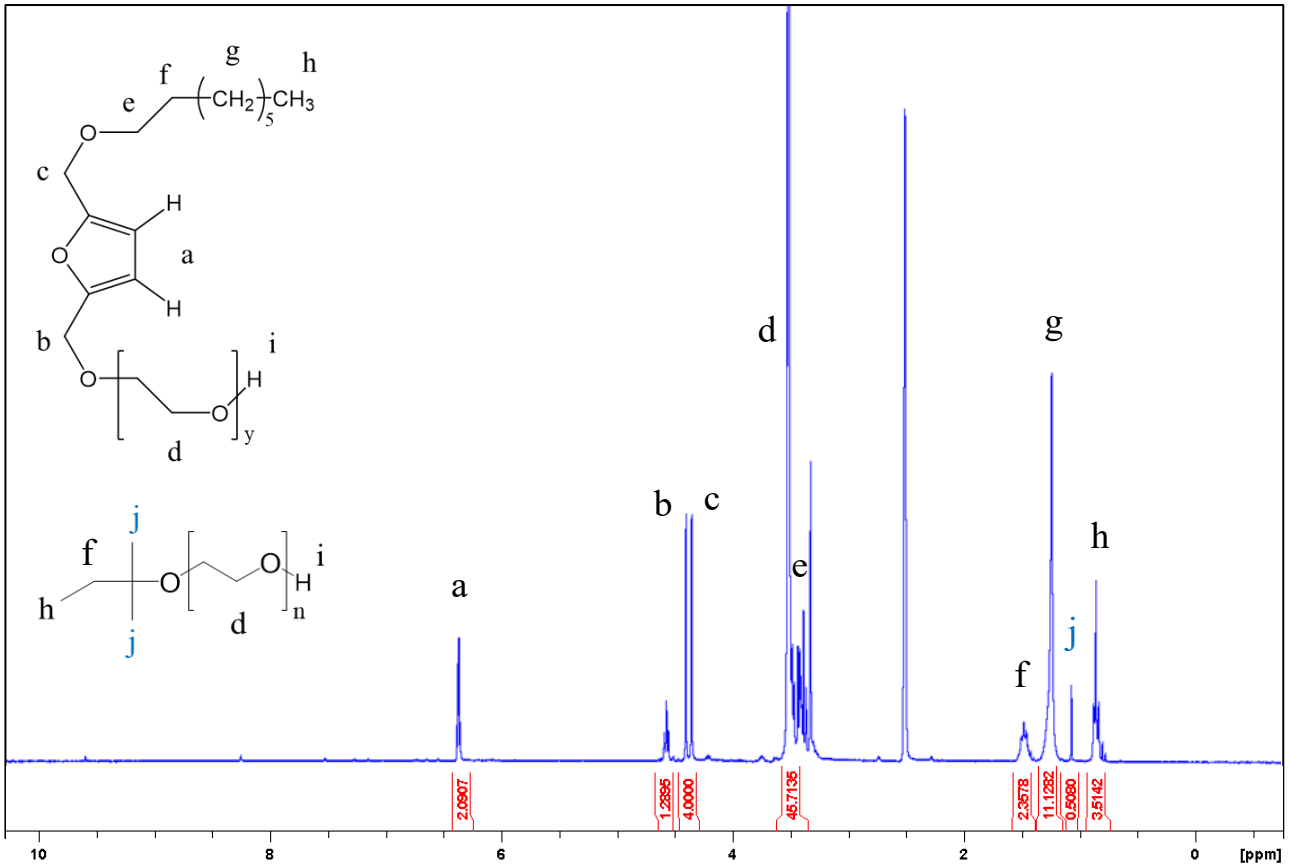

Figure A2.8. 300 MHz ^{1}H NMR spectrum of C_8-F-EO_{10} in d_6-DMSO: δ 6.3 (s, 2H), 4.6 (t, 1H), 4.4 (s, 2H), 4.3 (s,2H), 3.5 (m, 40H), 3.3 (t, 2H), 1.4 (p, 2H), 1.2 (m, 10H), 1.0 (s, 6H), 0.8 (t, 3H). Residual solvent peaks are found at 2.5 ppm for chloroform and 3.3 ppm for water.

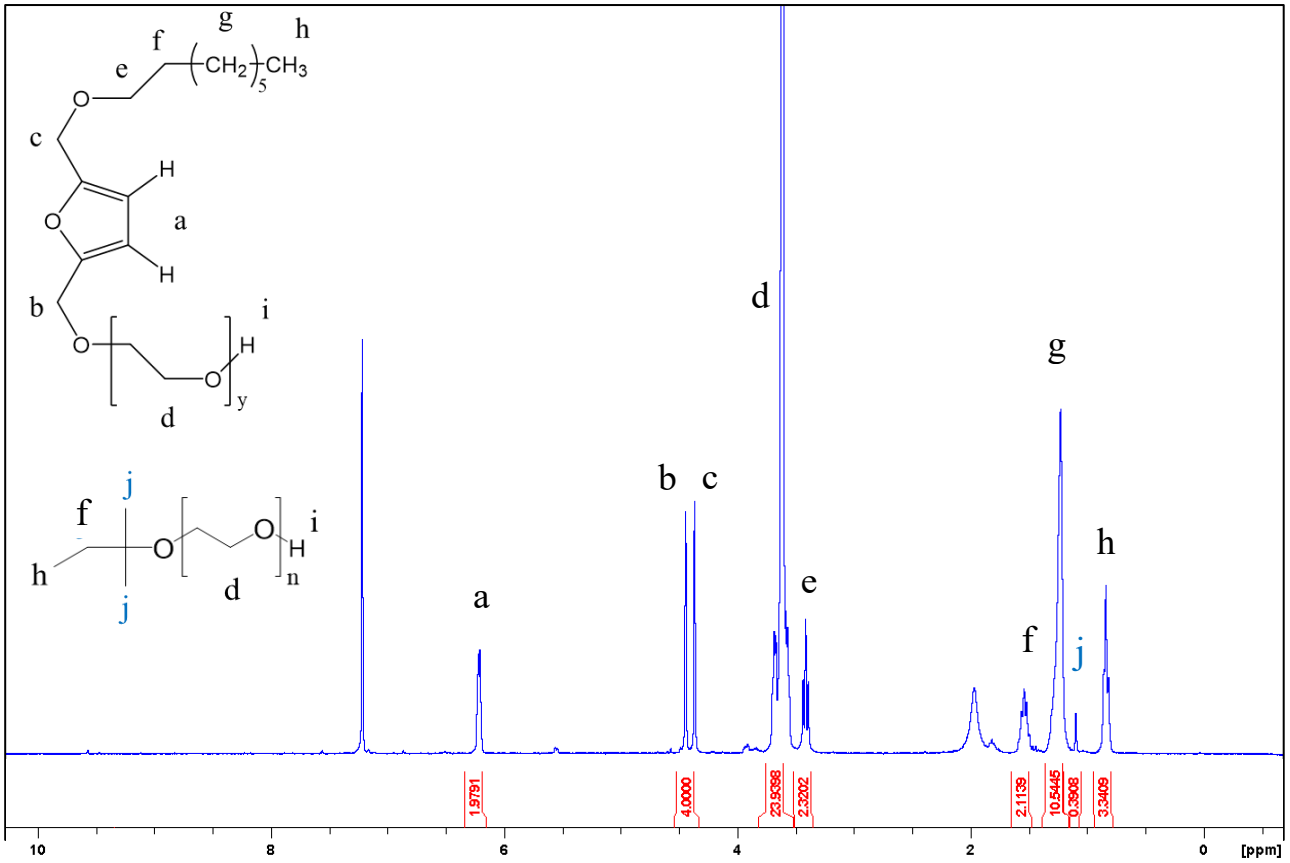

Figure A2.9. 300 MHz ^{1}H NMR spectrum of C_8-F-EO_6 in chloroform-*d*: δ 6.2 (d, 2H), 4.5 (s, 2H), 4.4 (s, 2H), 3.6 (m, 24H), 3.4 (t, 2H), 1.6 (p, 2H), 1.3 (m, 10H), 1.1 (s, 6H), 0.9 (t, 3H). Residual solvent peaks are found at 7.3 ppm for chloroform and 2.0 ppm for water.

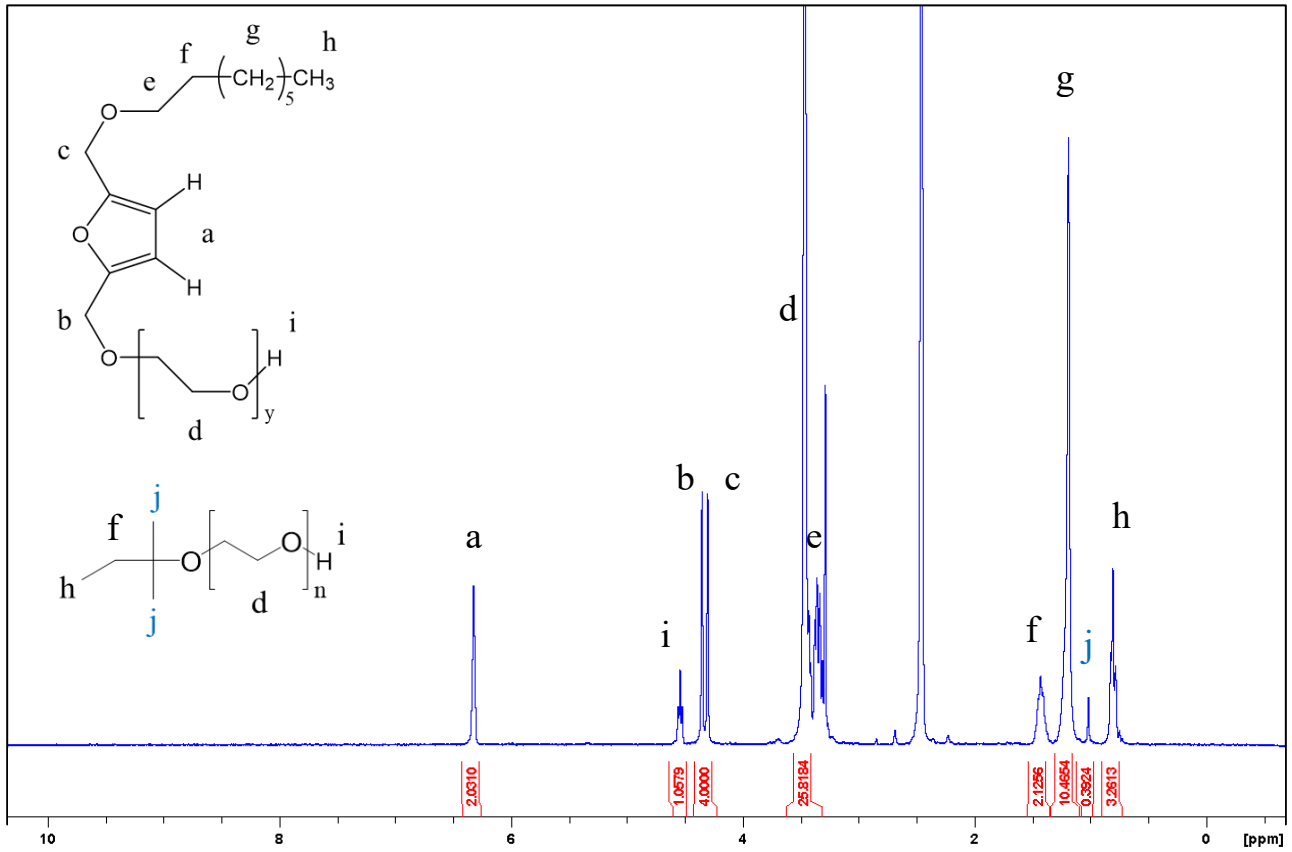

Figure A2.10. 300 MHz ^{1}H NMR spectrum of C_8-F-EO_6 in d_6-DMSO: δ 6.3 (s, 2H), 4.6 (t, 1H), 4.4 (s, 2H), 4.3 (s, 2H), 3.5 (m, 24H), 3.3 (t, 2H), 1.4 (p, 2H), 1.2 (m, 10H), 1.0 (s, 6H), 0.8 (t, 3H). Residual solvent peaks are found at 2.5 ppm for DMSO and 3.3 ppm for water.

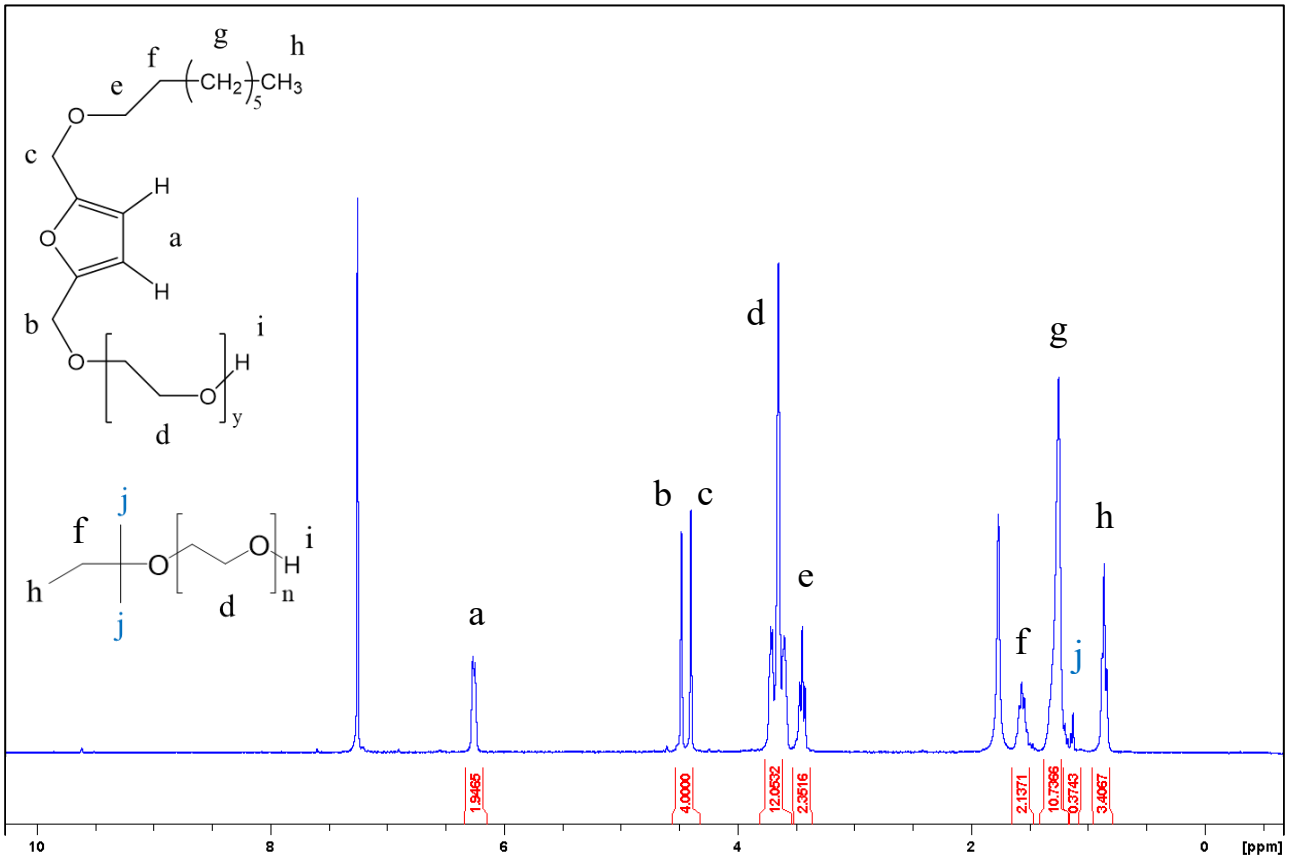

Figure A2.11. 300 MHz ^{1}H NMR spectrum of C_8-F-EO_3 in chloroform-*d*: δ 6.2 (d, 2H), 4.5 (s, 2H), 4.4 (s, 2H), 3.6 (m, 12H), 3.4 (t, 2H), 1.6 (p, 2H), 1.3 (m, 10H), 1.1 (s, 6H), 0.9 (t, 3H). Residual solvent peaks are found at 7.3 ppm for chloroform and 1.8 ppm for water.

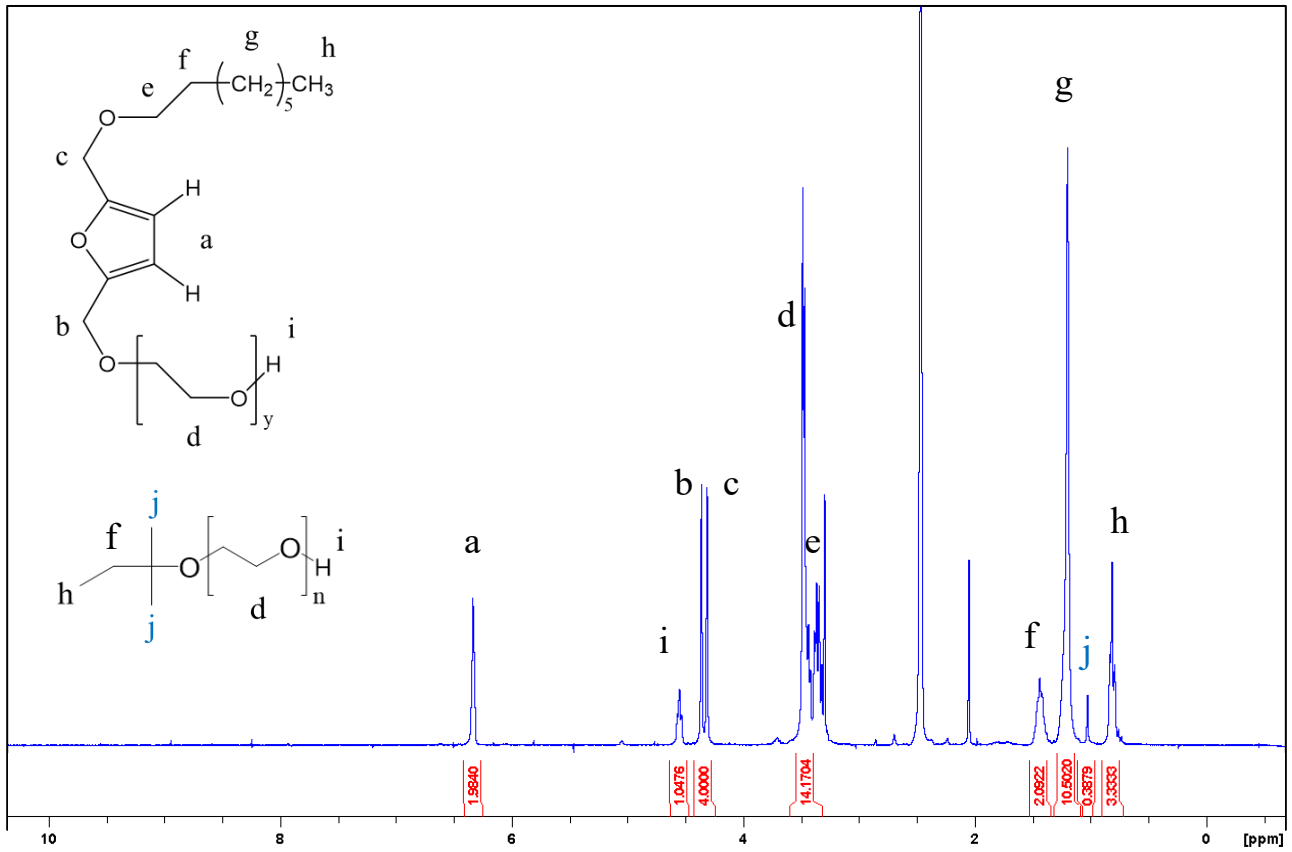

Figure A2.12. 300 MHz ^{1}H NMR spectrum of C_8-F-EO_3 in d_6-DMSO: δ 6.3 (s, 2H), 4.6 (t, 1H), 4.4 (s, 2H), 4.3 (s, 2H), 3.5 (m, 12H), 3.3 (t, 2H), 1.4 (p, 2H), 1.2 (m, 10H), 1.0 (s, 6H), 0.8 (t, 3H). Residual solvent peaks are found at 2.5 ppm for DMSO, 2.1 ppm for acetone, and 3.3 ppm for water.

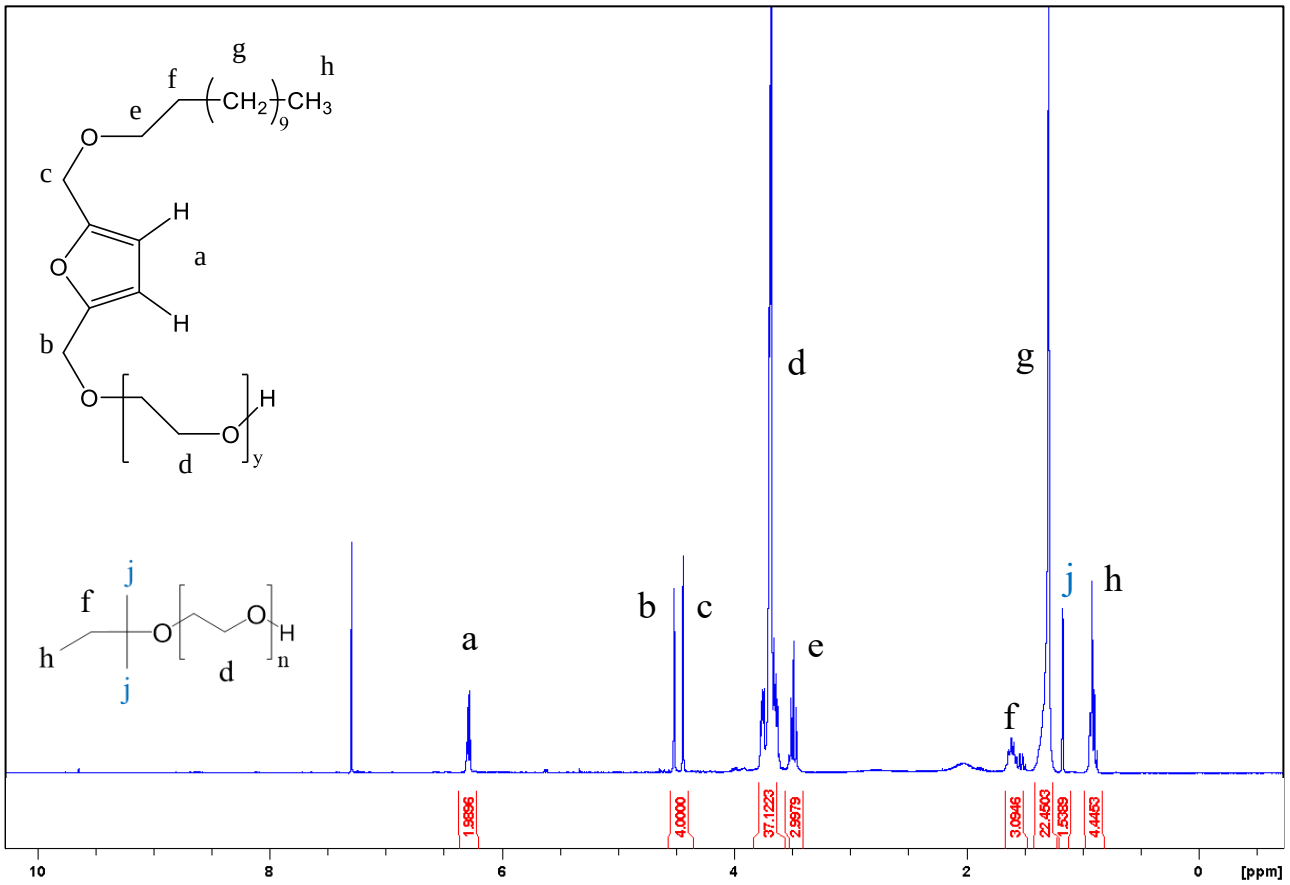

Figure A2.13. 300 MHz ^{1}H NMR spectrum of C_{12}-F-EO_8 in chloroform-*d*: δ 6.2 (d, 2H), 4.5 (s, 2H), 4.4 (s, 2H), 3.6 (m, 28H), 3.4 (t, 2H), 1.6 (p, 2H), 1.3 (m, 18H), 1.1 (s, 6H), 0.9 (t, 3H). Residual solvent peaks are found at 7.3 ppm for chloroform and 2.0 ppm for water.

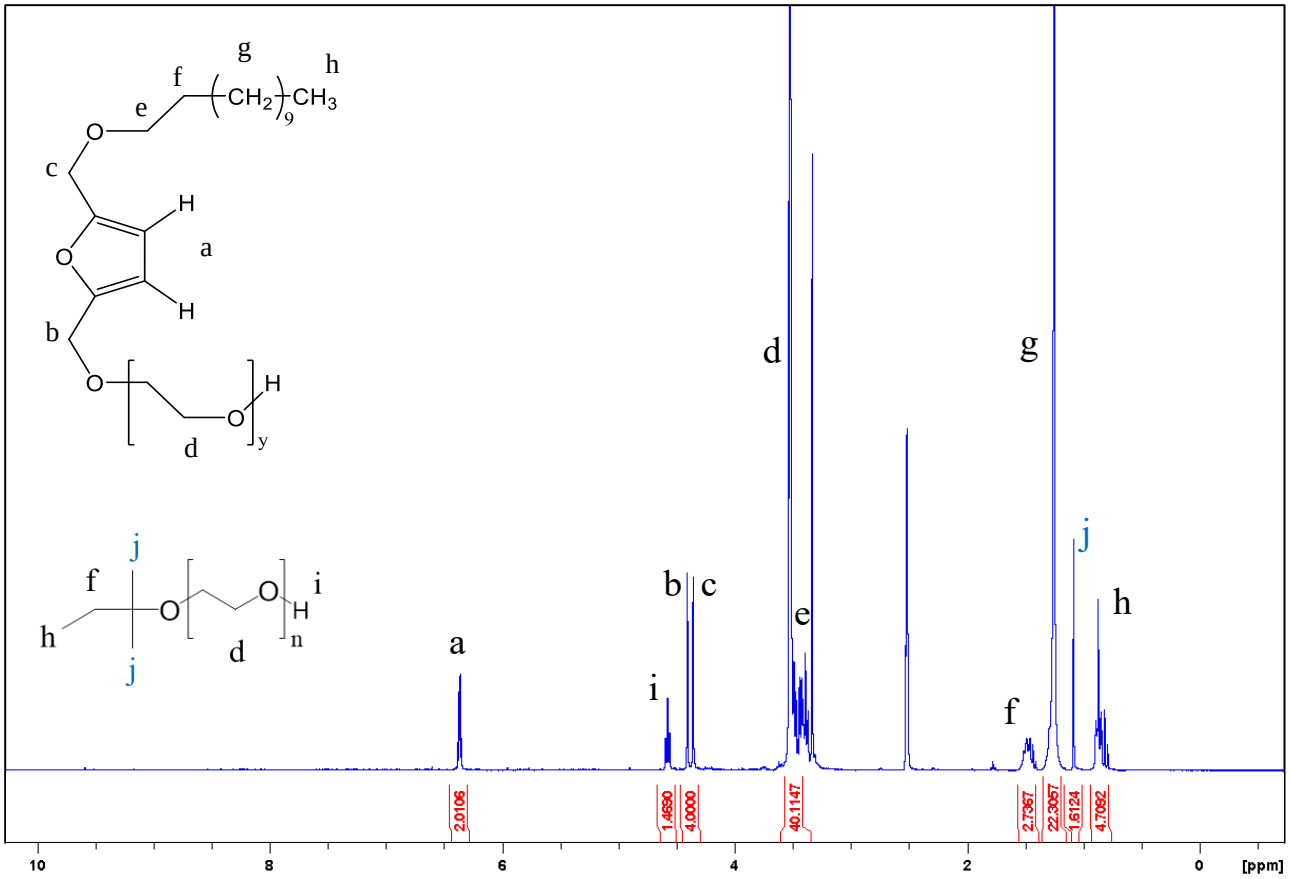

Figure A2.14. 300 MHz ^{1}H NMR spectrum of C_{12}-F-EO_8 in *d*$_6$-DMSO: δ 6.3 (s, 2H), 4.6 (t, 1H), 4.4 (s, 2H), 4.3 (s, 2H), 3.5 (m, 28H), 3.3 (t, 2H), 1.4 (p, 2H), 1.2 (m, 18H), 1.0 (s, 6H), 0.8 (t, 3H). Residual solvent peaks are found at 2.5 ppm for DMSO, 1.8 ppm for THF, and 3.3 ppm for water.

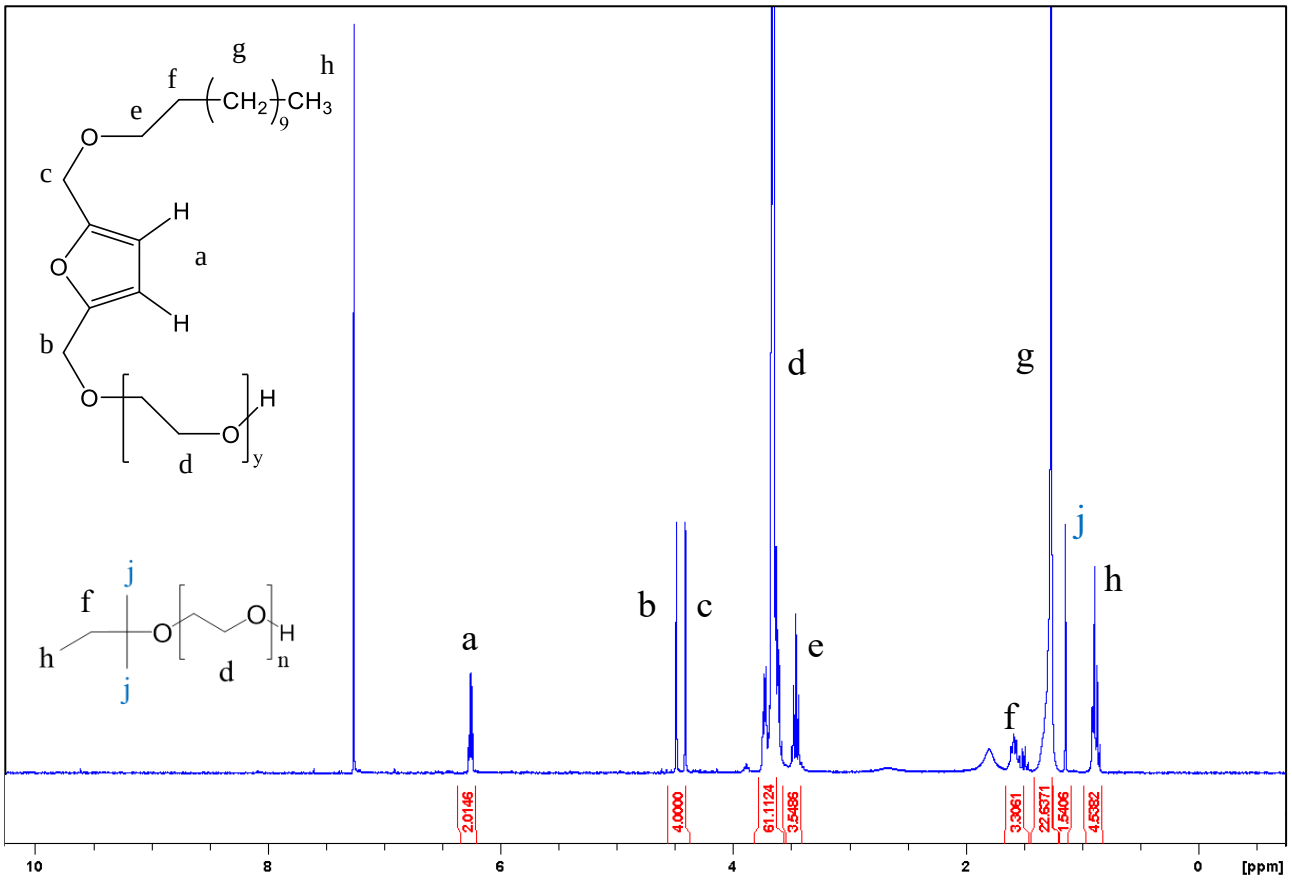

Figure S2.15. 300 MHz ^{1}H NMR spectrum of C_{12}-F-EO_{13} in chloroform-*d*: δ 6.2 (d, 2H), 4.5 (s, 2H), 4.4 (s, 2H), 3.6 (m, 48H), 3.4 (t, 2H), 1.6 (p, 2H), 1.3 (m, 18H), 1.1 (s, 6H), 0.9 (t, 3H). Residual solvent peaks are found at 7.3 ppm for chloroform and 2.1 ppm for water.

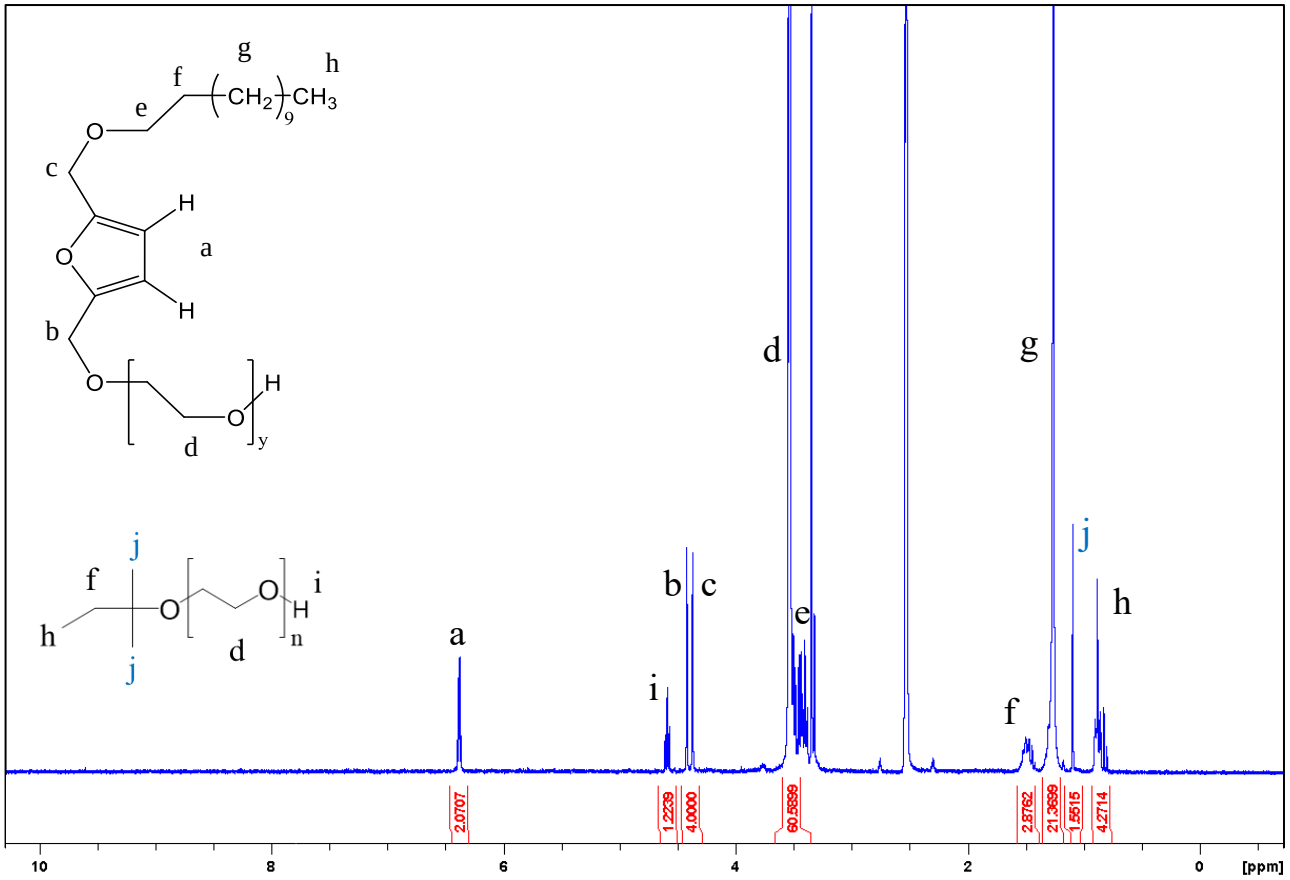

Figure A2.16. 300 MHz ^{1}H NMR spectrum of C_{12}-F-EO_{13} in *d*$_6$-DMSO: δ 6.3 (s, 2H), 4.6 (t, 1H), 4.4 (s, 2H), 4.3 (s, 2H), 3.5 (m, 48H), 3.3 (t, 2H), 1.4 (p, 2H), 1.2 (m, 18H), 1.0 (s, 6H), 0.8 (t, 3H). Residual solvent peaks are found at 2.5 ppm for DMSO and 3.3 ppm for water.

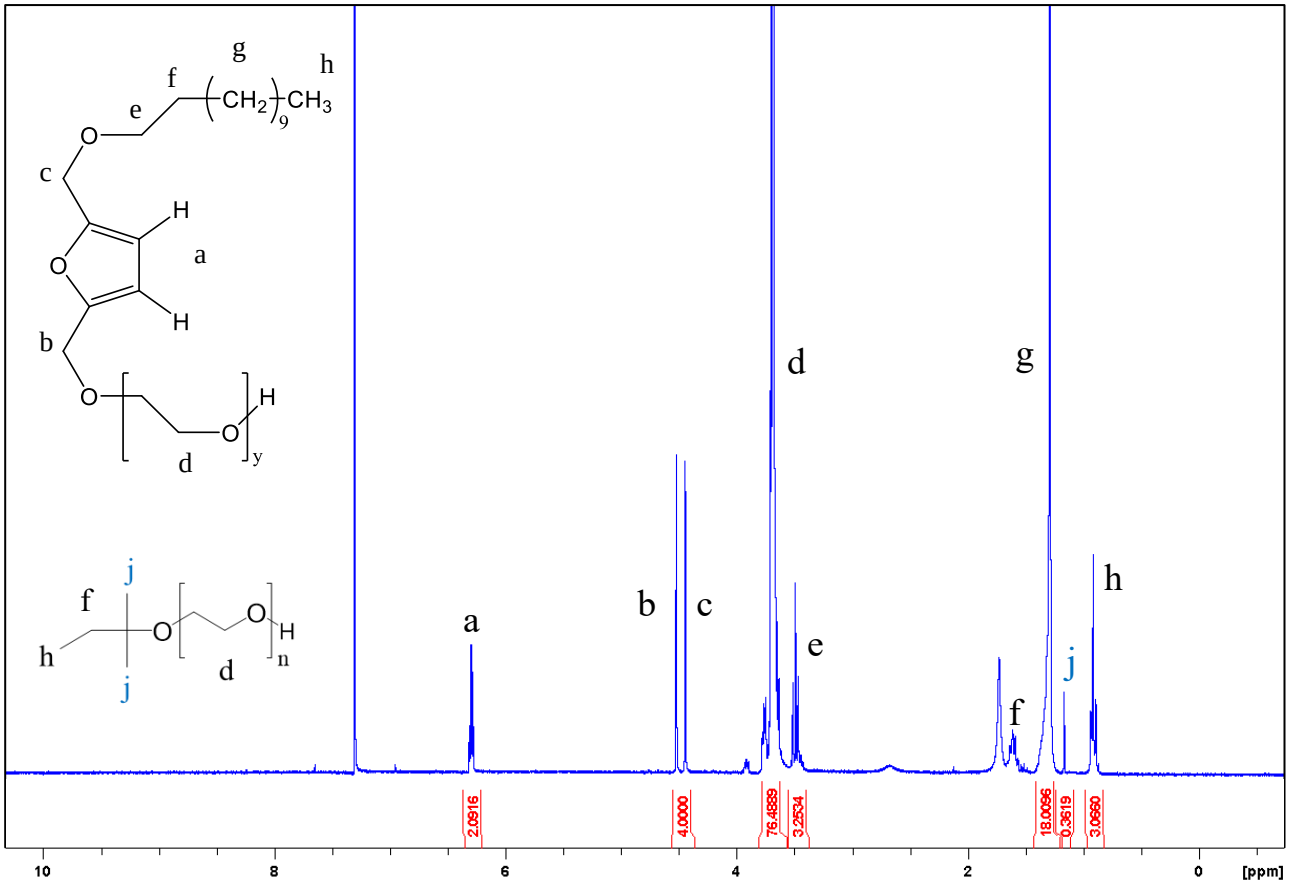

Figure A2.17. 300 MHz ^{1}H NMR spectrum of C_{12}-F-EO_{18} in chloroform-*d*: δ 6.2 (d, 2H), 4.5 (s, 2H), 4.4 (s, 2H), 3.6 (m, 72H), 3.4 (t, 2H), 1.6 (p, 2H), 1.3 (m, 18H), 1.1 (s, 6H), 0.9 (t, 3H). Residual solvent peaks are found at 7.3 ppm for chloroform and 1.7 ppm for water.

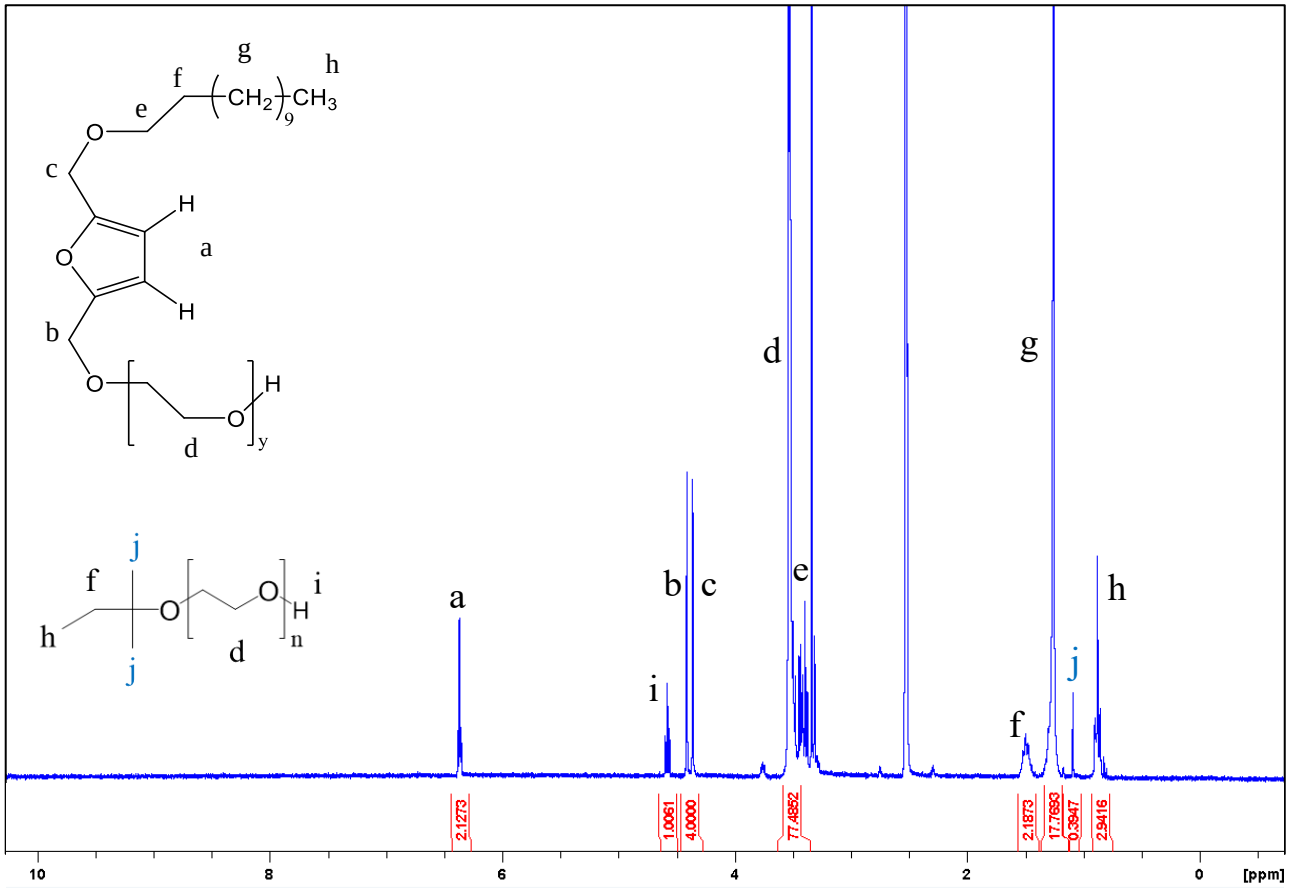

Figure A2.18. 300 MHz ^{1}H NMR spectrum of C_{12}-F-EO_{18} in d_6-DMSO: δ 6.3 (s, 2H), 4.6 (t, 1H), 4.4 (s, 2H), 4.3 (s,2H), 3.5 (m, 72H), 3.3 (t, 2H), 1.4 (p, 2H), 1.2 (m, 18H), 1.0 (s, 6H), 0.8 (t, 3H). Residual solvent peaks are found at 2.5 ppm for DMSO and 3.3 ppm for water.

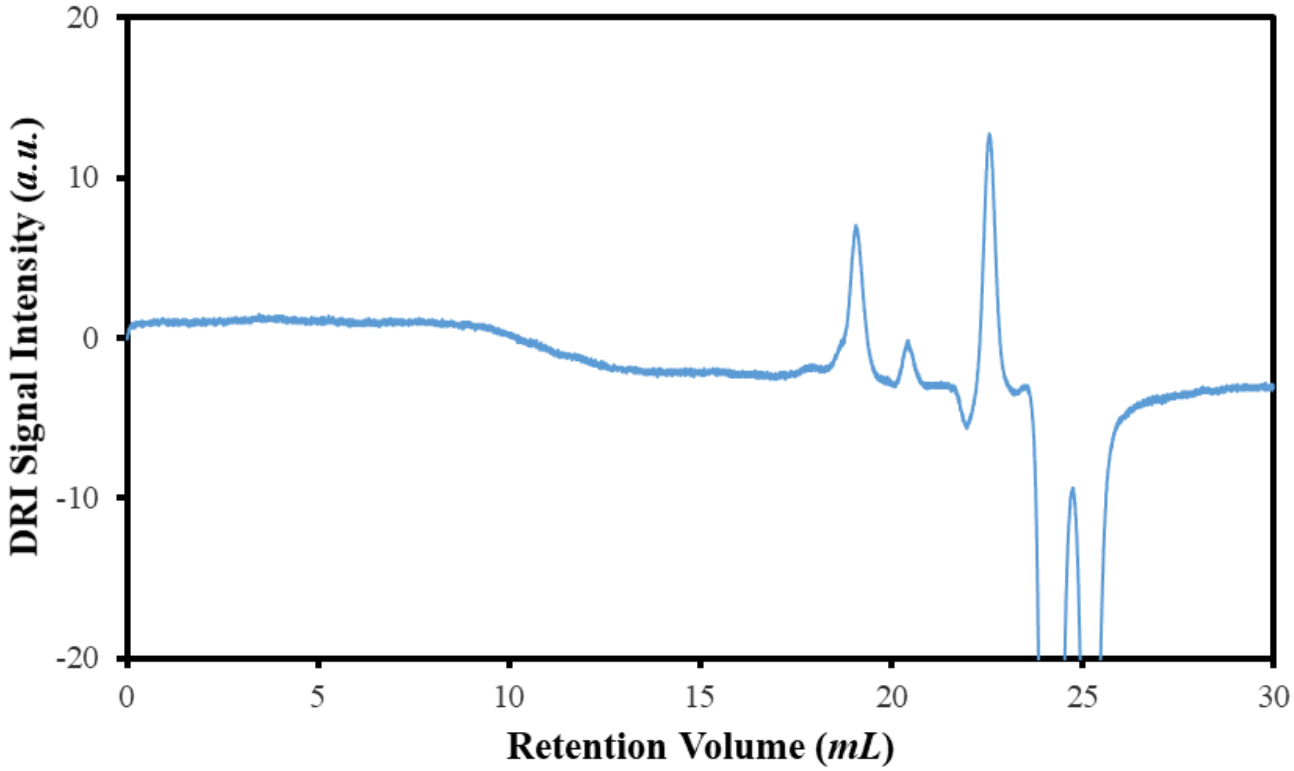

Figure A2.19. GPC trace obtained for THF solvent with the DRI detector.

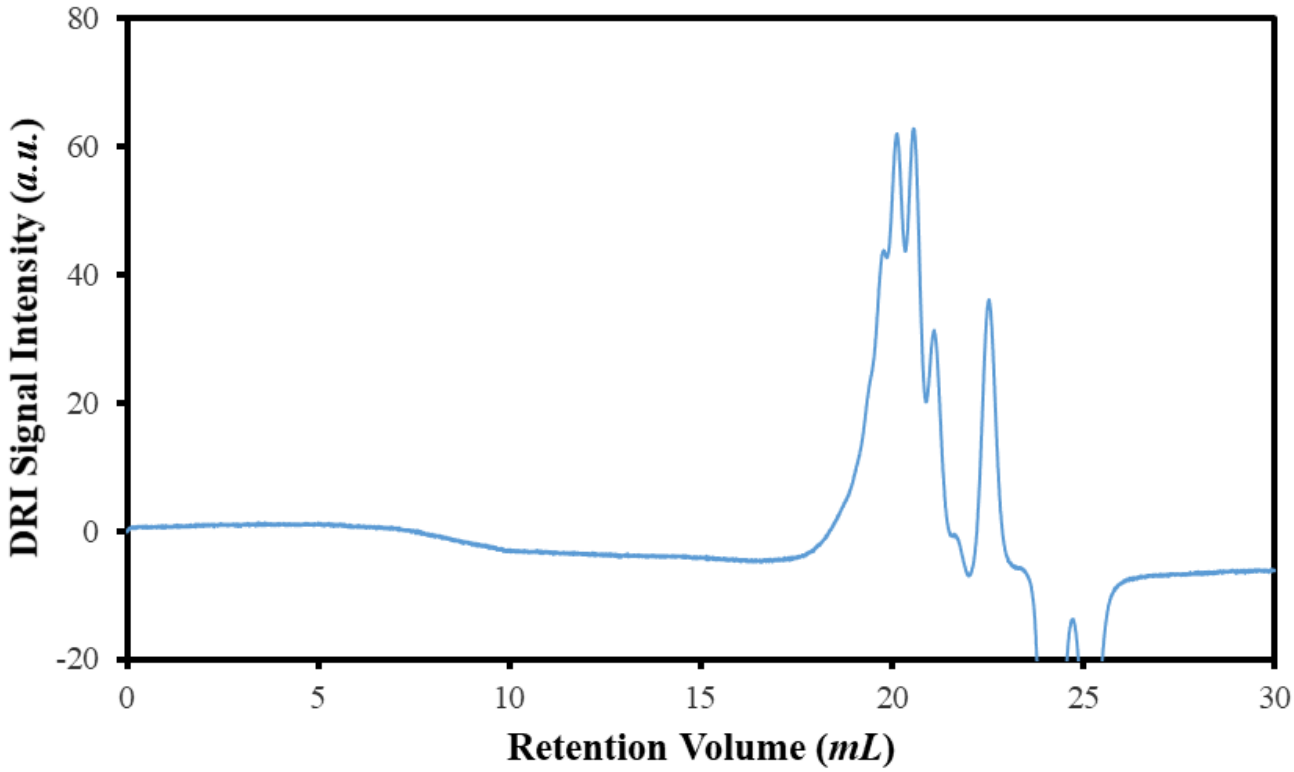

Figure A2.20. GPC trace obtained for Me-F-EO_3 with the DRI detector.

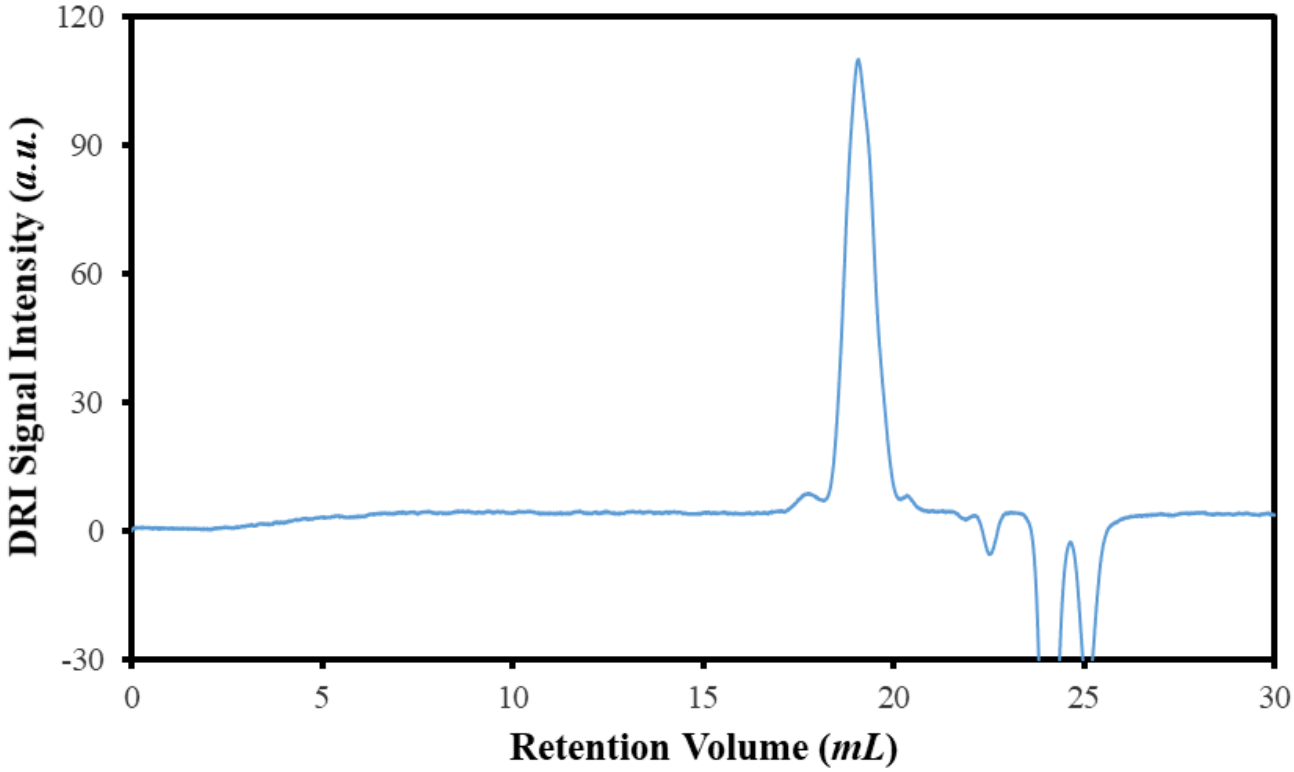

Figure A2.21. GPC trace obtained for Me-F-EO_6 with the DRI detector.

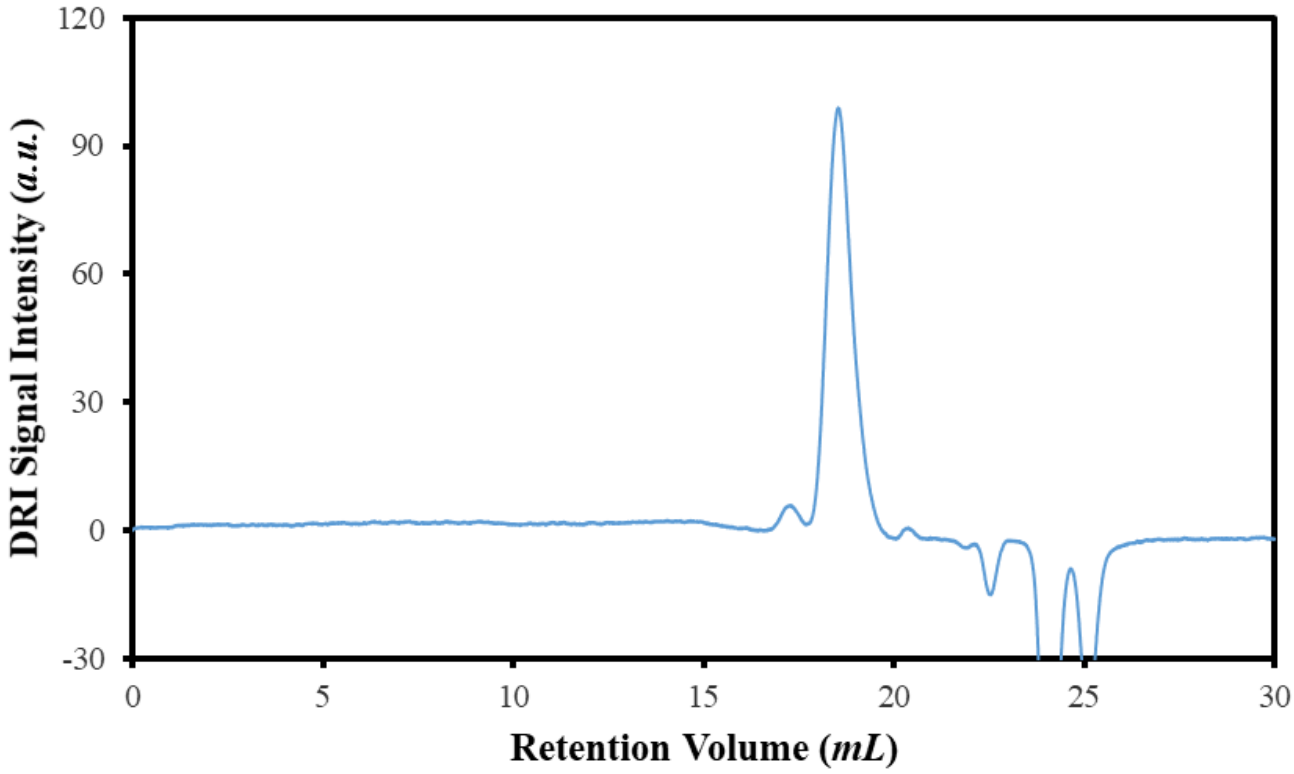

Figure A2.22. GPC trace obtained for Me-F-EO_8 with the DRI detector.

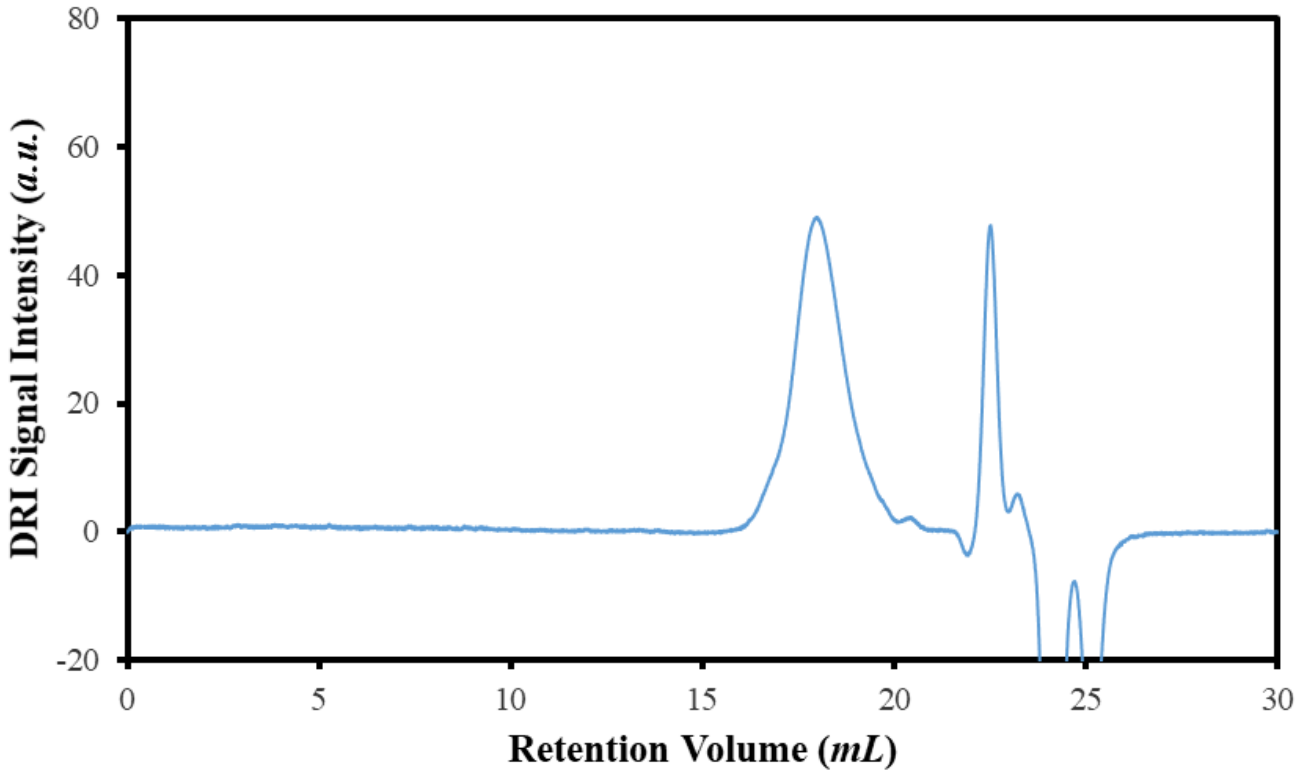

Figure A2.23. GPC trace obtained for Me-F-EO_{10} with the DRI detector.

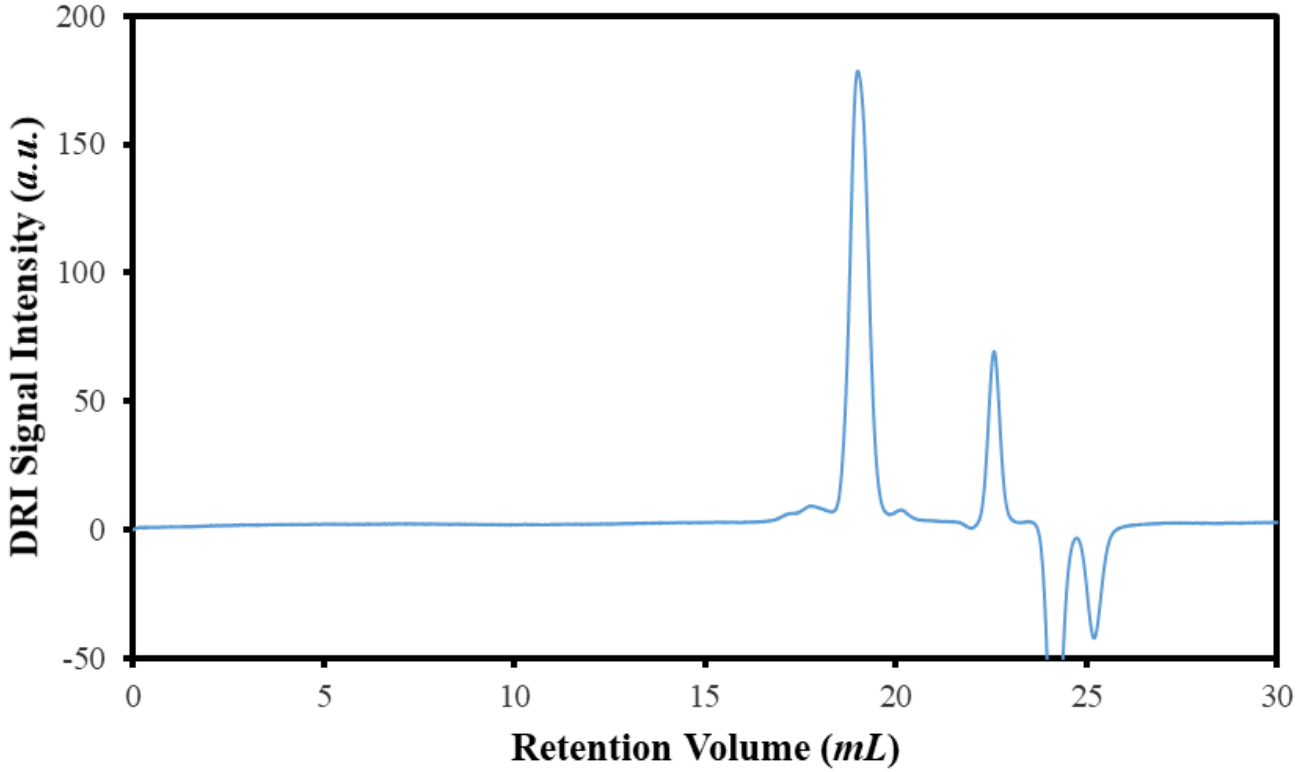

Figure A2.24. GPC trace obtained for C_8-F-EO_3 with the DRI detector.

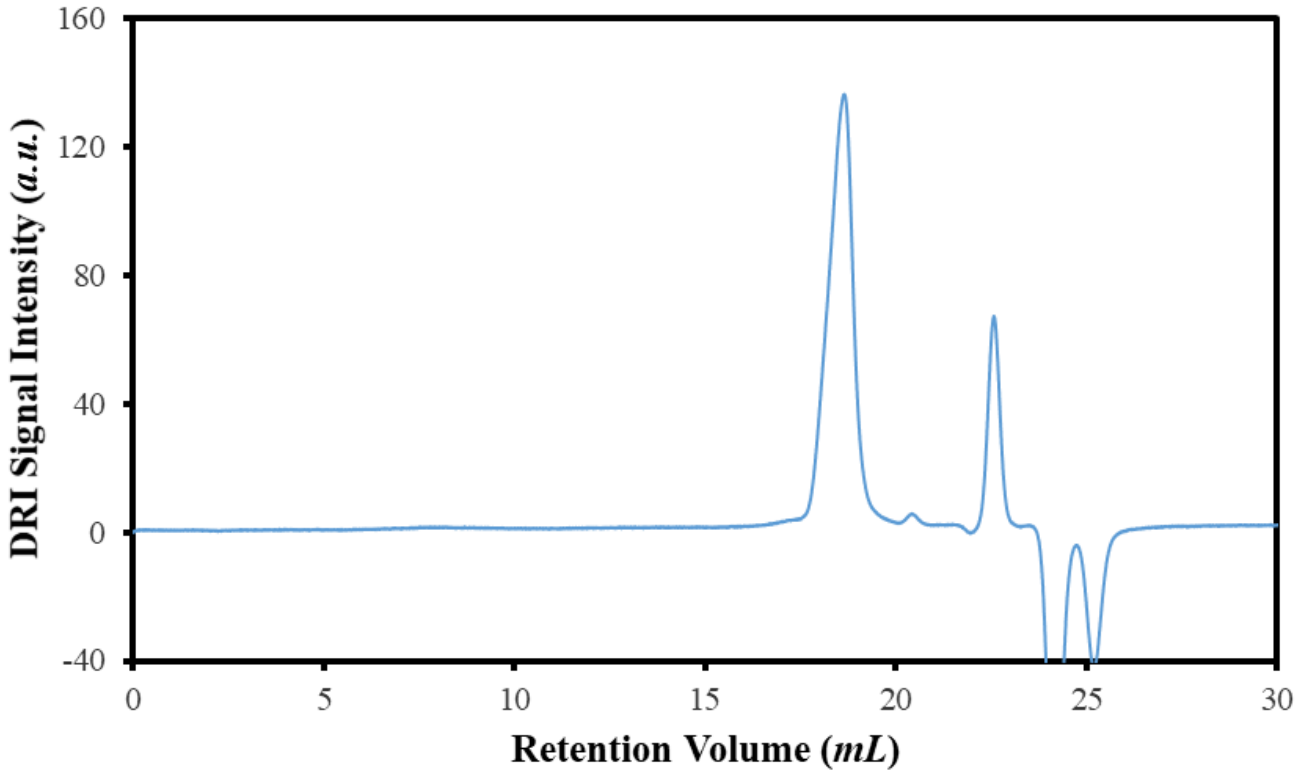

Figure A2.25. GPC trace obtained for C_8-F-EO_6 with the DRI detector.

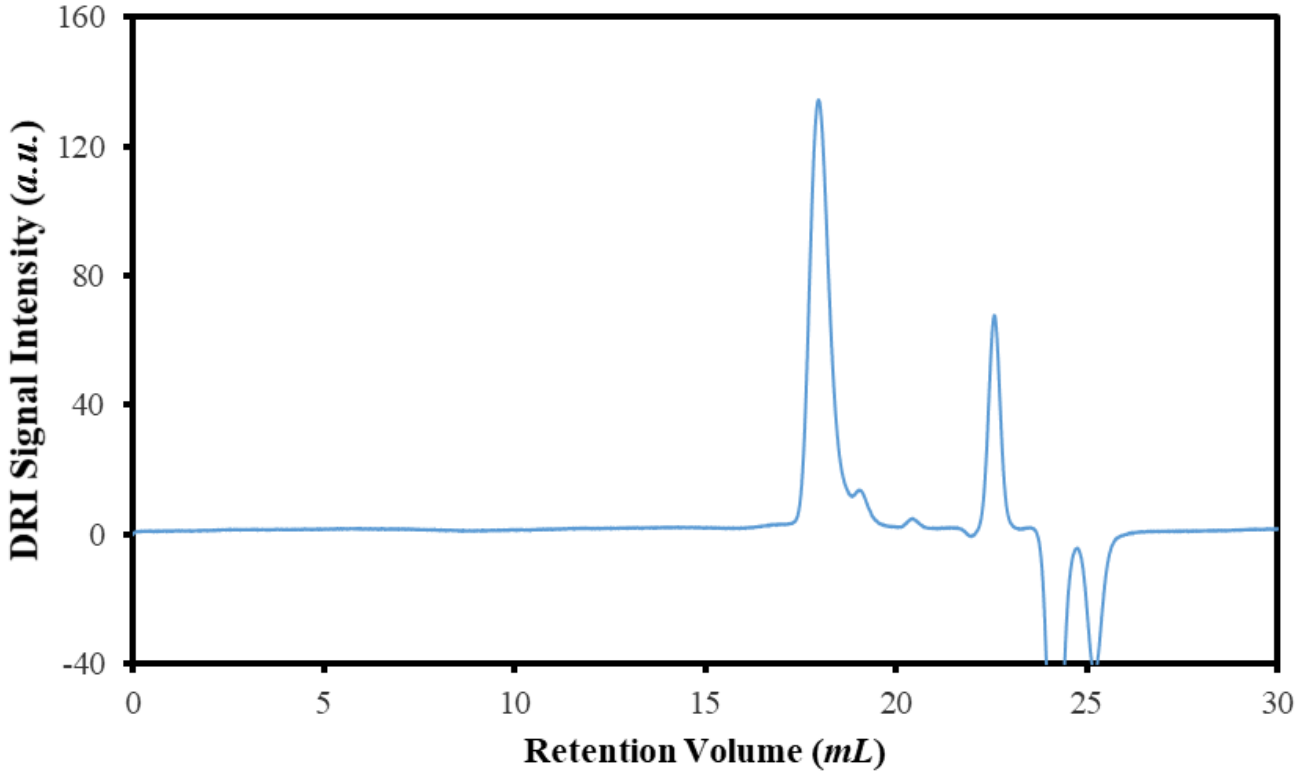

Figure A2.26. GPC trace obtained for C_8-F-EO_{10} with the DRI detector.

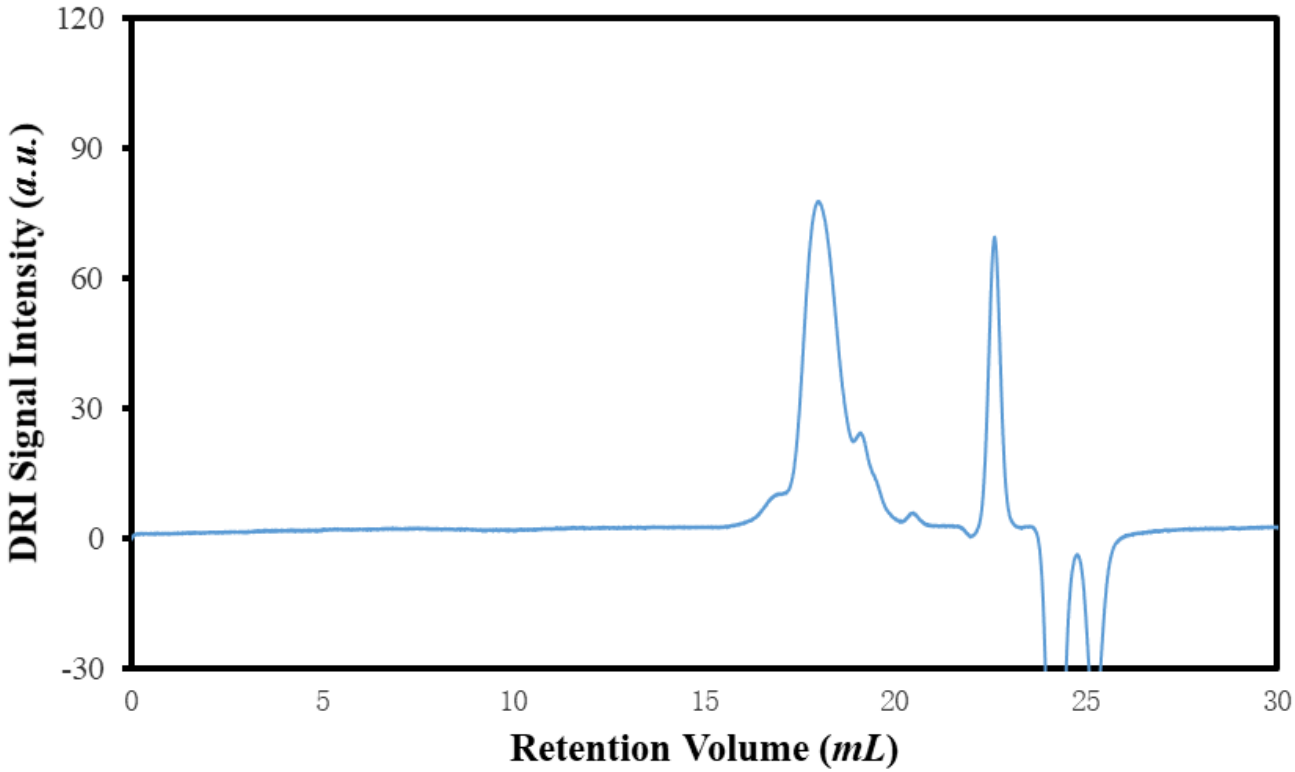

Figure A2.27. GPC trace obtained for C_{12}-F-EO_8 with the DRI detector.

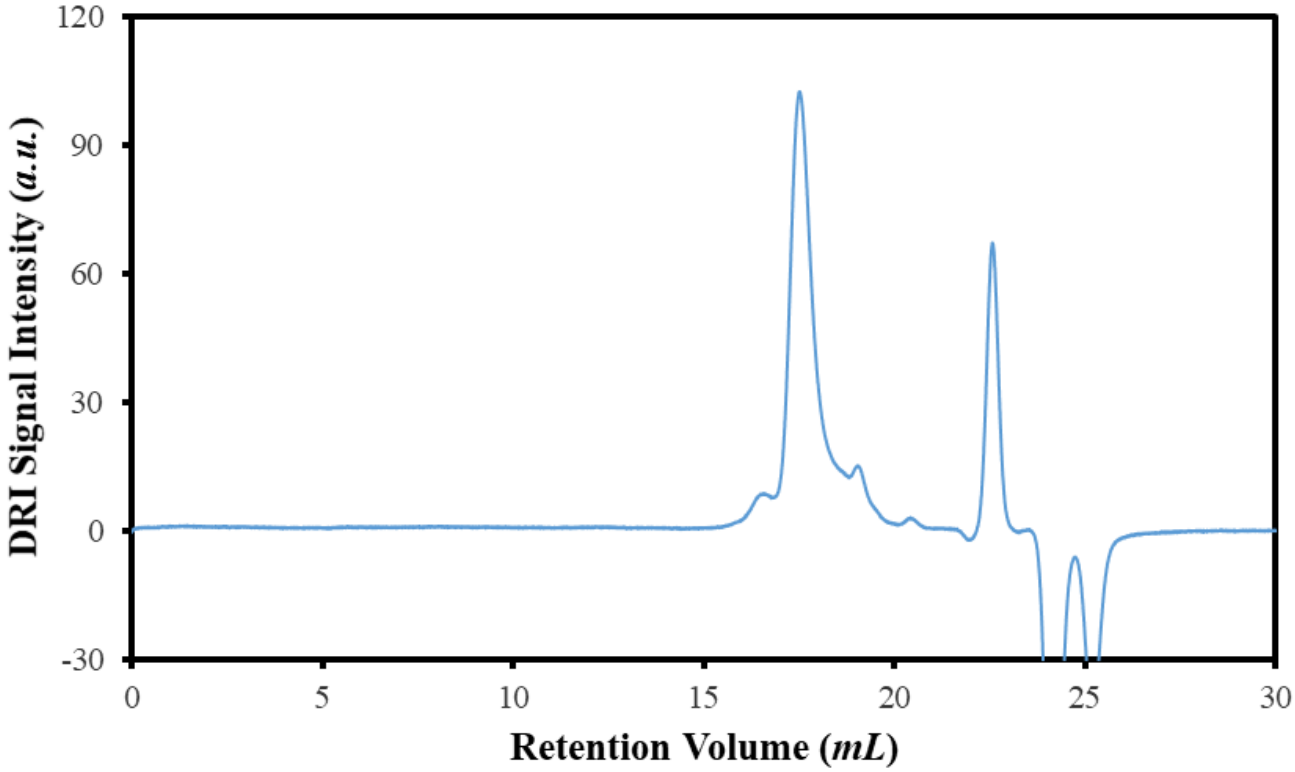

Figure A2.28. GPC trace obtained for C_{12}-F-EO_{13} with the DRI detector.

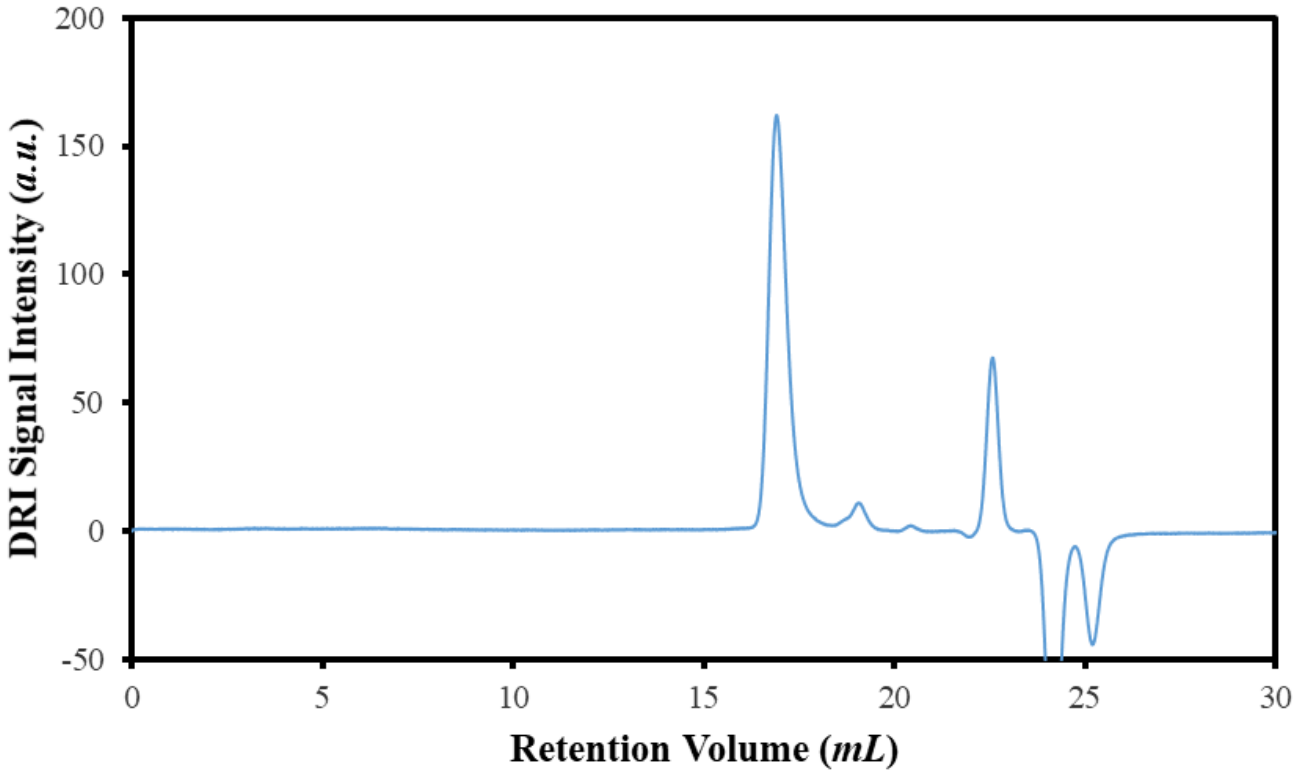

Figure A2.29. GPC trace obtained for C_{12}-F-EO_{18} with the DRI detector.

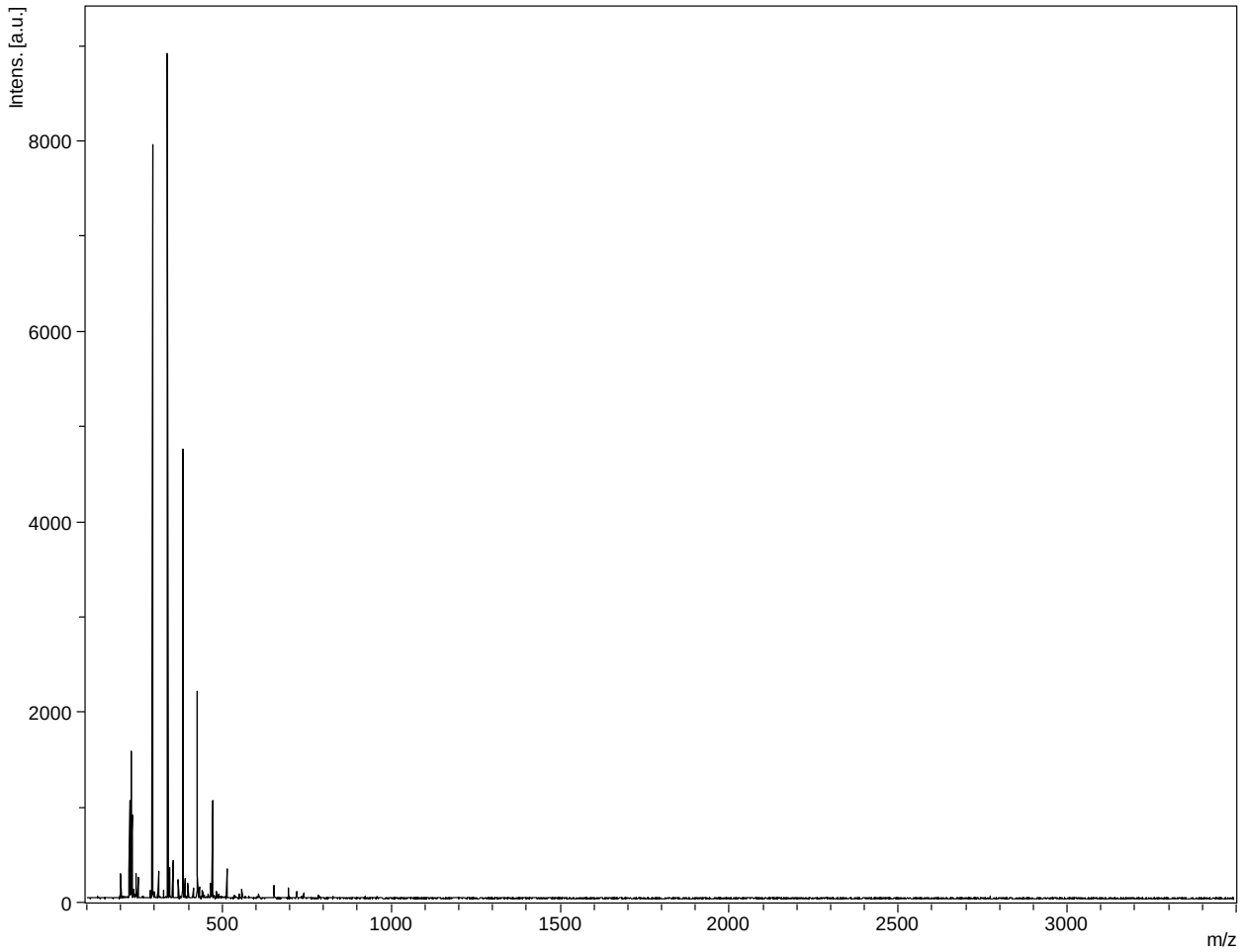

Figure A2.30. MALDI-ToF MS of Me-F-EO_3. Minor peaks are generated by complexes formed between Me-F-EO_3 and sodium or potassium ions present in the synthesis and purification processes.

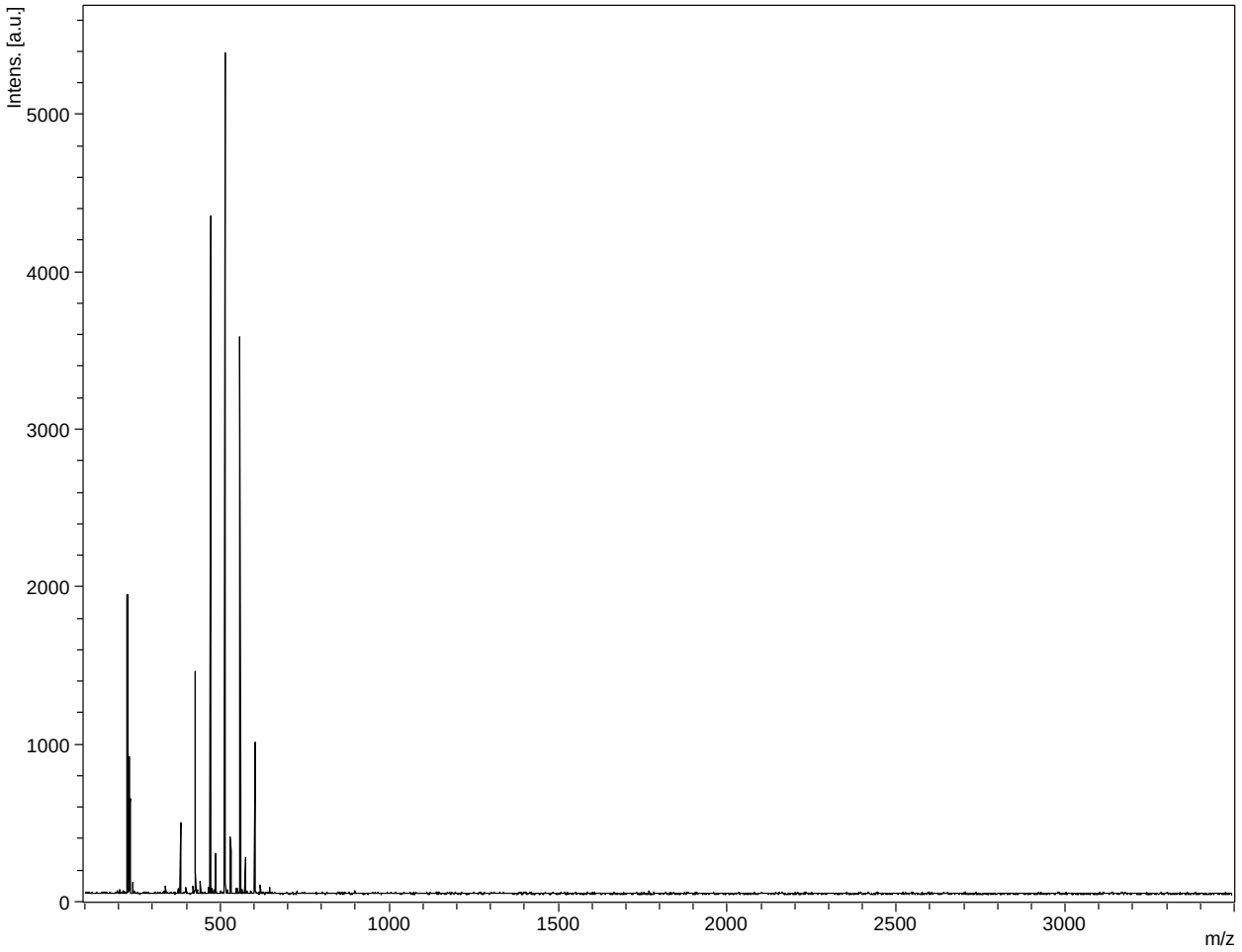

Figure A2.31. MALDI-ToF MS of Me-F-EO_6. Minor peaks are generated by complexes formed between Me-F-EO_6 and sodium or potassium ions present in the synthesis and purification processes.

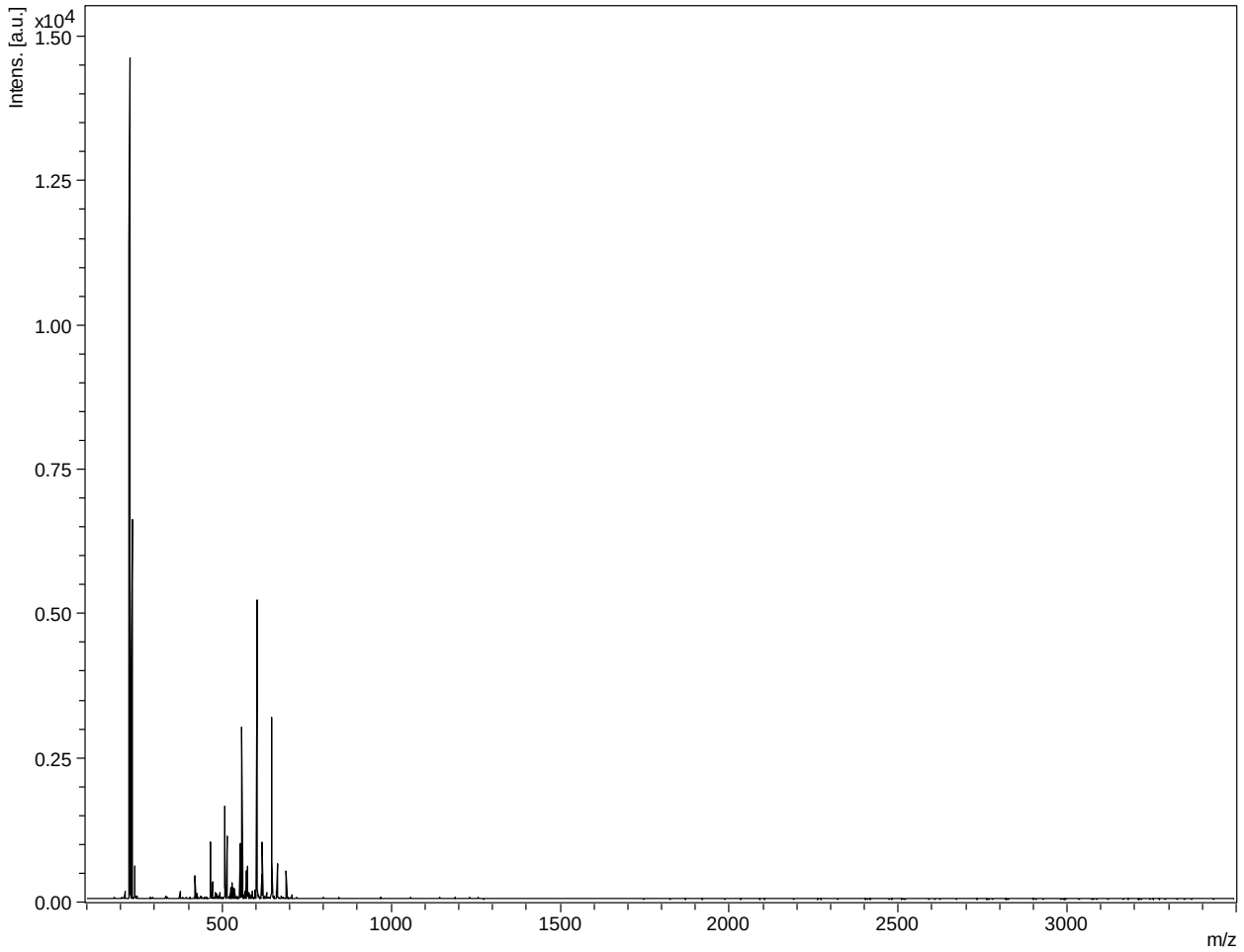

Figure A2.32. MALDI-ToF MS spectrum of Me-F-EO_8. Minor peaks are generated by complexes formed between Me-F-EO_8 and sodium or potassium ions present in the synthesis and purification processes.

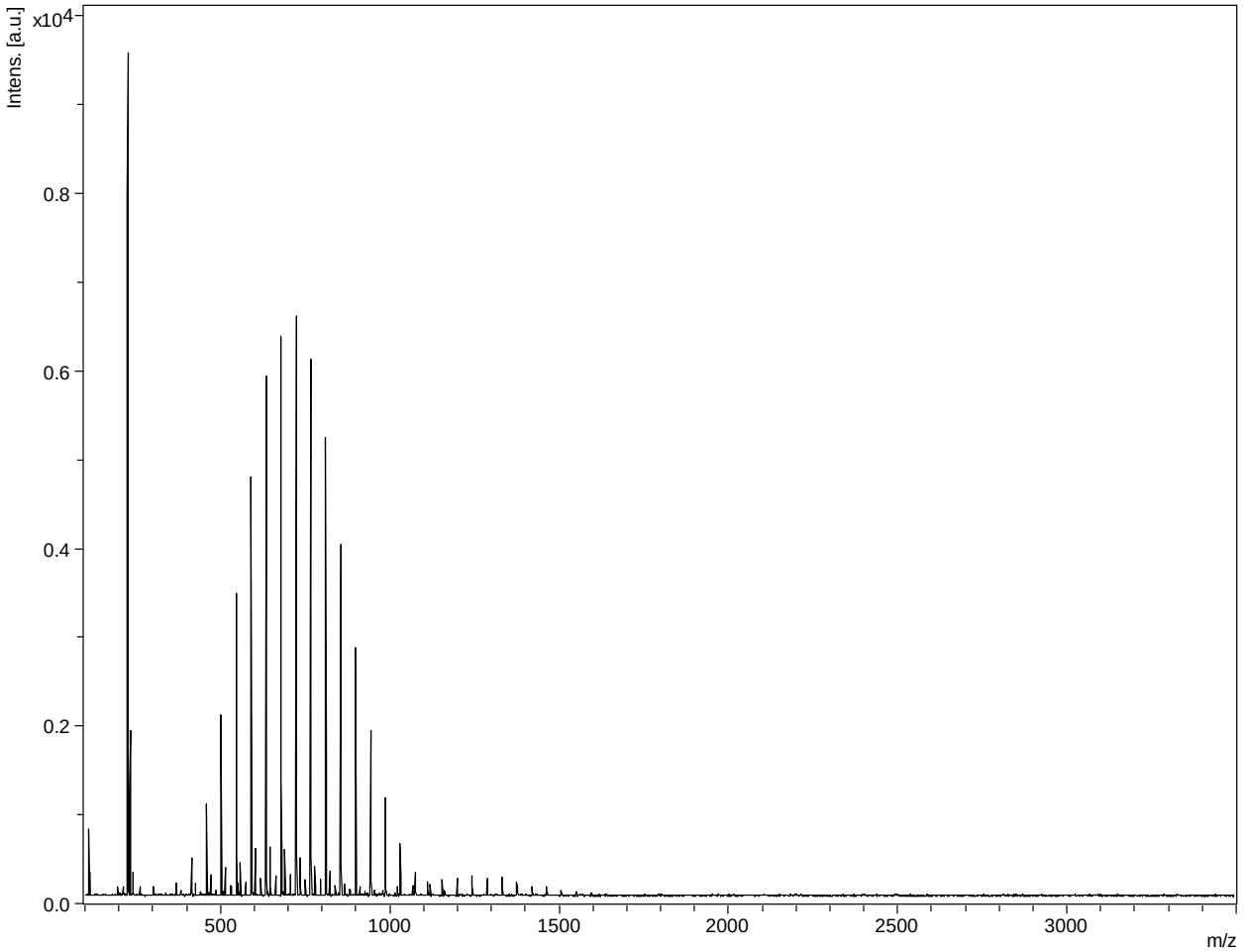

Figure A2.33. MALDI-ToF MS of Me-F-EO_{10}. Major peaks are generated by complexes formed between Me-F-EO_{10} and potassium ions present in the purification processes. Complexes also form between Me-F-EO_{10} and lithium or sodium ions.

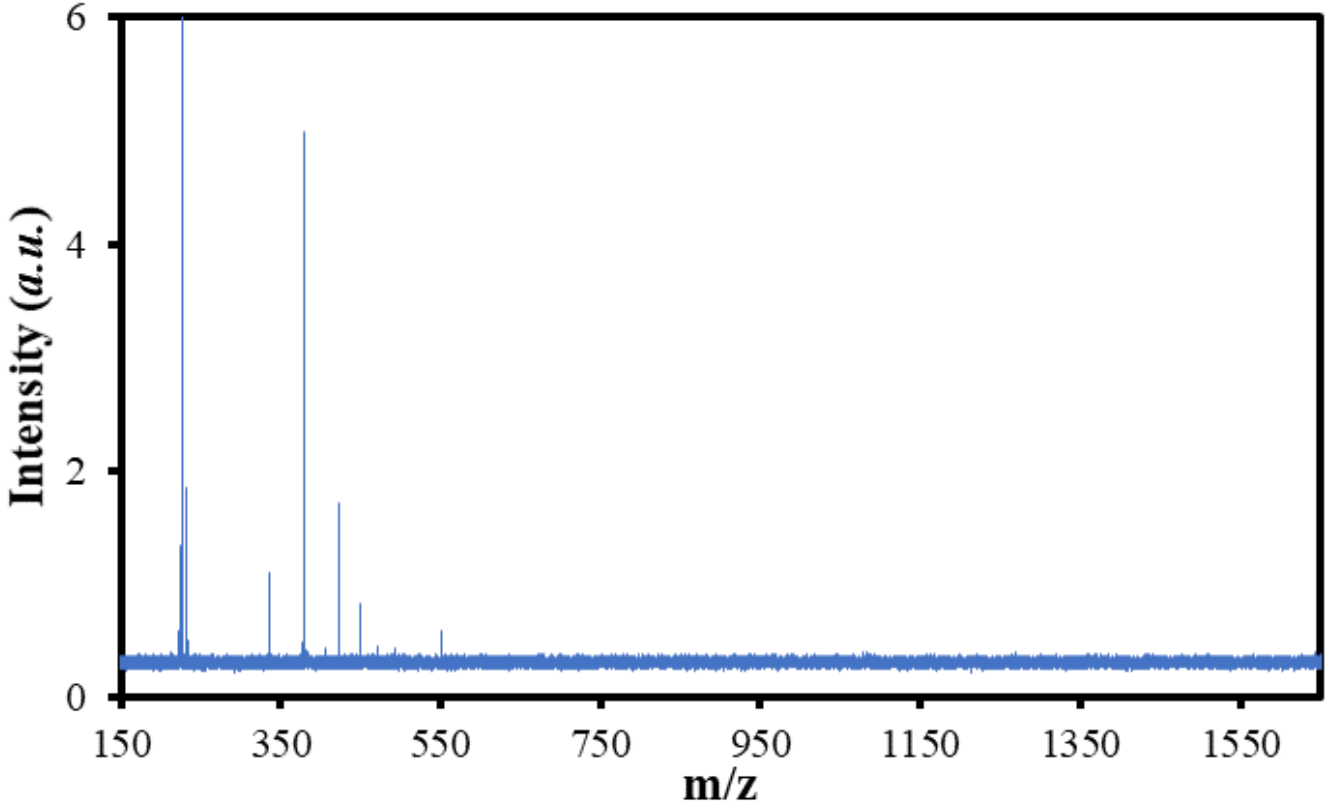

Figure A2.34. MALDI-ToF MS of C_8-F-EO_3.

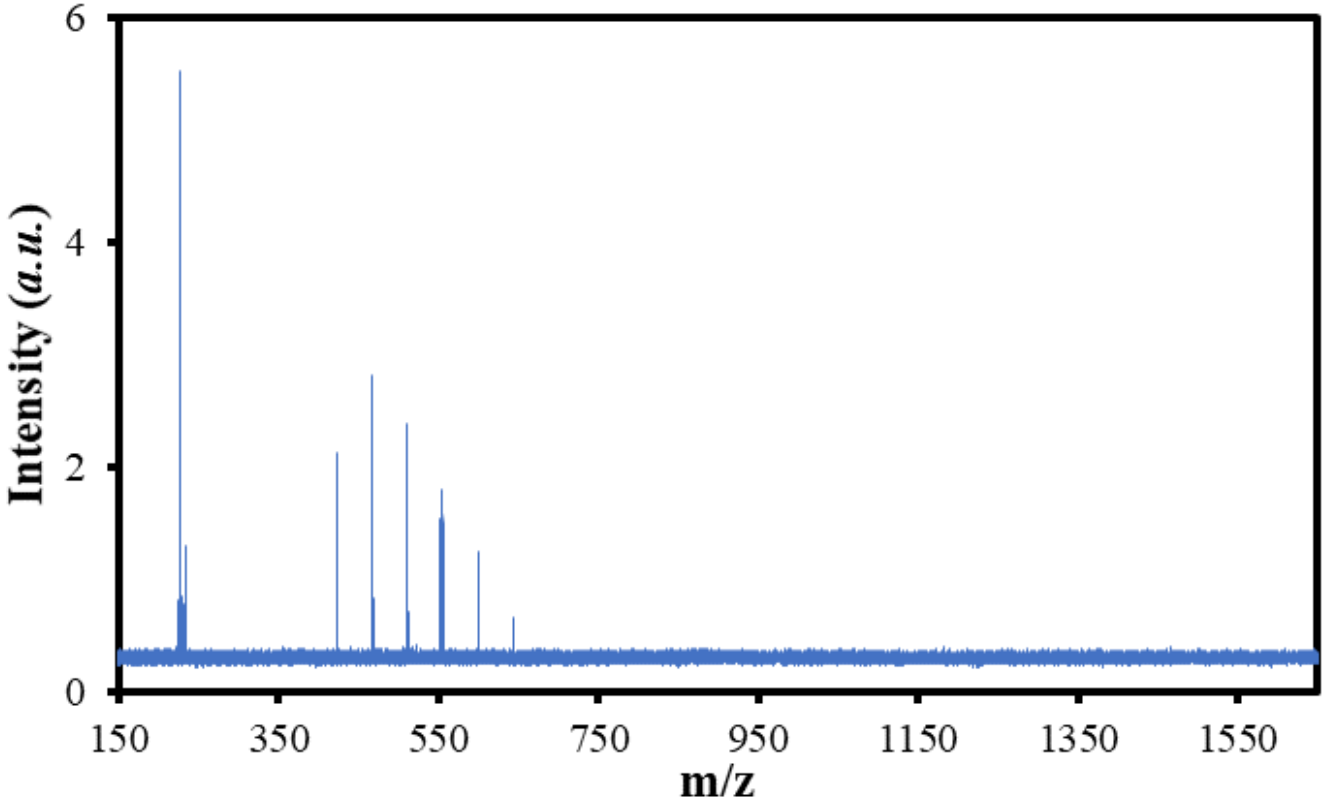

Figure A2.35. MALDI-ToF MS of C_8-F-EO_6.

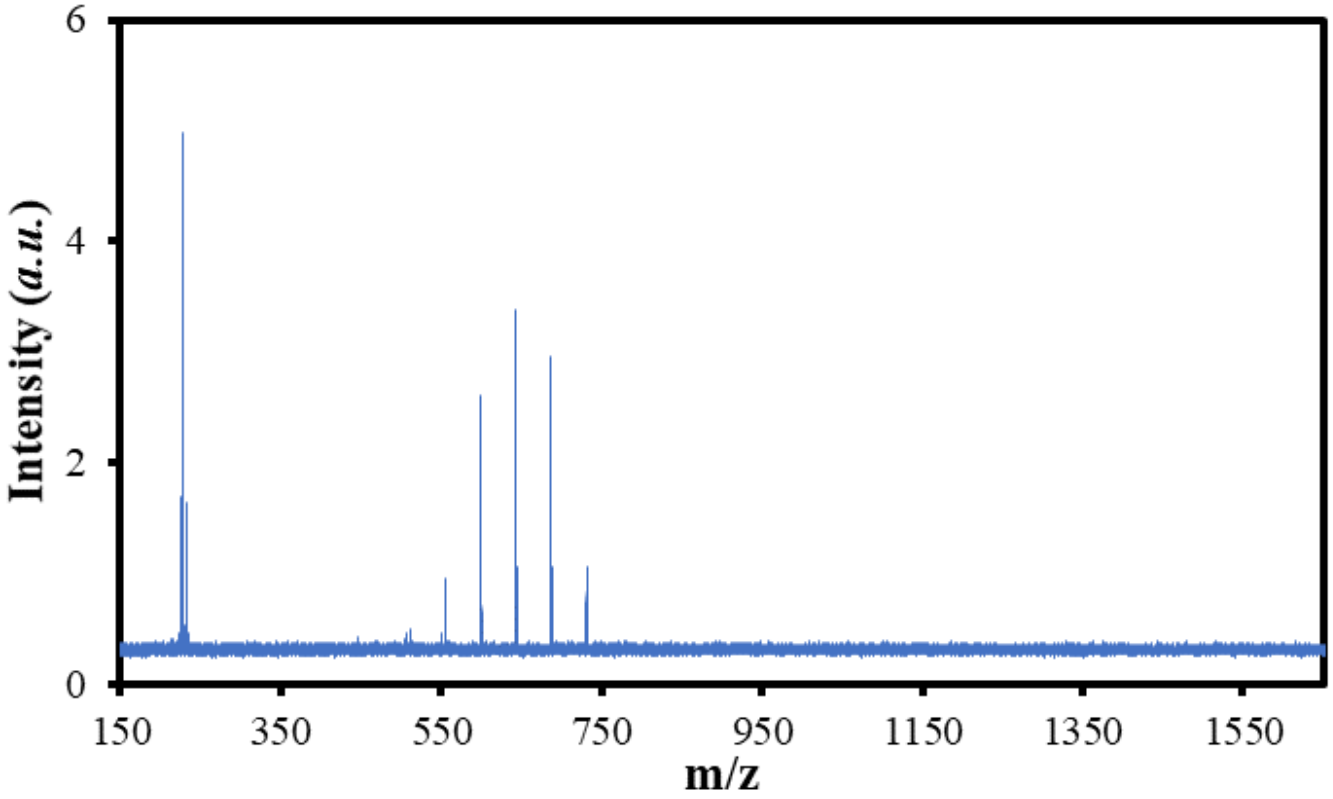

Figure A2.36. MALDI-ToF MS of C_8-F-EO_{10}.

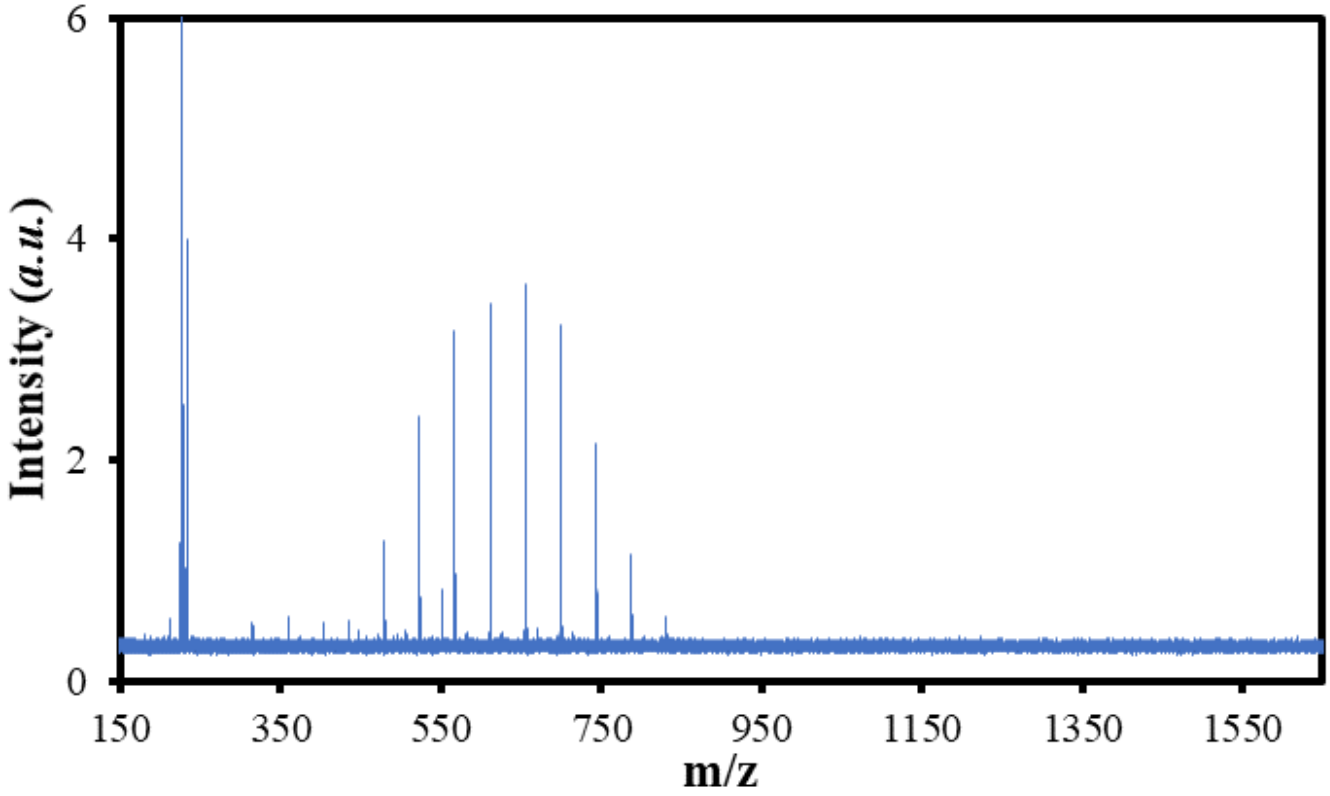

Figure A2.37. MALDI-ToF MS of C_{12}-F-EO_8. *tert*-Pentoxide-modified OEOs are observed as minor peaks in the 271 to 535 m/z range.

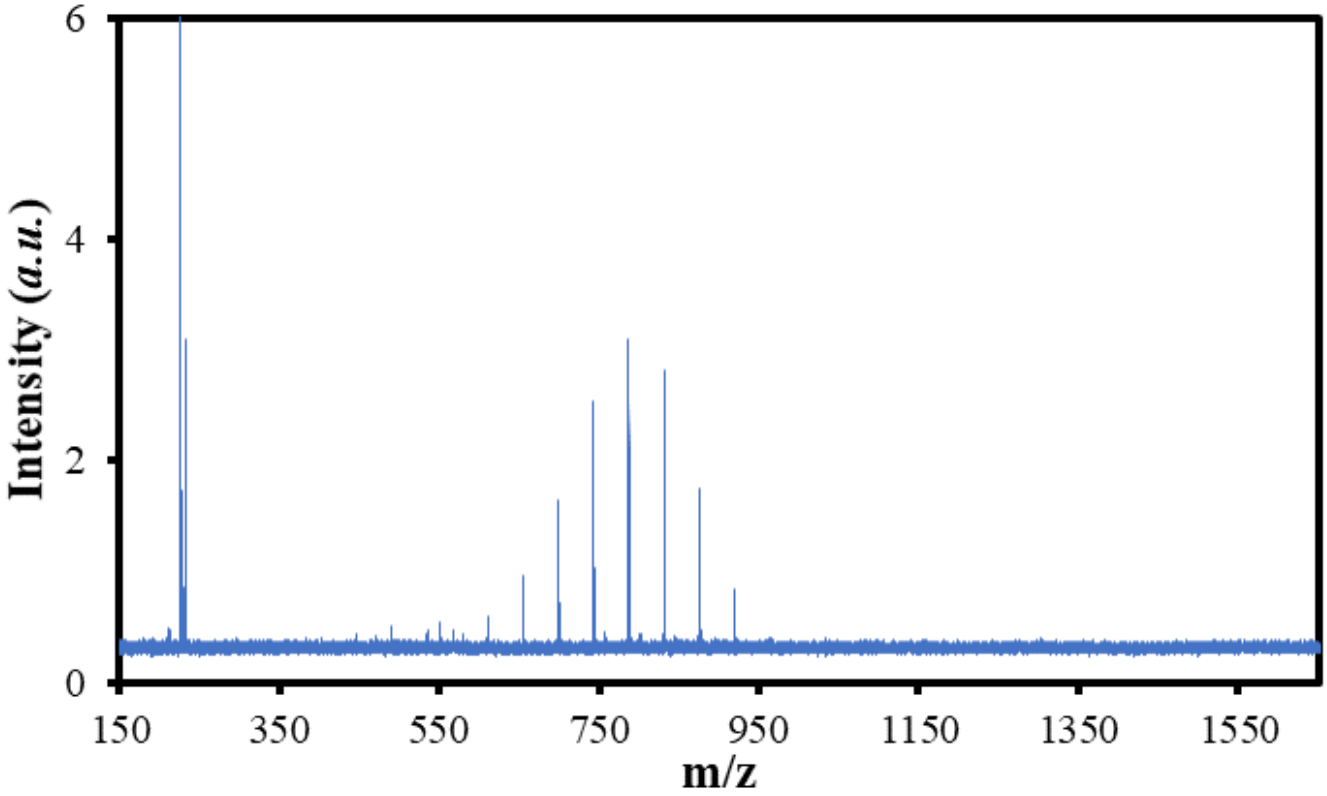

Figure A2.38. MALDI-ToF MS of C_{12}-F-EO_{13}. *tert*-Pentoxide-modified OEOs are observed as minor peaks in the 535 to 667 m/z range.

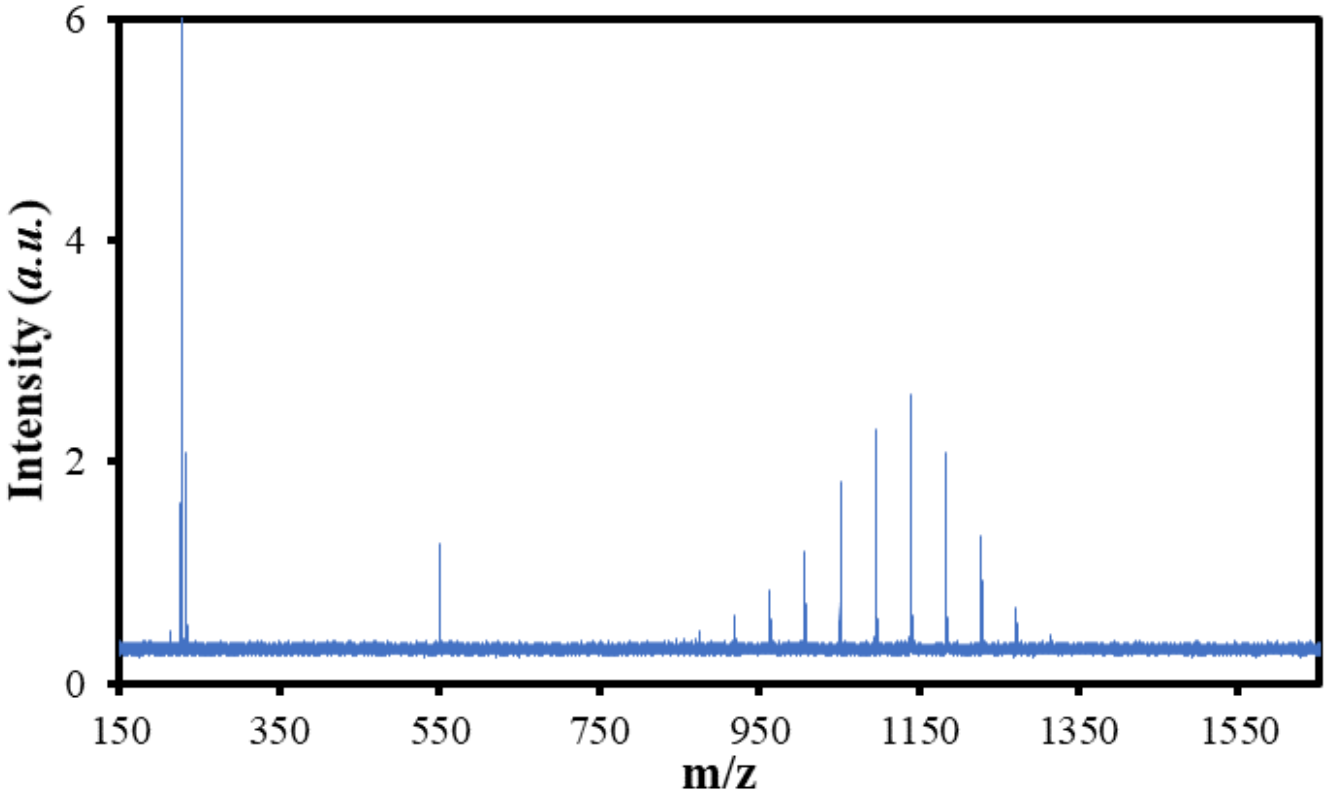

Figure S2.39. MALDI-ToF MS of C_{12}-F-EO_{18}.

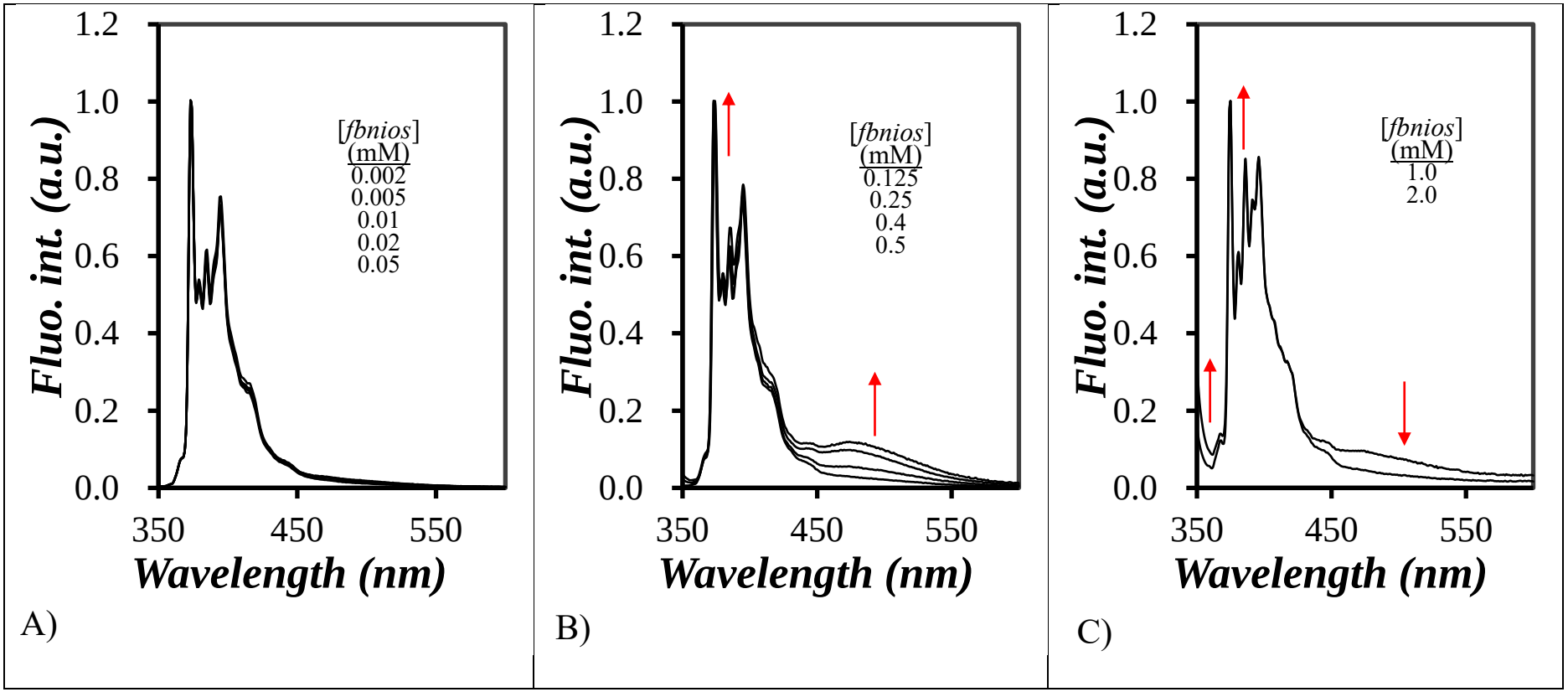

Figure A3.1. SSF spectra of 5×10^{-7} M pyrene in aqueous solutions of C_8-F-EO_3 at concentrationa ranging from A) 0.002 to 0.05 mM, B) 0.125 to 0.5 mM, and C) 1.0 to 2.0 mM. The turbidity of C_8-F-EO_3 solution significantly increases when C_8-F-EO_3 concentration is higher than 0.5 mM, so light scattering is observed in 350~365 nm range in C).

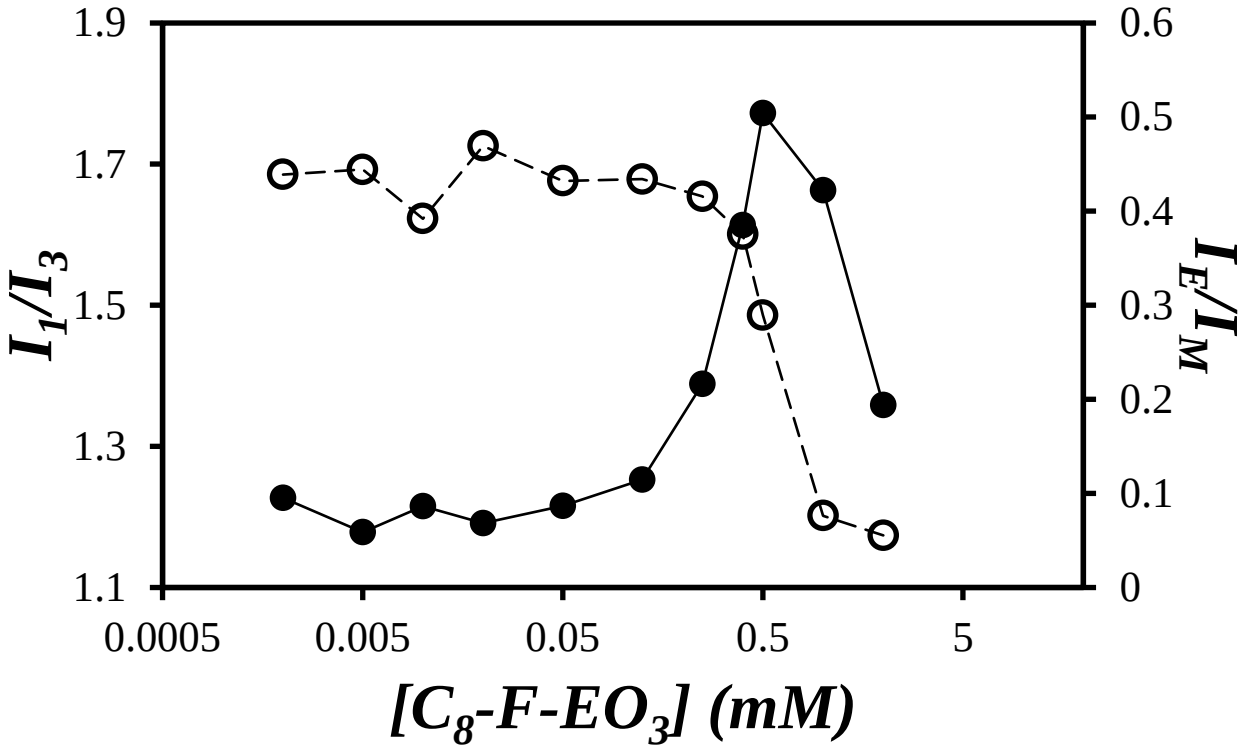

Figure A3.2. Plot of the (●, solid line) I_E/I_M and (○, dashed line) I_1/I_3 ratios as a function of C_8-F-EO_3 concentration. [*Py*] = 5×10^{-7} M.

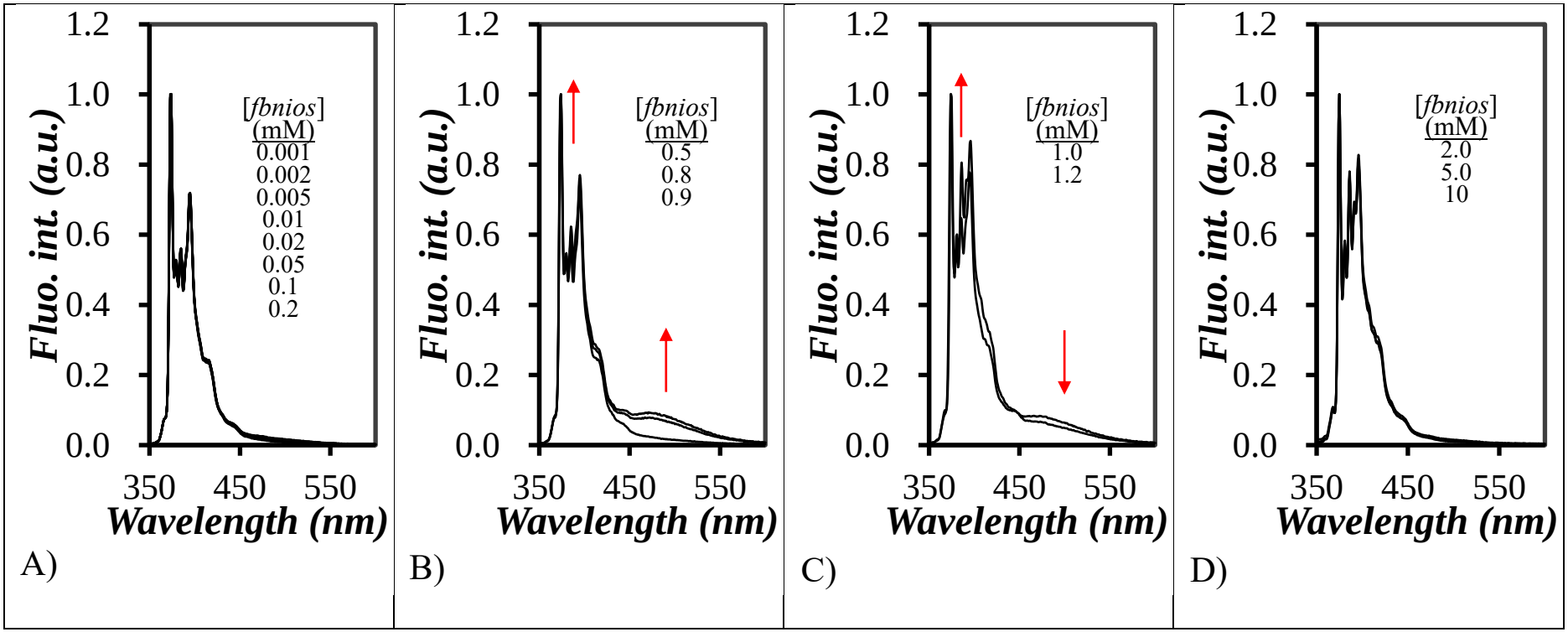

Figure A3.3. SSF spectra of 5×10^{-7} M pyrene in aqueous solutions of C_8-F-EO_6 at concentrations ranging from A) 0.001 to 0.2 mM, B) 0.5 to 0.9 mM, C) 1.0 to 1.2 mM, and D) 2.0 to 10 mM. λ_{ex} = 336 nm.

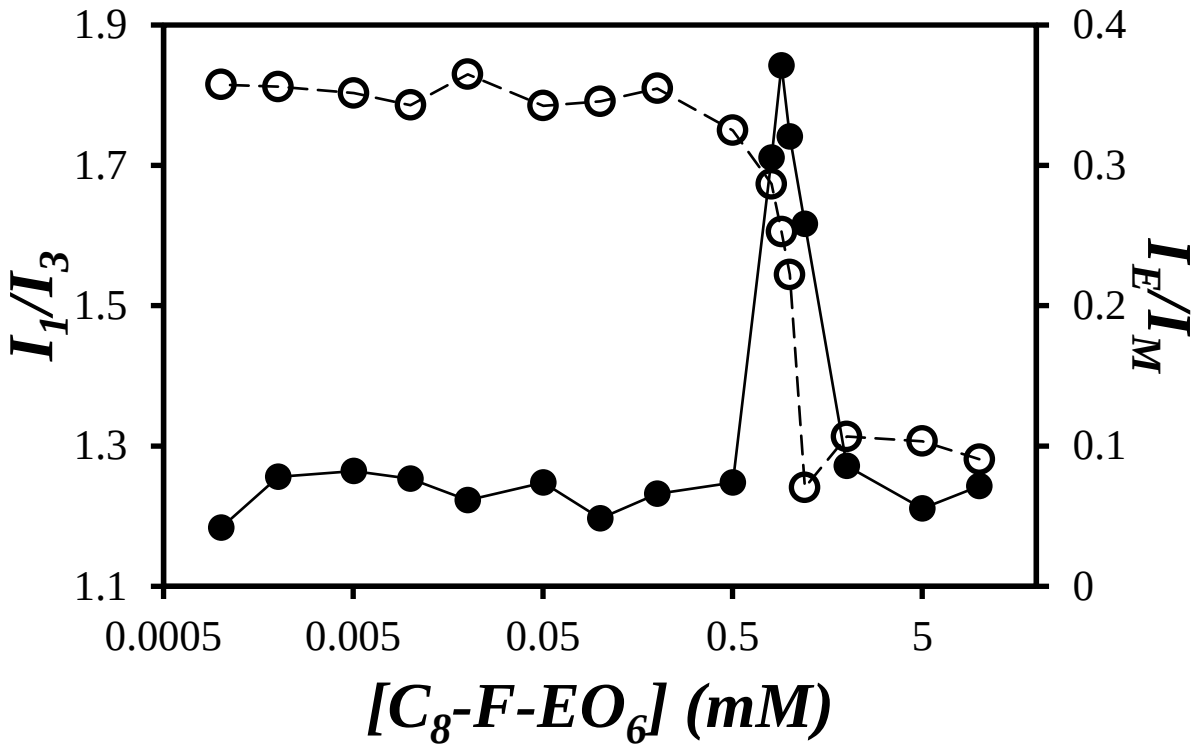

Figure A3.4. Plot of the (●, solid line) I_E/I_M and (○, dashed line) I_1/I_3 ratios as a function of C_8-F-EO_6 concentration. [*Py*] = 5×10^{-7} M.

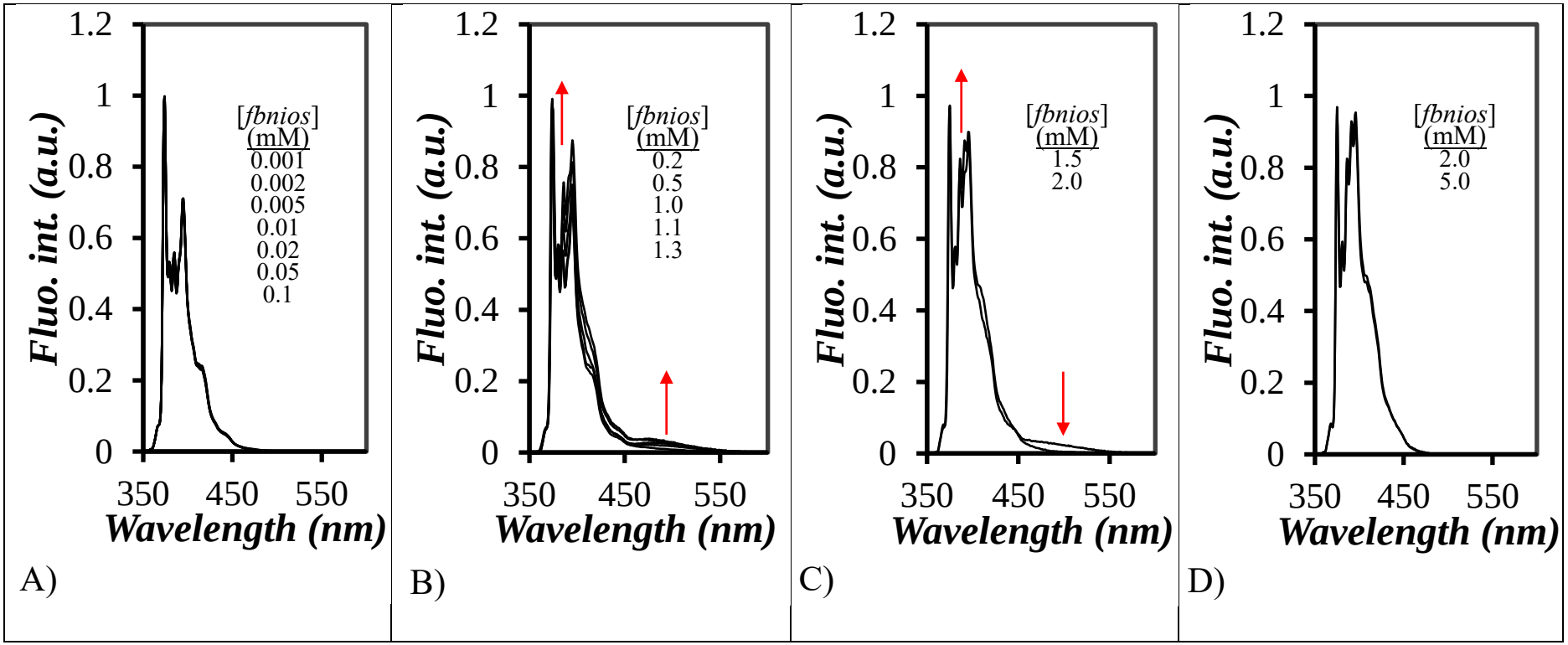

Figure A3.5. Corrected SSF spectra of 5×10^{-7} M pyrene in aqueous solutions of C_8-F-EO_{10} at concentrations ranging from A) 0.001 to 0.1 mM, B) 0.2 to 1.3 mM, C) 1.5 to 2.0 mM, and D) 2.0 to 10.0 mM. λ_{ex} = 336 nm.

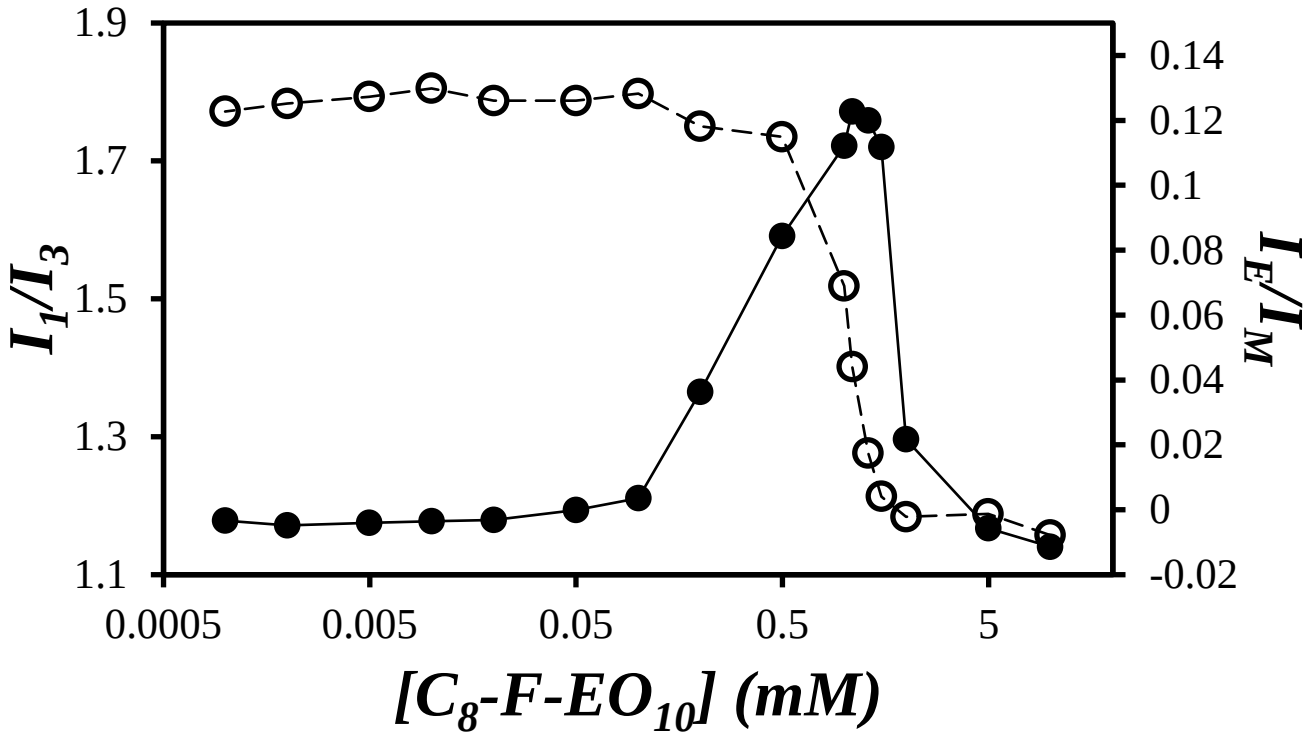

Figure A3.6. Plot of the corrected (●, solid line) I_E/I_M and (○, dashed line) I_1/I_3 ratios as a function of C_8-F-EO_{10} concentration. [*Py*] = 5×10^{-7} M.

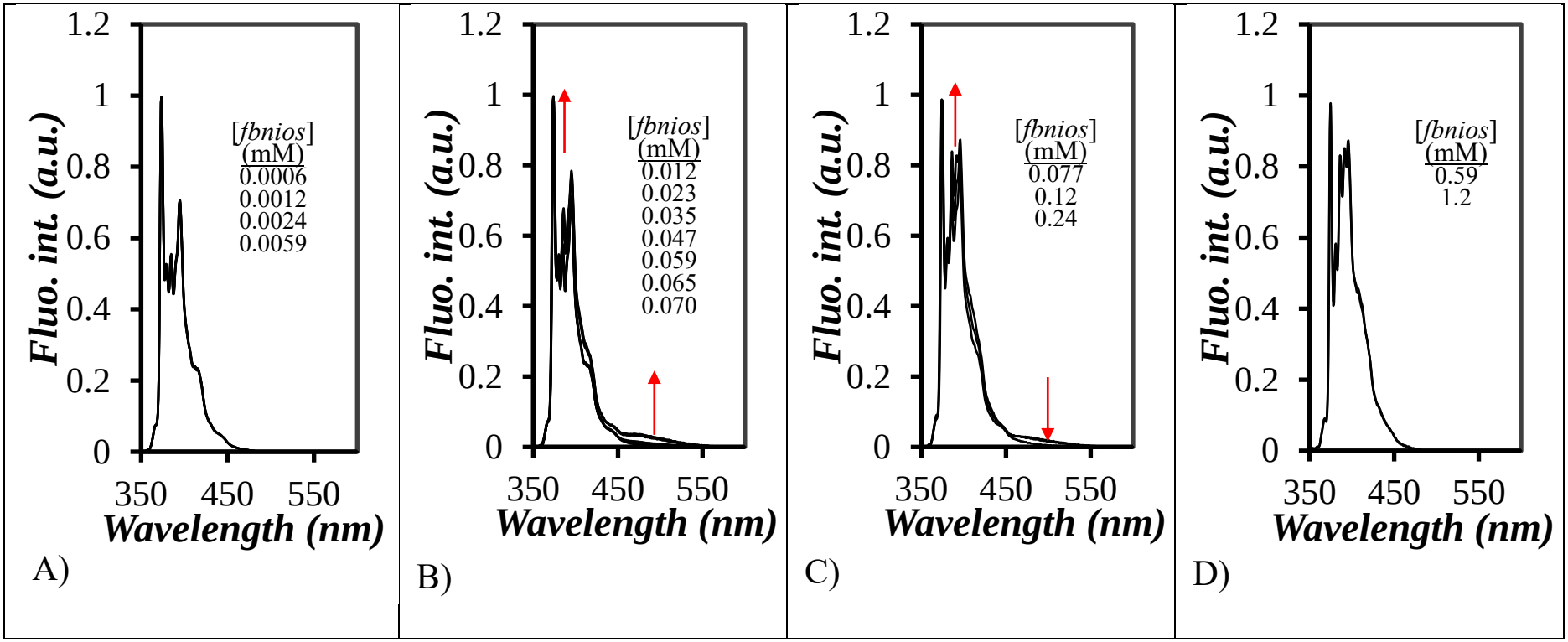

Figure A3.7. Corrected SSF spectra of 5×10^{-7} M pyrene in aqueous solutions of C_{12}-F-EO_8 at concentrations ranging from A) 0.0006 to 0.0059 mM, B) 0.012 to 0.070 mM, C) 0.077 to 0.24 mM, and D) 0.59 to 1.2 mM. λ_{ex} = 336 nm.

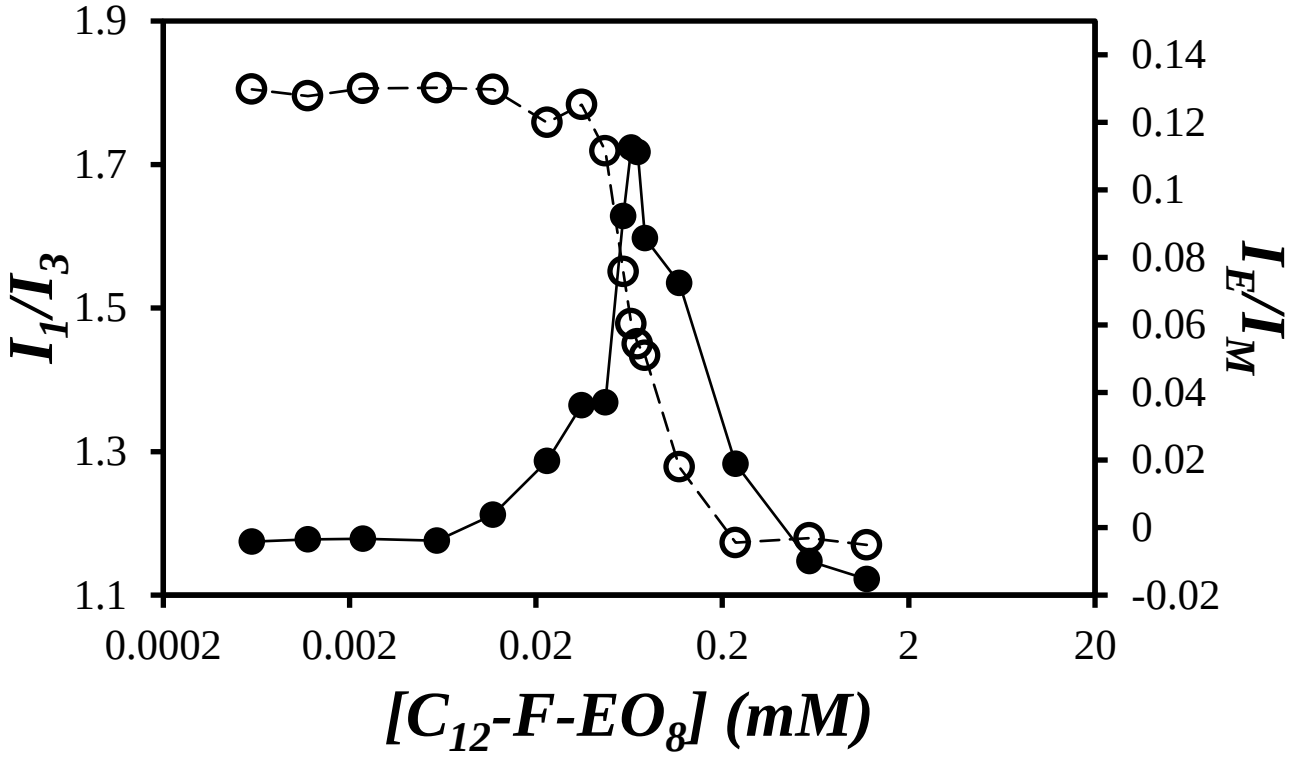

Figure A3.8. Plot of the corrected (●, solid line) I_E/I_M and (○, dashed line) I_1/I_3 ratios as a function of C_{12}-F-EO_8 concentration. [*Py*] = 5×10^{-7} M.

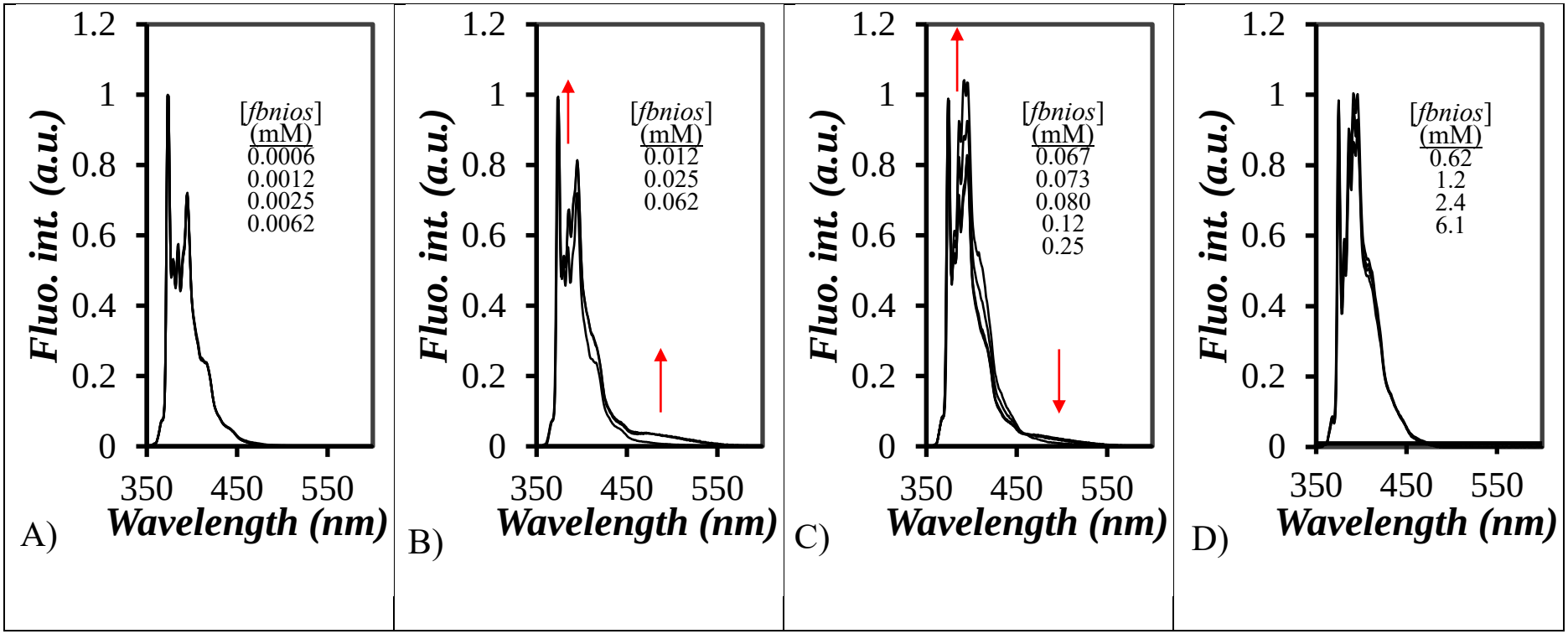

Figure A3.9. Corrected SSF spectra of 5×10^{-7} M pyrene in aqueous solutions of C_{12}-F-EO_{13} at concentrations ranging from A) 0.0006 to 0.0062 mM, B) 0.012 to 0.062 mM, C) 0.067 to 0.25 mM, and D) 0.62 to 6.1 mM. λ_{ex} = 336 nm.

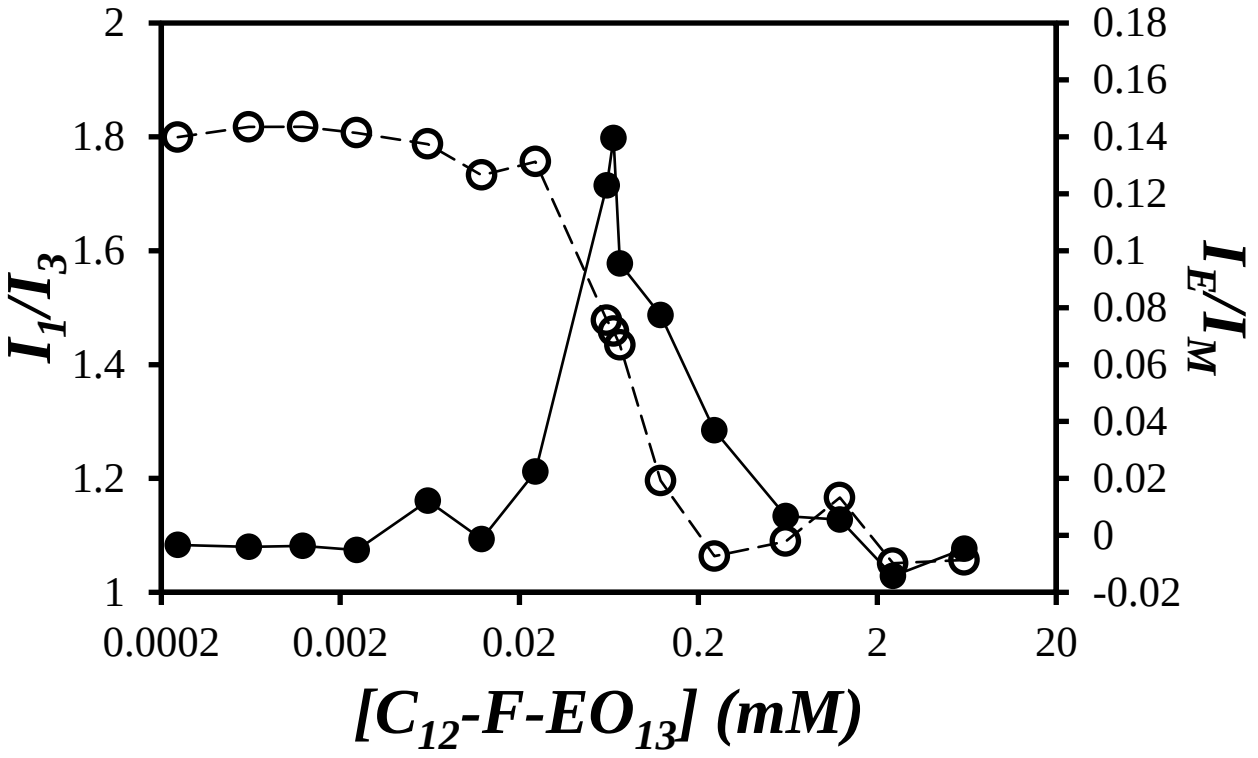

Figure A3.10. Plot of the corrected (●, solid line) I_E/I_M and (○, dashed line) I_1/I_3 ratios as a function of C_{12}-F-EO_{13} concentration. [*Py*] = 5×10^{-7} M.

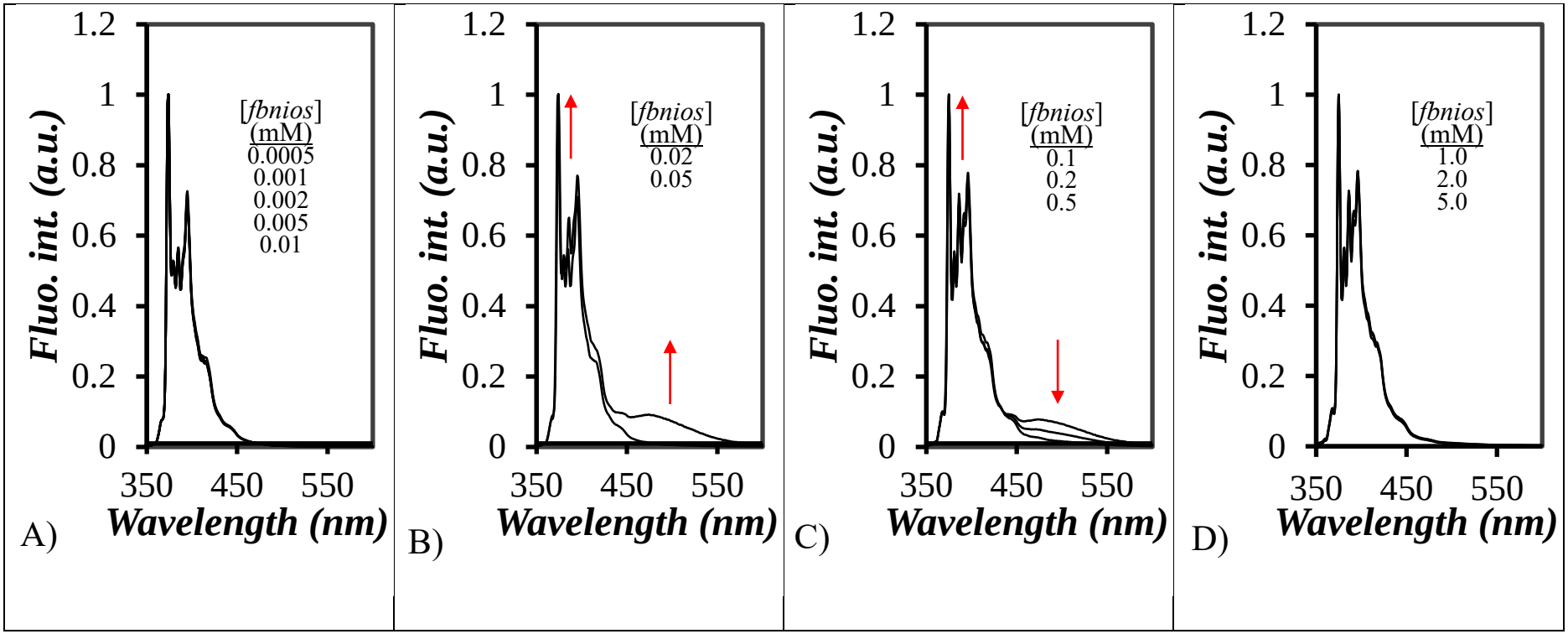

Figure A3.11. SSF spectra of 5×10^{-7} M pyrene in aqueous solutions of C_{12}-F-EO_{18} at concentrations ranging from A) 0.0005 to 0.01 mM, B) 0.02 to 0.05 mM, C) 0.1 to 0.5 mM, and D) 1.0 to 5.0 mM. λ_{ex} = 336 nm.

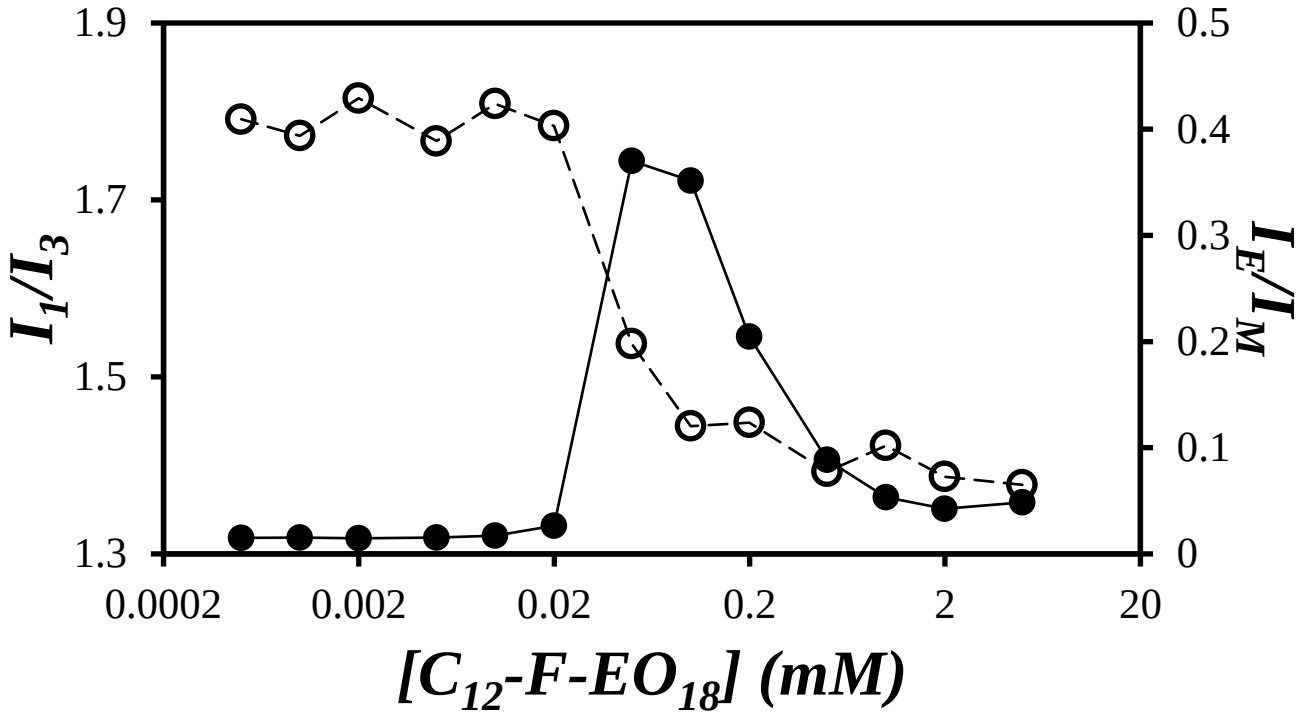

Figure A3.12. Plot of the (●, solid line) I_E/I_M and (○, dashed line) I_1/I_3 ratios as a function of C_{12}-F-EO_{18} concentration. [*Py*] = 5×10^{-7} M.

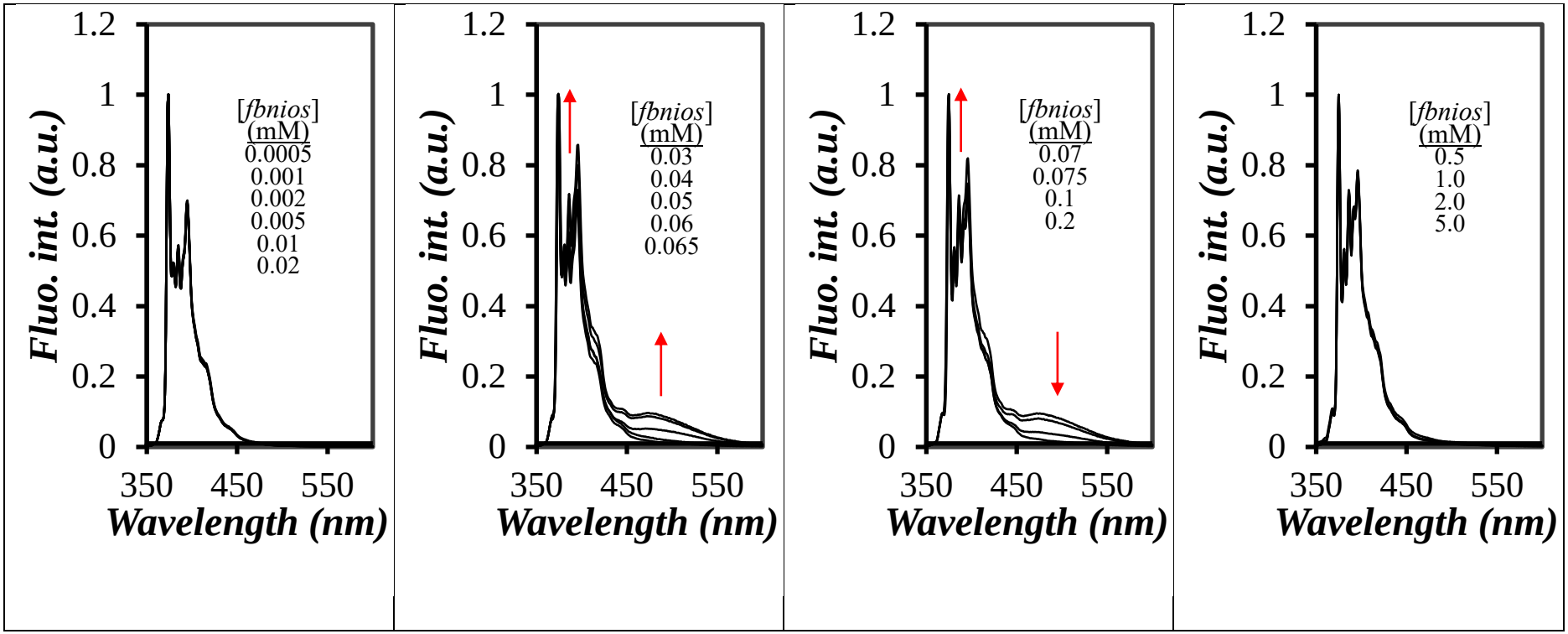

Figure A3.13. SSF spectra of 5×10^{-7} M pyrene in aqueous solutions of C_{12}-F-EO_{23} at concentrations ranging from A) 0.0005 to 0.02 mM, B) 0.03 to 0.065 mM, C) 0.07 to 0.2 mM, and D) 0.5 to 5.0 mM. λ_{ex} = 336 nm.

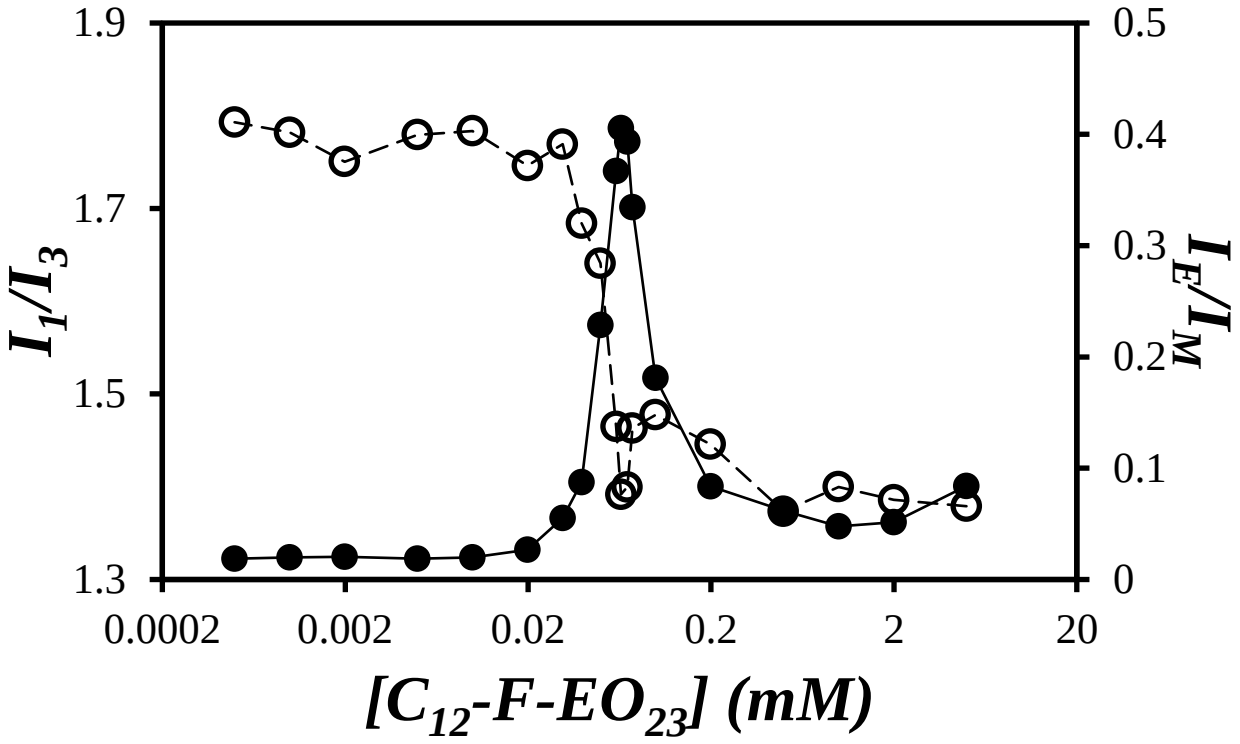

Figure A3.14. Plot of the (●, solid line) I_E/I_M and (○, dashed line) I_1/I_3 ratios as a function of C_{12}-F-EO_{23} concentration. [*Py*] = 5×10^{-7} M.